

EXPERIMENTAL MODAL ANALYSIS OF A STEEL GRID FRAME

A THESIS SUBMITTED TO
THE GRADUATE SCHOOL OF NATURAL AND APPLIED SCIENCES
OF
THE MIDDLE EAST TECHNICAL UNIVERSITY

BY

HÜSEYİN KAYA

IN PARTIAL FULFILLMENT OF THE REQUIREMENTS FOR THE DEGREE
OF
MASTER OF SCIENCE
IN
THE DEPARTMENT OF CIVIL ENGINEERING

JANUARY 2004

Approval of the Graduate School of Natural and Applied Sciences.

Prof. Dr Canan ÖZGEN

Director

I certify that this thesis satisfies all the requirements as a thesis for the degree of Master of Science.

Prof. Dr Erdal ÇOKCA

Head of Department

This is to certify that we have read this thesis and that in our opinion it is fully adequate, in scope and quality, as a thesis for the degree of Master of Science.

Assist. Prof. Dr Ahmet TÜRER

Supervisor

Examining Committee Members

Prof. Dr. Polat GÜLKAN

Assist. Prof Dr. Ahmet TÜRER

Assist Prof. Dr. Ahmet YAKUT

Dr. Oğuzhan HASANÇEBİ

M. S. Halim ÇERMİKLİ

ABSTRACT

EXPERIMENTAL MODAL ANALYSIS OF A STEEL GRID FRAME

Kaya, Hüseyin

M. S., Department of Civil Engineering

Supervisor: Assist. Prof. Dr. Ahmet Türer

January 2004, 220 pages

In this study, experimental modal analysis was studied. Experimental modal analysis includes modal testing, modal parameter estimation and calibration. For this purpose a 4 span skewed steel frame was constructed in Structural Mechanics Laboratory of Civil Engineering Department of METU. The model was transported to Vibration and Acoustic Laboratory of Mechanical Engineering Department of METU. The tests were conducted by cooperation with Vibration and Acoustics Laboratory. Due to lack of experimental modal analysis software in Structural Mechanics Laboratory, modal parameter estimation and finite element updating softwares were written in Matlab platform. The written softwares were executed on the data obtained from modal testing.

15 reasonable modes are extracted from the FRFs that are obtained from modal testing. 59.23 percent consistency is found for the nominal modal comparison. At the end of calibration process 76.14 percent consistency is achieved between the experimental results and analytical results.

Keywords: Experimental Modal Analysis, Modal Testing, Modal Parameter Estimation, Vibration, Finite Element Analysis, Simulated Annealing and Calibration.

ÖZ

ÇELİK BİR GRİD ÇERÇEVENİN DENEYSEL MODAL ANALİZİ

Kaya, Hüseyin

Yüksek Lisans, İnşaat Mühendisliği Bölümü

Tez Yöneticisi: Yard. Doç. Dr. Ahmet Türer

Ocak 2004, 220 sayfa

Bu tezde, deneysel modal analiz çalışılmıştır. Deneysel modal analiz, dinamik test, dinamik parametre tahmini ve kalibrasyon konularını içermektedir. Bu amaç için, Orta Doğu Teknik Üniversitesi İnşaat Mühendisliği Bölümü Yapı Mekaniği Laboratuvarında tek açıklıklı 4 bölmeli yan çelik çerçeve inşa edilmiştir. İnşa edilen yapı Orta Doğu Teknik Üniversitesi Makine Mühendisliği Bölümü Titreşim ve Akustik Laboratuvarına taşınmıştır. Deneyler Titreşim ve Akustik Laboratuvarı ile işbirliği içerisinde yapılmıştır. Modal parametre tahmini için laboratuvarımızda herhangi bir ticari yazılım bulunmamasından dolayı, Modal parametre tahmini ve kalibrasyon için Matlab platformunda programlar yazılmıştır. Yazılan programlar dinamik test sonucu elde edilen bilgiler üzerinde uygulanmıştır.

Dinamik test sonucu elde edilen bilgilerden, kabul edilebilir 15 mod çıkarılmıştır. Nominal model karşılaştırmasında %59.23 uyum saptanmıştır. Kalibrasyon işlemi sonucunda deneysel ve analitik sonuçlar arasındaki uyum %76.14 'e yükselmiştir

Anahtar kelimeler: Deneysel Modal Analiz, Modal Test, Modal Parametre Tahmini, Titreşim, Sonlu Elemanlar Analizi, Kalibrasyon.

To My Parents and My Fiancé;

ACKNOWLEDGEMENTS

I would like to express my profound appreciation to Assist. Prof. Dr. Ahmet TÜRER, my supervisor, without whose patient supervision, invaluable guidance and continuous encouragement this work could have never been accomplished at all. It has been a pleasure to work under his supervision.

I would like to thank Ali Faik ULUSOY, for his helpful ideas and support in Optimization Process.

Finally, special thanks go to my family and my fiancé for their patience and loving encouragement, who deserve much more attention than I could devote to them during this study.

TABLE OF CONTENTS

ABSTRACT	iii
ÖZ	v
DEDICATION	vii
ACKNOWLEDGEMENT	viii
TABLE OF CONTENTS	ix

CHAPTER

1. INTRODUCTION.....	1
1.1 Background	1
1.2 Finite Element Method (FEM).....	2
1.3 Modal Testing Method.....	3
1.4 Applications of Modal Test Models.....	4
1.4.1 Updating of the Analytical Models (Calibration)	5
1.4.2 Structural Dynamic Modification	6
1.5 Sources of Lack of Precision in Modal Testing	8
1.6 Objectives, and Scope of This Thesis	10
2. THEORY OF VIBRATION	12
2.1 Introduction	12
2.2 Single Degree of Freedom Systems	12
2.2.1 Time Domain: Impulse Response Function	17
2.2.2 Frequency Domain: Frequency Response Function	18
2.2.3 Laplace Domain: Transfer Function	25

2.3	Multiple Degree of Freedom Systems.....	33
2.4	Damping Mechanisms.....	39
3. MODAL DATA ACQUISITION & EXPERIMENTAL MODAL ANALYSIS		
METHODS		41
3.1	Introduction	41
3.2	Modal Data Acquisition	42
3.2.1	Sampling	43
3.2.2	Quantization	47
3.2.3	ADC Errors	48
3.2.3.1	Aliasing	48
3.2.3.2	Quantization Error.....	49
3.2.4	Discrete Fourier Transform.....	49
3.2.4.1	Discrete Fourier Transform Errors.....	51
3.2.4.1.1	Leakage Error.....	51
3.2.5	Transducer Considerations.....	55
3.3	Experimental Modal Analysis Methods.....	58
3.3.1	Frequency Response Function Model.....	59
3.3.2	Frequency Response Function Testing Method.....	60
3.3.3	Excitation	63
3.3.3.1	Classification of Excitation	63
4. MODAL PARAMETER ESTIMATION		67
4.1	Introduction	67
4.2	Modal Parameters:	67
4.3	Complex Mode Indication Function (CMIF).....	69
4.3.1	Theory of SVD and CMIF	69
4.4	Enhanced Frequency Response Function (eFRF).....	74
4.5	Pole Estimation	75
4.6	Scaling Computation.....	79

5. MODAL DATA PRESENTATION/VALIDATION	81
5.1 Introduction	81
5.2 Measurement Synthesis.....	82
5.3 Visual Verification (Animation)	83
5.4 Finite Element Analysis	83
5.5 Modal Assurance Criterion	84
6. EXPERIMENTAL MODAL ANALYSIS SOFTWARE	86
6.1 Introduction	86
6.2 Structure of EMAS.....	87
6.2.1 Commands.....	88
6.2.1.1 Input File Editor	89
6.2.1.1.1 NODE.....	90
6.2.1.1.2 NODEGEN	91
6.2.1.1.3 ELEMTYPE.....	92
6.2.1.1.4 ELEM.....	93
6.2.1.1.5 ELEMGEN.....	93
6.2.1.1.6 CONSTNODE.....	95
6.2.1.1.7 CONSTDOF.....	96
6.2.1.1.8 MASTERNODE	97
6.2.1.1.9 MASTERDOF.....	97
6.2.1.1.10 ALLMASTERDOF	97
6.2.1.2 Frequency Response Function Loader	98
6.2.1.2.1 How Does FRFL Program Work	99
6.2.1.3 Modal Parameter Estimation.....	100
6.2.1.3.1 How Does MPE Program Work.....	101
6.2.1.4 FRF Generator.....	108
7. VERIFICATION OF EMAS.....	112
7.1 Introduction	112

7.2	Verification of EMAS using 3. d.o.f Model.....	112
7.2.1	Enhanced FRF Plots & eFRF Plots with Synthesized Peaks	114
7.2.2	MPE Results.....	118
7.2.3	Measurement Synthesis.....	119
7.2.4	Visual Verification	124
7.2.5	Modal Assurance Criterion (MAC) Correlation	125
7.2.6	Comparison of Results Obtained from MPE Part of EMAS Against Theoretical Results.....	126
8.	EXPERIMENTAL STUDY	128
8.1	Introduction	128
8.2	Specifications of Model	128
8.3	Boundary Conditions	132
8.4	Excitation	134
8.5	Sensors	135
8.6	Dynamic Signal Analyzer	137
8.7	Modal Data Acquisition & Parameters	139
8.8	Input File of Model	142
8.9	Data Loading	143
8.10	Modal Parameter Estimation.....	143
8.10.1	First Experiment (Excitation at Node 1)	143
8.10.2	Second Experiment (Excitation at Node 33).....	146
9.	FE UPDATING.....	149
9.1	Introduction	149
9.2	Finite Element Analysis	150
9.3	Objective Function Calculation.....	151
9.4	Modification of FE Model in order to Correlate FEM and EMA Results (FEU Strategy)	152
9.4.1	Simulated Annealing	152

9.4.1.1	Physical Origin of SA	153
9.4.2	How Does SA Work?	154
9.4.3	Formation of the Candidate Model	155
9.4.4	Number of Iterations of the Inner Loop (<i>I</i>)	157
9.4.5	Metropolis Test	158
9.5	Matlab Based FEU Software (FEUS)	160
10.	APPLICATION OF FE UPDATING SOFTWARE ON SKEWED STEEL GRID FRAME	166
10.1	Introduction	166
10.2	Input File of the Skewed Steel Grid Frame	166
10.3	Groups, and Parameters for Each Group	169
10.3.1	Mass groups and Parameters:	169
10.3.2	Spring Groups and Parameters	171
10.3.3	Frame Groups and Parameters	172
10.4	Parameters Defined for FEU Process	177
10.4.1	Nominal Models' Comparisons and FEU Results	177
10.4.1.1	EMA Result Set 1	178
10.4.1.2	EMA Results Set 2	181
10.4.1.3	EMA Set 3	182
10.5	Optimized Group Parameters	187
11.	DISCUSSION OF RESULTS & CONCLUSION	189
11.1	An Overview of This Study	189
11.2	Discussion of Results of Modal Testing	190
11.3	Discussion of Results of Finite Element Updating	191
11.3.1	Optimized Mass Parameters	193
11.3.2	Optimized Spring Parameters	193
11.3.3	Optimized Frame Parameters	194
11.4	A Few Comment about FEU	197

11.5	Future Studies.....	199
REFERENCES.....		200
APPENDICES		
A.	Report generated by EMAS for 3 d.o.f. system	207
B.	Input file of skewed frame used in FEUS	210
C.	Mode shapes extracted from the first experiment	215
D.	Mode shapes extracted from the second experiment	218

CHAPTER 1

INTRODUCTION

1.1 Background

The understanding of the physical nature of vibration phenomena has always been important for researchers and engineers, even more as today as structures are becoming lighter and more flexible due to increased demands for efficiency, speed, safety and comfort. When any structure vibrates, it causes major problems and operating limitations ranging from discomfort (including noise), malfunction, reduced performance and fatigue. Two approaches may be considered to resolve the vibration problem: first, prevention, through proper design, and second, cure, by modification of structure or a vibration control design. In any case, a thorough understanding of vibration of the structure is essential. Hence, accurate mathematical models are required to describe the vibration characteristics of the structure. For simple structures, such as beams and plates, good analytical predictions using closed form solutions can be easily found in various reference books and tables (Such as Chopra, 1995, Chandrupatla *et al.*, 1997). However, for more complex structures, more powerful tools are needed. Today, analytical tools and experimental tools are used to model the dynamic behavior of the structures.

The most widely used analytical tool is the Finite Element Method (FEM) (Cook *et al.*, 1989, Chandrupatla *et al.*, 1997), while the experimental counterparts are largely based on modal testing and analysis (Ewins, 1995). Due to different built-in limitations, assumptions and choices, each approach has its own advantages and disadvantages.

1.2 Finite Element Method (FEM)

The main assumption in Finite Element Method (FEM) is that a continuous structure can be discretized by describing it as an assembly of finite (discrete) elements, each with a number of boundary points which are commonly referred to as nodes. For structural dynamic analysis, element mass, stiffness and damping matrices are generated first and then assembled into global system matrices. Dynamic analysis of the produced model gives the modal properties; the natural frequencies (Eigenvalues) and corresponding mode shapes (Eigenvectors). The modal solution can subsequently be used to calculate forced vibration response levels for the structure under study. Element system matrices have been developed for many simple structures, such as beams, plates, shells and bricks. Most general-purpose FE programs have a wide range of choice of element types, and the user must select the appropriate elements for the structure under investigation and its particular application. Further theoretical background and practical implementation of the FE method are given in various text books, such as those by Cook *et al.*, (1989), Chandrupatla *et al.*, (1997), Bathe (1996).

The FE method is extensively used in industry as it can produce a good representation of a true structure. However, for complicated structures, due to

limitations in the method and application, a FE model can lead to errors. The sources of errors in Finite Element models are:

1. Inaccuracy in estimation of the physical properties of the structure.
2. Poor quality of mesh generation and selection of individual shape functions.
3. Poor approximation of boundary conditions.
4. Poor estimation or omission of damping properties of the system.
5. Computational errors which are mainly due to rounding off. (ill conditioned matrices)
6. Linear Modeling of highly nonlinear structures. (Geometric and material nonlinearities)

The result of a finite element analysis is mainly dependent on the judgment and experience of the operator and the software package used.

1.3 Modal Testing Method

The experimental approach to modeling the dynamic behavior of structures (modal testing) relies mostly on extracting the vibration characteristics of a structure from measurements. The procedure consists of three steps:

1. Acquiring the modal data.
2. Analyzing the measured modal data.
3. Constructing the dynamic model behavior by using extracted modal parameters from the analyzed data.

Vibration measurements are taken directly from a physical structure, without any assumptions about the structure, and that is the reason why modal testing models are considered to be more reliable than Finite Element models. However, due to a number of limitations and errors, the model created from the measured data may not represent the actual behavior of the structure as closely as desired.

The theoretical background of modal testing and practical aspects of vibration measurement techniques are discussed by Ewins, (1995).

In general, limitations and errors of modal testing are:

- Random errors due to noise.
- Loose attachment of transducers to the structure.
- Non-linear behavior of the structure or attached mechanical devices
- Poor modal analysis of experimental data (user experience).
- Limited number of measured degrees of freedom.
- Not all modes being excited due to excitation at a node.
- Difficulty in measuring rotational degrees of freedom.

1.4 Applications of Modal Test Models

It is generally believed that more confidence can be placed in experimental data since measurements are taken on the true structure. Therefore, the mathematical models, which have been created as a result of modal testing, can be used in various ways to avoid or to cure the problems encountered in structural dynamics. In this Section, the applications of modal testing methods for improving the structural dynamics will be considered.

1.4.1 Updating of the Analytical Models (Calibration)

One of the applications of the result of a modal test is the updating of an analytical model (usually a model derived using finite element method). Model updating can be defined as adjustment of an existing analytical model which represents the structure under study, using experimental data (Catbas *et al.*, 1998, Ventura *et al.*, 2001, Dascotte, 2001, Haapaniemi *et al.*, 2002). Therefore, updated FE model more accurately reflects the dynamic behavior of that structure. Model updating can be divided into three steps:

1. Comparison of FE model and modal testing results.
2. Modifying FE model in order to correlate FEM and modal testing results.
3. Analyzing updated FE model and return to step 1 until convergence is achieved.

Comparison can be defined as the initial step to assess the quality of the analytical model. If the difference between analytical and experimental data is within some preset tolerances, the analytical model can be judged to be adequate and no updating is necessary.

Most difficulties are encountered in the second step. The difficulties in locating the errors in a theoretical model are mostly due to measurement process and can be summarized as:

1. Insufficient experimental modes;

2. Insufficient experimental coordinates;
3. Size and mesh incompatibility of the experimental and FE models;
4. Experimental random and systematic errors.
5. Absence of damping in the FE model

In spite of extensive research over the last two decades, model updating is still far from mature and no reliable and general applicable procedures have been formulated so far.

1.4.2 Structural Dynamic Modification

Structural dynamic modification can be defined as the study of changes (in natural frequencies and mode shapes) of measured dynamic properties of the test structure due to modified mass or stiffness or damping of the structure. In principle, the modification process is a form of optimization of the structure to bring its modal properties of the structures to some desired condition (Wallack *et al.*, 1989 and Schwarz *et al.*, 1997).

For example a bridge with certain vibration problems should be modified. Sometimes, the effect of an addition to a structure must be known. For instance, addition of a storey to an existing building or addition of a missile to a fighter jet plane. Modeling the existing structure might be too costly and unnecessary. The existing structure can be modal tested and effect of the new addition (i.e. additional floor or missile) can be evaluated using structural dynamic modification.

This method saves large amounts of redesign time as it reduces the cycle time in the test, analysis, redesign, shop drawings, install redesign, and retest cycle. In practice, the measured properties of existing structure at the boundary level are only

translational degrees of freedom (d.o.f.). However for structural dynamic modification, rotational d.o.f.s are also needed for proper assembly. Deficiency in rotational degrees of freedom has problems in dealing with real-world problems such as addition of a plate, beam, and rotor or other structural elements with bending resistance.

Moreover, there is a need for sufficient modal vector information to carry out real world structural modification. This demands that more data be taken, but the number of data points is limited by the time available from the highly-trained modal staff. Generally, most modal tests are limited to 50-60 x - y - z degrees of freedom. This is usually too few for the structural modification to be implemented without excessive retesting. Sometimes it is desired to construct a mathematical model of a complete structural assembly formed by the assembly of several individual substructures. There are a number of methods for assembling such a model which are extensions of modification methods and called “structural assembly methods”. The essential difference is that here the modifications are themselves dynamic systems, rather than simple mass or stiffness elements. It is possible to combine subsystem or component models derived from different sources or analyses for example from a mixture of analytical and experimental studies. Again the same problems encountered with modification methods are encountered.

There are other quantitative applications of the modal test models, which demand a high degree of both accuracy and completeness (enough points and enough d.o.f.s on the test structure) of the test data. These applications are:

- Response predictions for the test structure if it is subjected to other excitations.

- Force determination, from measured responses.
- Damage detection. (Operating curves).

1.5 Sources of Lack of Precision in Modal Testing

Laboratory experiments and practical measurements serve several purposes, some of which do not demand high accuracy. Some experiments are exploratory in the sense of looking for the existence and direction of some effect before trying to establish its magnitude; others are chiefly instructional, to demonstrate theoretical principles. Some industrial measurements are needed only to control and repeat a process in accordance with previously established values. Errors in such cases may be harmless. However, engineering applications of some experiments demand test data of high quality. In these cases, large errors may arise if test data with poor quality are used. In recent years there has been a strong demand for modal testing with high quality suitable for advanced applications such as structural modification and model updating.

In Section 1.4, it is explained in general terms how the mathematical models which have been created as a result of modal tests, can be used in various ways to apply in vibration-related problems encountered in theory and practice, and how these applications are hindered from a lack of precision in modal testing. In this Section, the problem of the sources of the lack of precision in modal testing is studied more systematically. In the following paragraphs attention is drawn to the reasons why the experimental modal test data can depart from the true values it purports to measure. The sources of a lack of precision in modal testing procedure can be categorized in three groups: (i) Experimental data acquisition errors (ii) Signal

processing errors and (iii) Modal analysis errors, each of them has been categorized itself in below (Ashory, 1999).



Figure 1-1 Three stages of the modal testing

Experimental data acquisition errors:

a) Quality :

1) Mechanical errors :

- Mass loading effect of transducers
- Shaker-structure interaction
- Supporting of the structure

2) Measurement noise

3) Nonlinearity

b) Quantity :

- Measuring enough points on the structure
- Measuring enough Degrees of Freedom (i.e. Rotational DOFs)

(ii) signal processing errors :

- Leakage

- Aliasing
- Effect of window functions
- Effect of Discrete Fourier Transform
- Effect of averaging

(iii)modal analysis errors :

- Circle-Fit Modal Analysis
- Line-Fit Modal Analysis
- Global Modal Analysis

1.6 Objectives, and Scope of This Thesis

This work is an attempt to:

- Carry out a literature survey on the subjects of Theory of Vibration, modal testing, modal analysis and FE updating.
- Construct single span skewed steel grid frame in the Structural Mechanics Laboratory for the application of modal testing.
- Study one of the non-destructive modal testing methods of sweep sine forced vibration method on the constructed frame.
- Study global modal parameter estimation method of “Complex Mode Indicator Function” (CMIF).
- Write graphical user interfaced program about “General purpose modal parameter estimation and mode animation”.
- Study a robust global search and optimization technique of “Simulated Annealing (SA)” for FEU purposes.

- Write a graphical user interfaced program about Finite Element Updating.
- Application of the written FEU Software on modal data obtained from single span skewed steel grid frame model.

CHAPTER 2

THEORY OF VIBRATION

2.1 Introduction

One who wants to study modal testing and modal analysis should briefly have background about dynamics but specially “Theory of vibration”. The following Section briefly explains theory of vibration, starting with single degree of freedom systems and continues to multi degree of freedom systems (Allemang, 1998, Chopra, 1995, Ewins, 1995).

2.2 Single Degree of Freedom Systems

In order to understand modal analysis, single degree of freedom systems must be understood. In particular, the complete familiarity with single degree of freedom systems (as presented and evaluated in the time, frequency (Fourier), and Laplace domains) serves as the basis for many of the models that are used in modal parameter estimation. The single degree of freedom approach is obviously trivial for the modal analysis case. The importance of this approach results from the fact that the multiple degree of freedom case can be viewed as a linear superposition of

single degrees of freedom systems. Single degree of freedom system is described in Figure 2-1.

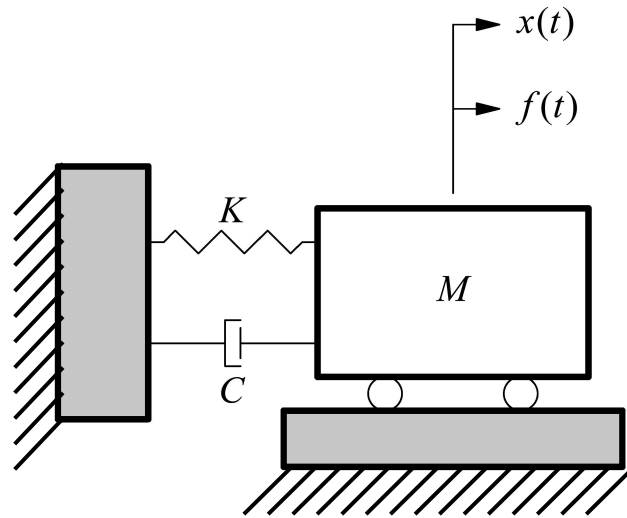


Figure 2-1 Single Degree of Freedom System

Free body diagram of Figure 2-1 is shown in Figure 2-2.

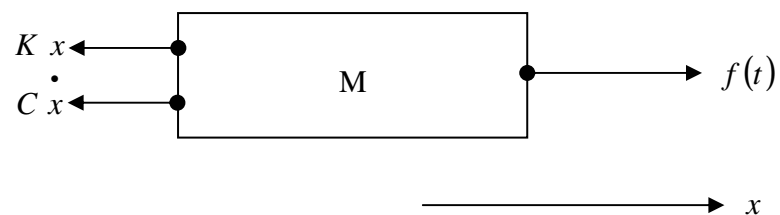


Figure 2-2 Free Body Diagram of SDOF system

The general mathematical representation of a single degree of freedom system is obtained from Newton's Law of Motion and expressed in Equation 2-1, where total forces acting on the system is equaled to mass (M) times acceleration.

$$M \ddot{x}(t) + C \dot{x}(t) + K x(t) = f(t) \quad \text{Equation 2-1}$$

Where;

- M = Mass of the system
- C = Damping of the system
- K = Stiffness of the system
- f(t) = General force function

By setting $f(t) = 0$, the homogeneous form of Equation 2-2 can be solved.

$$M \ddot{x}(t) + C \dot{x}(t) + K x(t) = 0 \quad \text{Equation 2-2}$$

From differential equation theory, the solution can be assumed to be of the form $x(t) = X e^{st}$, where s is a complex valued number to be determined. Taking appropriate derivatives and substituting into Equation 2-2 yields:

$$(M s^2 + C s + K) X e^{st} = 0 \quad \text{Equation 2-3}$$

Thus, for a non-trivial solution:

$$M s^2 + C s + K = 0 \quad \text{Equation 2-4}$$

Where:

s = Complex-valued frequency variable (Laplace variable)

Equation 2-4 is the characteristic equation of the system, whose roots λ_1 and λ_2 are:

$$\lambda_{1,2} = -\frac{C}{2M} \pm \left\{ \left(\frac{C}{2M} \right)^2 - \left(\frac{K}{M} \right) \right\}^{\frac{1}{2}} \quad \text{Equation 2-5}$$

Thus the general solution of Equation 2-2 is:

$$x(t) = Ae^{\lambda_1 t} + Be^{\lambda_2 t} \quad \text{Equation 2-6}$$

A and B are constants determined from the initial conditions imposed on the system at time $t = 0$.

For most real structures, unless active damping systems are present, the damping ratio is rarely greater than ten percent. For this reason, all further discussion is restricted to under damped systems ($\zeta < 1$). With reference to Equation 2-6, this means that the two roots, $\lambda_{1,2}$, are always complex conjugates. Also, the two coefficients (A and B) are complex conjugates of one another (A and A^*). For an under damped system, the roots of the characteristic equation can be written as:

$$\lambda_1 = \sigma_1 + j\omega_1 \quad \lambda_2 = \sigma_1 - j\omega_1 \quad \text{Equation 2-7}$$

Where;

- σ_1 = Damping Factor

- w_1 = Damped Natural Frequency

The roots of characteristic Equation 2-4 can also be written as:

$$\lambda_1, \lambda_1^* = -\zeta_1 \Omega_1 \pm j \Omega_1 \sqrt{1 - \zeta_1^2} \quad \text{Equation 2-8}$$

Where;

Ω_1 = Undamped Natural Frequency

ζ_1 = Percent damping with respect to critical damping.

The damping factor, σ_1 , is defined as the real part of a root of the characteristic equation. This parameter has the same units as the imaginary part of the root of the characteristic equation, radians per second. The damping factor describes the exponential decay or growth of the oscillation. In real-world structures energy of the system is dissipated through damping mechanism. Therefore there is always exponential decay in oscillation. Exponential growth of the oscillation is theoretical and is not valid for real world structures.

Critical damping (C_c), is defined as being the damping which reduces the radical in the solution of the characteristic equation to zero. This form of damping representation is a physical approach and therefore involves the appropriate units for equivalent viscous damping.

$$\left(\frac{C_c}{2M}\right)^2 - \left(\frac{K}{M}\right) = 0 \rightarrow \frac{C_c}{2M} = \sqrt{\frac{K}{M}}$$

$$C_c = 2M \sqrt{\frac{K}{M}} = 2M \Omega_1 \quad \text{Equation 2-9}$$

The damping ratio, ζ , is the ratio of the actual system damping to the critical system damping. The damping ratio is dimensionless since the units are normalized.

$$\zeta_1 = \frac{C}{C_c} = \frac{-\sigma_1}{\Omega_1} \quad \text{Equation 2-10}$$

2.2.1 Time Domain: Impulse Response Function

The impulse response function of a single degree of freedom system can be determined from Equation 2-6 assuming that the initial conditions are zero and that the system excitation, $f(t)$, is a unit impulse. The response of the system, $x(t)$, to such a unit impulse is known as the impulse response function, $h(t)$, of the system. Therefore:

$$h(t) = A e^{\lambda_1 t} + A^* e^{\lambda_1^* t} \quad \text{Equation 2-11}$$

$$h(t) = e^{\sigma_1 t} \left[A e^{(+j w_1 t)} + A^* e^{(-j w_1 t)} \right] \quad \text{Equation 2-12}$$

Thus, the coefficients (A and A^*) control the amplitude of the impulse response, the real part of the pole is the decay rate and the imaginary part of the pole is the frequency of oscillation. Figure 2-3 illustrates the impulse response function, for a single degree of freedom system.

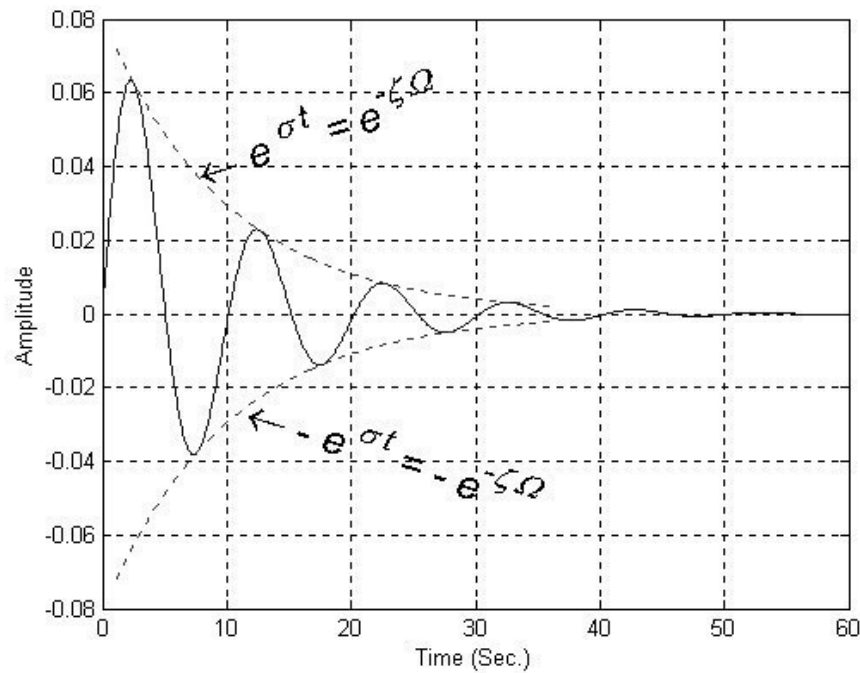


Figure 2-3 Time Domain: Impulse Response Function

2.2.2 Frequency Domain: Frequency Response Function

An equivalent equation of motion for Equation 2-1 is determined for the Fourier or frequency (ω) domain. This representation has the advantage of converting a differential equation to an algebraic equation. This is accomplished by taking the Fourier transform (Meirovitch, 1996) of Equation 2-1.

Letting the forcing function of Equation 2-1 be in the form of

$$F(t) = F(\omega)e^{j\omega t} \quad \text{Equation 2-13}$$

Therefore the solution of Equation 2-1 will be in the form of;

$$X(t) = X(\omega)e^{j\omega t} \quad \text{Equation 2-14}$$

Thus;

$$\dot{X}(t) = j\omega X(\omega)e^{j\omega t} \quad \text{Equation 2-15}$$

$$\ddot{X}(t) = -\omega^2 X(\omega)e^{j\omega t} \quad \text{Equation 2-16}$$

Substituting Equation 2-14 , Equation 2-15 and Equation 2-16 into Equation 2-1 yields;

$$\left[-M \omega^2 X(\omega)e^{j\omega t} + j C \omega X(\omega)e^{j\omega t} + K X(\omega)e^{j\omega t} \right] = F(\omega)e^{j\omega t} \quad \text{Equation 2-17}$$

After rearranging the common terms in Equation 2-17;

$$\left[-M \omega^2 + j C \omega + K \right] X(\omega)e^{j\omega t} = F(\omega)e^{j\omega t} \quad \text{Equation 2-18}$$

Simplifying Equation 2-18 yields;

$$\left[-M \omega^2 + j C \omega + K \right] X(\omega) = F(\omega) \quad \text{Equation 2-19}$$

Restating Equation 2-19 yields:

$$B(\omega) X(\omega) = F(\omega) \quad \text{Equation 2-20}$$

Where;

- $B(\omega) = -M \omega^2 + j C \omega + K$

Equation 2-20 states that the system response $X(\omega)$ is directly related to the system forcing function $F(\omega)$ through the quantity $B(\omega)$, the impedance function. If the system forcing function $F(\omega)$ and its response $X(\omega)$ are known, $B(\omega)$ can be calculated. That is:

$$B(\omega) = \frac{F(\omega)}{X(\omega)} \quad \text{Equation 2-21}$$

More frequently, the system response, $X(\omega)$ due to a known input $F(\omega)$ is of interest.

$$X(\omega) = \frac{F(\omega)}{B(\omega)} \quad \text{Equation 2-22}$$

Equation 2-22 becomes:

$$X(\omega) = H(\omega) F(\omega) \quad \text{Equation 2-23}$$

Where:

- $H(\omega) = \frac{1}{-M \omega^2 + j C \omega + K}$

The quantity $H(\omega)$ is known as the ***Frequency Response Function*** of the system.

The frequency response function relates the Fourier transform of the system input to the Fourier transform of the system response. From Equation 2-23, the frequency response function can be defined as:

$$H(\omega) = \frac{X(\omega)}{F(\omega)} \quad \text{Equation 2-24}$$

Going back to Equation 2-19, the frequency response function can be written as,

$$H(\omega) = \frac{1}{-M\omega^2 + jC\omega + K} = \frac{1/M}{-\omega^2 + j\left(\frac{C}{M}\right)\omega + \left(\frac{K}{M}\right)} \quad \text{Equation 2-25}$$

The denominator of Equation 2-25 is known as the “characteristic equation” of the system and is in the same form as Equation 2-4. The characteristic values of this complex equation are in general complex even though the equation is a function of a real valued independent variable “ ω ”. The characteristic values of this equation are known as the complex roots of the characteristic equation or the complex poles of the system. These characteristic values are also called the “modal frequencies”.

The frequency response function $H(\omega)$ can also be written as a function of the complex poles as follows:

$$H(\omega) = \frac{1/M}{(j\omega - \lambda_1)(j\omega - \lambda_1^*)} = \frac{A}{(j\omega - \lambda_1)} + \frac{A^*}{(j\omega - \lambda_1^*)} \quad \text{Equation 2-26}$$

Where;

λ_1 = Complex Pole

$$\lambda_1 = \sigma_1 + j \omega_1$$

$$\lambda_1^* = \sigma_1 - j \omega_1$$

$$\sigma_1 = -\zeta_1 \Omega_1$$

$$\omega_1 = \Omega_1 \sqrt{1 - \zeta_1^2}$$

Since the frequency response function is a complex valued function of a real valued independent variable (ω), the frequency response function, real-imaginary, magnitude-phase, and log magnitude-phase graphs as shown in Figure 2-4 through Figure 2-9.

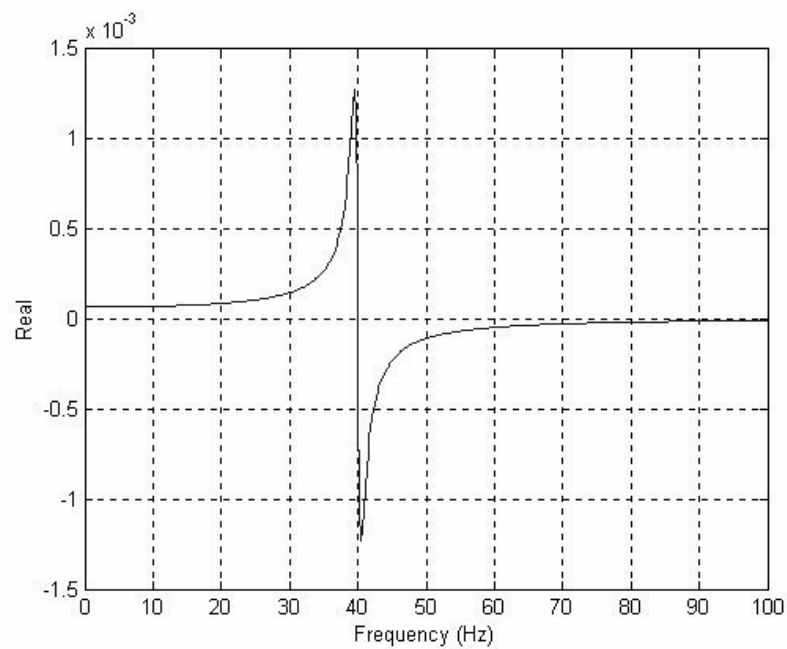


Figure 2-4 Frequency Response Function (Real part vs. frequency)

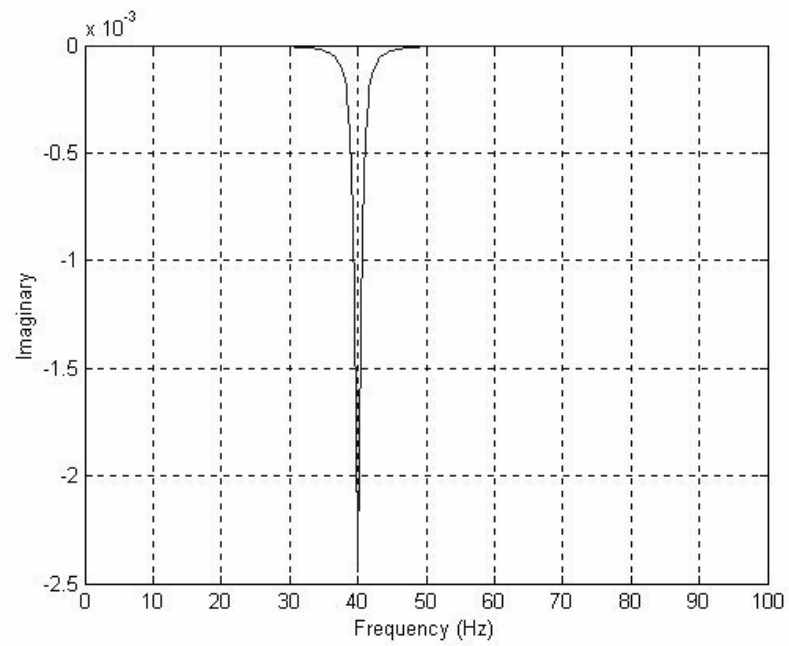


Figure 2-5 Frequency Response Function (Imaginary part vs. frequency)

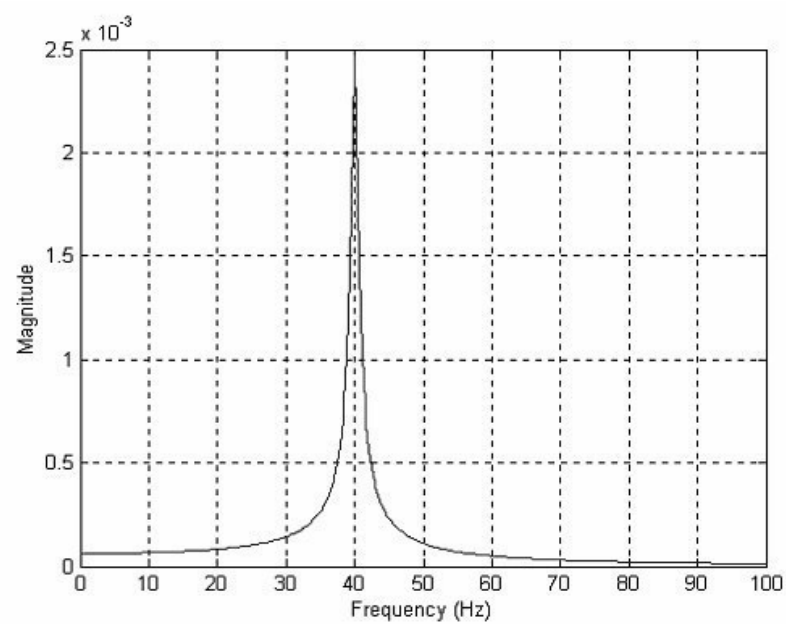


Figure 2-6 Frequency Response Function (Magnitude vs. frequency)

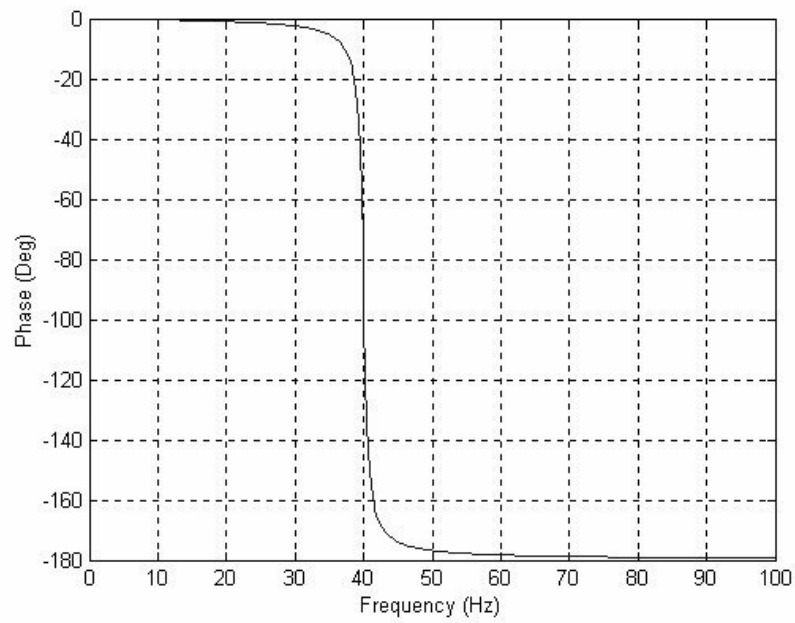


Figure 2-7 Frequency Response Function (Phase vs. frequency)

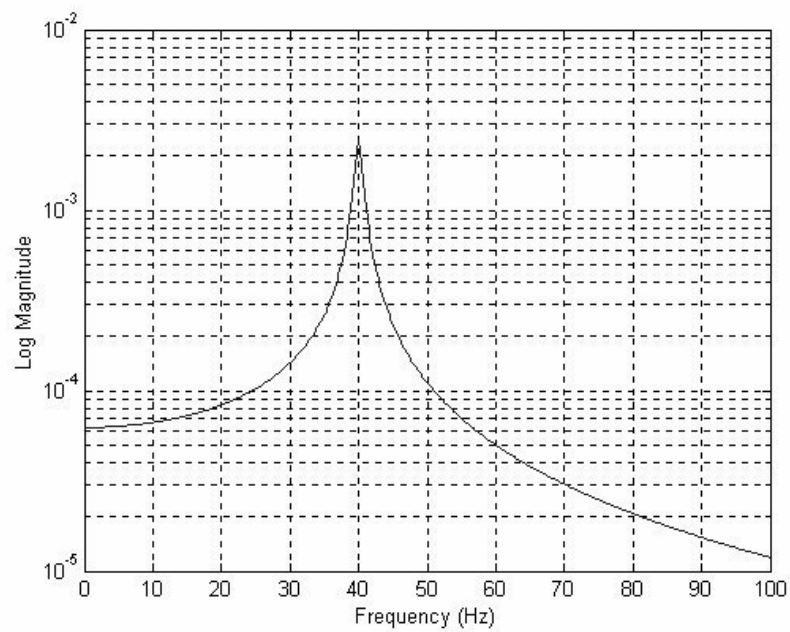


Figure 2-8 Frequency Response Function (Log Magnitude vs. frequency)

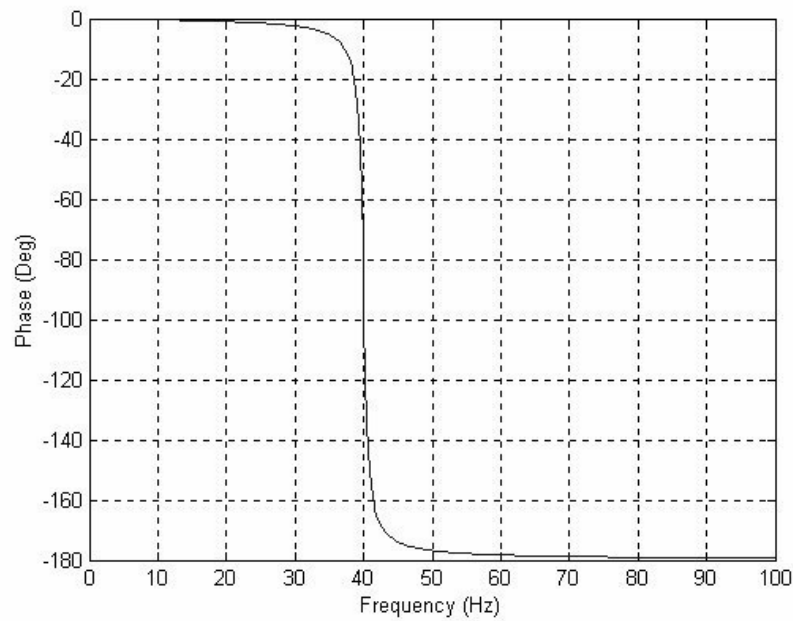


Figure 2-9 Frequency Response Function (Phase vs. frequency)

2.2.3 Laplace Domain: Transfer Function

Just as in Section 2.2.1.2 for the frequency domain, the equivalent information can be represented in the Laplace domain by way of the Laplace transform. The only significant difference between the two domains is that the Fourier transform is defined from negative infinity to positive infinity while the Laplace transform is defined from zero to positive infinity with initial conditions. The Laplace representation, also, has the advantage of converting a differential equation to an algebraic equation. Theory behind Laplace transform is shown in almost every classical text concerning vibrations (Meirovitch, 1996). The development using Laplace transforms begins by taking the Laplace transform of Equation 2-1. Thus, Equation 2-1 becomes:

$$\left[M s^2 + C s + K \right] X(s) = F(s) + \left[M s + C \right] X(0) + M \dot{X}(0) \quad \text{Equation 2-27}$$

$X(0)$ and $\dot{X}(0)$ are the initial displacements and velocities at time $t = 0$, respectively

If the initial conditions are taken as zero, Equation 2-27 becomes:

$$\left[M s^2 + C s + K \right] X(s) = F(s) \quad \text{Equation 2-28}$$

Then Equation 2-28 becomes:

$$B(s) X(s) = F(s) \quad \text{Equation 2-29}$$

Where:

- $B(s) = M s^2 + C s + K$

Therefore, using the same logic as in the frequency domain case, the transfer function can be defined in the same way that the frequency response function was defined previously.

$$X(s) = H(s) F(s) \quad \text{Equation 2-30}$$

Where:

- $H(s) = \frac{1}{M s^2 + C s + K}$

The quantity $H(s)$ is defined as the “transfer function” of the system. In other words, a transfer function relates the Laplace transform of the system input to the Laplace

transform of the system response. From Equation 2-30, the transfer function can be defined as:

$$H(s) = \frac{X(s)}{F(s)} \quad \text{Equation 2-31}$$

Going back to Equation (2.22), the transfer function can be written:

$$H(s) = \frac{1}{M s^2 + C s + K} = \frac{1/M}{s^2 + \left(\frac{C}{M}\right)s + \left(\frac{K}{M}\right)} \quad \text{Equation 2-32}$$

Note that Equation 2-32 is valid under the assumption that the initial conditions are zero.

The denominator term is once again referred to as the characteristic equation of the system. As noted in the previous two cases, the roots of the characteristic equation are given in Equation 2-5. The transfer function, $H(s)$, can now be rewritten, just as in the frequency response function case, as:

$$H(s) = \frac{1/M}{(s - \lambda_1)(s - \lambda_1^*)} = \frac{A}{(s - \lambda_1)} + \frac{A^*}{(s - \lambda_1^*)} \quad \text{Equation 2-33}$$

Since the transfer function is a complex valued function of a complex independent variable (s), the transfer function is represented, as shown in Figures 2-7 through 2-9, as a pair of surfaces. Remember that the variable s in Equation (2.27) is a complex variable, that is, it has a real part and an imaginary part. Therefore, it can be viewed as a function of two variables which represent a surface.

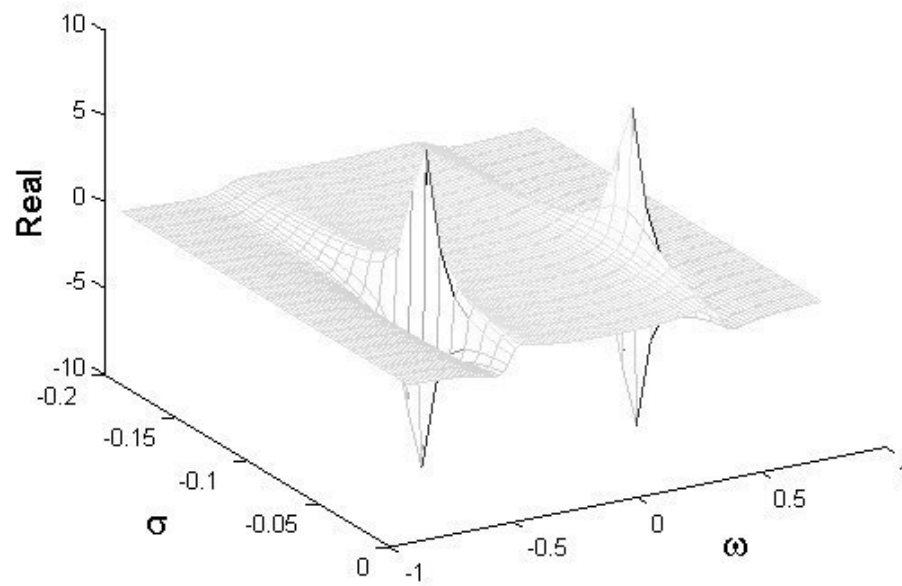


Figure 2-10 Transfer Function (Real Format)

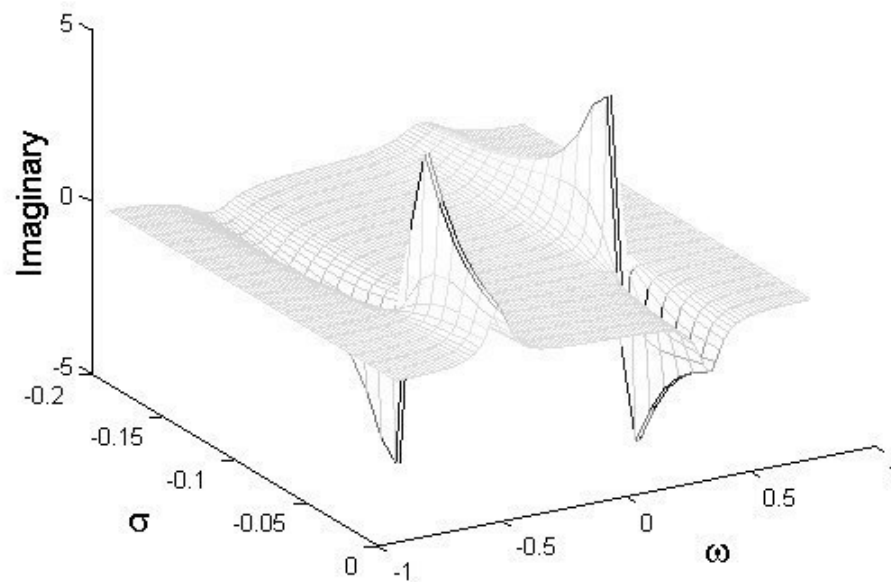


Figure 2-11 Transfer Function (Imaginary Format)

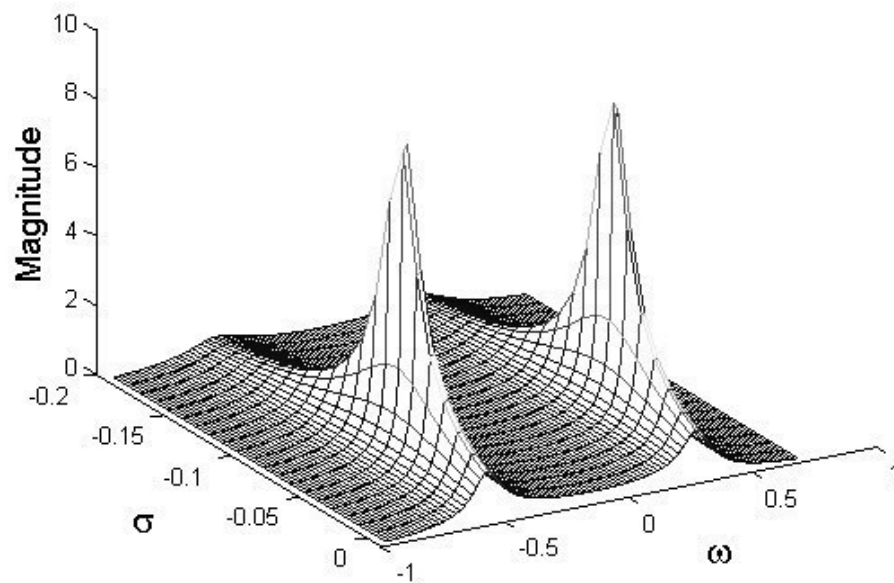


Figure 2-12 Transfer Function (Magnitude Format)

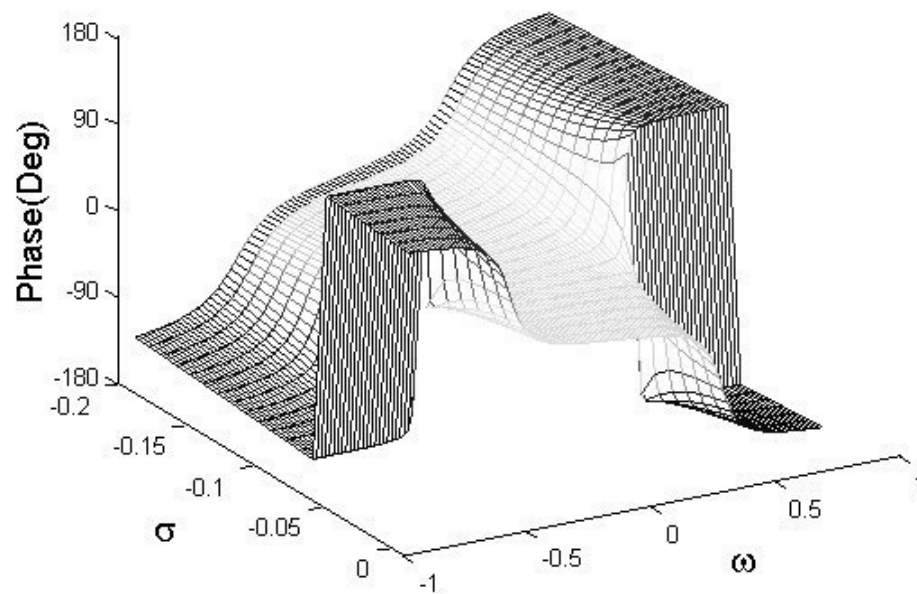


Figure 2-13 Transfer Function (Phase Format)

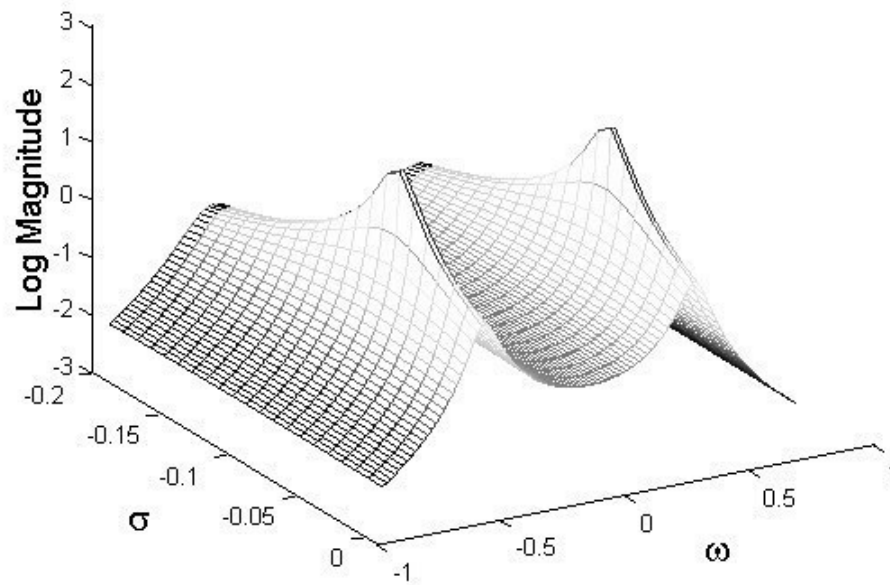


Figure 2-14 Transfer Function (Log Magnitude Format)

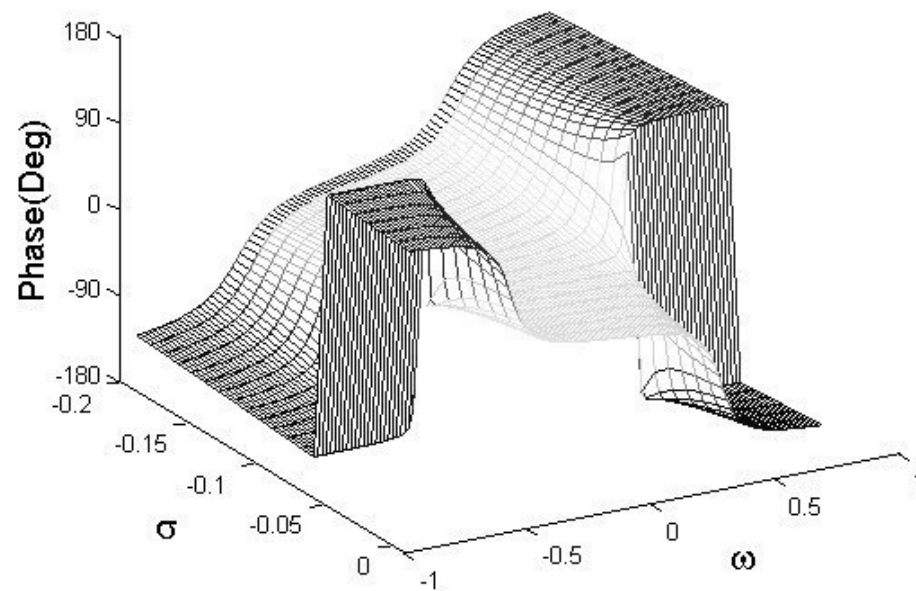


Figure 2-15 Transfer Function (Phase Format)

The definition of undamped natural frequency, damped natural frequency, damping factor, percent of critical damping, and residue are all relative to the information represented by Figure 2-11 through Figure 2-15. The projection of this information onto the plane of zero amplitude yields the information as shown in Figure 2-16.

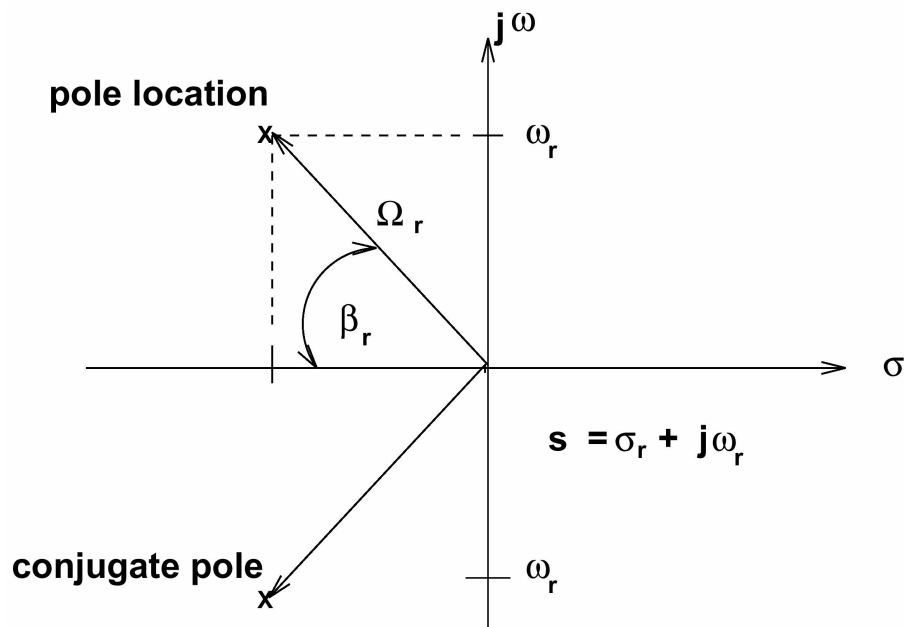


Figure 2-16 Transfer Function - Laplace Plane Projection

Where;

σ_r = Damping coefficient

ω_r = Damped natural frequency

Ω_r = Undamped natural frequency

$\zeta_r = \cos \beta_r$ = Damping factor (percent of critical damping)

The concept of residues is now defined in terms of the partial fraction expansion of the transfer function equation. Equation 2-33 can be expressed in terms of partial fractions as follows:

$$H(s) = \frac{1/M}{(s - \lambda_1)(s - \lambda_1^*)} = \frac{A}{(s - \lambda_1)} + \frac{A^*}{(s - \lambda_1^*)} \quad \text{Equation 2-34}$$

The residues of the transfer function are defined as being the constants A and A^* . The terminology and development of residues comes from the evaluation of analytic functions in complex analysis. The residues of the transfer function are directly related to the amplitude of the impulse response function. In general, the residue A can be a complex quantity.

It can be noted that the Laplace transform formulation is simply the general case of the Fourier transform development if the initial conditions are zero. The Frequency Response Function is the part of the transfer function evaluated along the $s = j\omega$ axis.

From an experimental point of view, the transfer function is not estimated from measured input-output data (modal testing). Instead, the Frequency Response Function is actually estimated via the discrete Fourier transform.

2.3 Multiple Degree of Freedom Systems

The real applications of modal analysis concepts begin when a continuous, non-homogeneous structure is described as a lumped mass, multiple degree-of-freedom systems. At this point, the modal frequencies, the modal damping, and the modal vectors, or relative patterns of motion, can be found via an estimate of the mass, damping, and stiffness matrices or via the measurement of the associated frequency response functions. The two-degree of freedom system, shown in Figure 2-11, is the most basic example of a multiple degree of freedom system. This example is useful for discussing modal analysis concepts since a theoretical solution can be formulated in terms of the mass, stiffness and damping matrices or in terms of the frequency response functions.

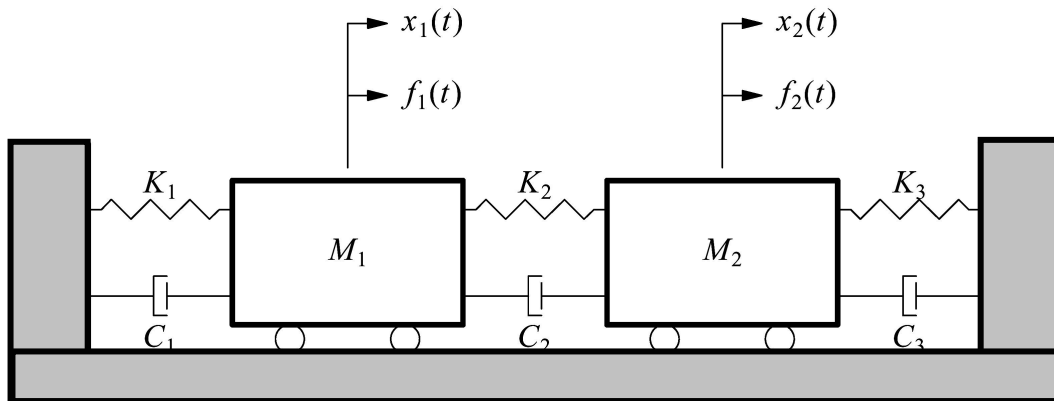


Figure 2-17 Multi-Degree of Freedom System

The equations of motion for the system in Figure 2-17, using matrix notation, are as follows:

$$\begin{bmatrix} M_1 & 0 \\ 0 & M_2 \end{bmatrix} \begin{bmatrix} \ddot{x}_1 \\ \ddot{x}_2 \end{bmatrix} + \begin{bmatrix} (C_1 + C_2) & -C_2 \\ -C_2 & (C_2 + C_3) \end{bmatrix} \begin{bmatrix} \dot{x}_1 \\ \dot{x}_2 \end{bmatrix} + \begin{bmatrix} (K_1 + K_2) & -K_2 \\ -K_2 & (K_2 + K_3) \end{bmatrix} \begin{bmatrix} x_1 \\ x_2 \end{bmatrix} = \begin{bmatrix} f_1 \\ f_2 \end{bmatrix}$$

Equation 2-35

The process of solving Equation 2-35 when the mass, damping, and stiffness matrices are known is shown in almost every classical text concerning vibrations and (examples are Cook, 1989, Meirovitch 1996, and Chandrupalta, 1997)

The development of the frequency response function solution for the multiple degree of freedom case is similar to the single degree-of-freedom case, which relates the mass, damping, and stiffness matrices to a transfer function model involving multiple degrees of freedom. Just as in the analytical case, where the ultimate solution can be described in terms of one degree of freedom systems, the frequency response functions between any input and response degree of freedom can be represented as a linear superposition of the single degree of freedom models derived previously.

As a result of the linear superposition concept, the equations for the impulse response function, the frequency response function, and the transfer function for the multiple degree of freedom system are defined as follows:

Impulse Response Function (Time domain):

$$[h(t)] = \sum_{r=1}^N [A_r] e^{\lambda_r t} + [A_r^*] e^{\lambda_r^* t} = \sum_{r=1}^{2N} [A_r] e^{\lambda_r t} \quad \text{Equation 2-36}$$

Frequency Response Function (Frequency Domain):

$$[H(\omega)] = \sum_{r=1}^N \frac{[A_r]}{j\omega - \lambda_r} + \frac{[A_r^*]}{j\omega - \lambda_r} = \sum_{r=1}^{2N} \frac{[A_r]}{j\omega - \lambda_r} \quad \text{Equation 2-37}$$

Transfer Function (Laplace Domain):

$$[H(s)] = \sum_{r=1}^N \frac{[A_r]}{s - \lambda_r} + \frac{[A_r^*]}{s - \lambda_r} = \sum_{r=1}^{2N} \frac{[A_r]}{s - \lambda_r} \quad \text{Equation 2-38}$$

Where:

t = Time variable

ω = Frequency variable

s = Laplace variable

p = Measured degree of freedom (output)

q = Measured degree of freedom (input)

r = Modal vector number

A_{pqr} = Residue

$A_{pqr} = Q_r \psi_{pr} \psi_{qr}$

Q_r = Modal scaling factor

ψ_{pr} = Modal coefficient

λ_r = System pole

N = Number of positive modal frequencies

It is important to note that the residue, A_{pqr} , in Equation 2-36 through Equation 2-38 is the product of the modal deformations at the input q and response p degrees of freedom and a modal scaling factor for mode r. Therefore, the product of these three terms is unique but each of the three terms by themselves is not unique. This is consistent with the arbitrary normalization of the modal vectors. Modal scaling, Q_r , refers to the relationship between the normalized modal vectors and the absolute scaling of the mass matrix (analytical case) and/or the absolute scaling of the residue information (experimental case). Modal scaling is normally presented as modal mass or modal A.

The driving point residue, A_{qqr} , is particularly important in deriving the modal scaling.

$$A_{qqr} = Q_r \psi_{qr} \psi_{qr} = Q_r \psi_{qr}^2 \quad \text{Equation 2-39}$$

For undamped and proportionally damped systems, the r-th modal mass of a multi degree of freedom system can be defined as:

$$M_r = \frac{1}{j^2 Q_r \omega_r} = \frac{\psi_{pr} \psi_{qr}}{j^2 A_{pqr} \omega_r} \quad \text{Equation 2-40}$$

Where:

M_r = Modal mass

Q_r = Modal scaling constant

ω_r = Damped natural frequency

If the largest scaled modal coefficient is equal to unity, Equation 2-40 will also compute a quantity of modal mass that has physical significance. The physical significance is that the quantity of modal mass computed under these conditions will be a number between zero and the total mass of the system. Therefore, under this scaling condition, the modal mass can be viewed as the amount of mass that is participating in each mode of vibration. Obviously, for a translational rigid body mode of vibration, the modal mass should be equal to the total mass of the system.

The **modal mass** defined in Equation 2-40 is developed in terms of displacement over force units. If measurements, and therefore residues, are developed in terms of any other units (velocity over force or acceleration over force), Equation 2-40 will have to be altered accordingly.

Once the modal mass is known, the *modal damping* and *modal stiffness* can be obtained through the following single degree of freedom equations:

Modal Damping

$$C_r = 2 \sigma_r M_r \quad \text{Equation 2-41}$$

Modal Stiffness

$$K_r = (\sigma_r^2 + \omega_r^2) M_r = \Omega_r^2 M_r \quad \text{Equation 2-42}$$

There are several references in the literature in which modal mass, stiffness, and damping matrices are calculated from estimated modal parameters (Potter, 1982, Shye, 1986, Richardson, 2000)

For systems with non-proportional damping, **modal mass** cannot be used for modal scaling. For non-proportional case, and increasingly for undamped and proportionally damped cases as well, the **modal A** scaling factor is used as the basis for the relationship between the scaled modal vectors and the residues determined from the measured frequency response functions. This relationship is as follows:

Modal A

$$M_{A_r} = \frac{\psi_{pr} \psi_{qr}}{A_{pqr}} = \frac{1}{Q_r} \quad \text{Equation 2-43}$$

This definition of **modal A** is also developed in terms of displacement over force units. Once **modal A** is known, **modal B** can be obtained through the following single degree of freedom equation:

Modal B

$$M_{B_r} = -\lambda_r M_{A_R} \quad \text{Equation 2-44}$$

For undamped and proportionally damped systems, the relationship between **modal mass** and **modal A** scaling factors can be stated.

$$M_{A_r} = \pm 2M_r \omega_r \quad \text{Equation 2-45}$$

In general, modal vectors are considered to be dimensionless since they represent relative patterns of motion. Therefore, the modal mass or modal A scaling terms carry the units of the respective measurement. For example, the development of the frequency response is based upon displacement over force units. The residue must therefore, have units of length over force-seconds. Since the modal A scaling coefficient is inversely related to the residue, modal A will have units of force-seconds over length. This unit combination is the same as mass over seconds. Likewise, since modal mass is related to modal A, for proportionally damped systems, through a direct relationship involving the damped natural frequency, the units on modal mass are mass units as expected.

2.4 Damping Mechanisms

In order to evaluate multiple degree of freedom systems that are present in the real world, the effect of damping on the complex frequencies and modal vectors must be considered. Many physical mechanisms are needed to describe all of the possible forms of damping that may be present in a particular structure or system. Some of the classical types are: 1) Structural Damping; 2) Viscous Damping; and 3) Coulomb Damping. It is generally difficult to ascertain which type of damping is present in any particular structure. Indeed most structures exhibit damping characteristics that result from a combination of all the above. Rather than consider the many different physical mechanisms, the probable location of each mechanism, and the particular mathematical representation of the mechanism of damping that is needed to describe the dissipative energy of the system, a model will be used that is only concerned with the resultant mathematical form. This model will represent a

hypothetical form of damping, which is proportional to the system mass or stiffness matrix. Therefore:

$$[C] = \alpha [M] + \beta [K] \quad \text{Equation 2-46}$$

Under this assumption, ***proportional damping*** is the case where the equivalent damping matrix is equal to a linear combination of the mass and stiffness matrices. For this mathematical form of damping, the coordinate transformation that diagonalizes the system mass and stiffness matrices also diagonalizes the system damping matrix. ***Non-proportional damping*** is the case where this linear combination does not exist. Therefore when a system with proportional damping exists, that system of coupled equations of motion can be transformed to a system of equations that represent an uncoupled system of single degree-of-freedom systems that are easily solved. With respect to modal parameters, a system with proportional damping has real-valued modal vectors (***real or normal modes***) while a system with non-proportional damping has complex-valued modal vectors (***complex modes***).

CHAPTER 3

MODAL DATA ACQUISITION & EXPERIMENTAL MODAL ANALYSIS METHODS

3.1 Introduction

Modal data acquisition and related experimental modal analysis methods will be explained in this chapter. Modal data acquisition can be seen as the first step of experimental modal analysis. Acquisition of data, which will be used in the formulation of a modal model, involves many important concerns.

These concerns include successful acquisition of data, prevention of various reading and signal related errors, post processing of measured data, sampling theorems, modal analysis and domain transformations will also be discussed in this Chapter.

A series of articles of Pete Aitavale are printed in annual journal of Society of Experimental Techniques starting from March 1998 till March 2003. These references are useful for understanding experimental modal analysis and modal data acquisition.

3.2 Modal Data Acquisition

In order to determine modal parameters, the measured input (excitation) and response data must be processed and put into a form that is compatible with the test and modal parameter estimation methods. Digital signal processing of the data is a very important step in Modal data acquisition. Signal processing is one of the technology areas where clear understandings of the Time-Frequency-Laplace domain (Avaible, 1998) relationships are important. The conversion of the data from the time domain into the frequency and Laplace domain is important both in the “measurement” and (subsequently) in the “modal parameter estimation” processes. The process of representing an analog signal as a series of digital values is a basic requirement of modern digital signal processing analyzers. In practice, the goal of the analog to digital conversion (ADC) process is to obtain the conversion while maintaining sufficient accuracy in terms of frequency, magnitude, and phase. When dealing strictly with analog devices, this concern was satisfied by the performance characteristics of each individual analog device. With the improvements in digital signal processing, the performance characteristics of the analog device are only the first criteria of consideration. The characteristics of the analog to digital conversion has become the primary concern. This process of analog to digital conversion involves two separate concepts, each of which are related to the dynamic performance of a digital signal processing analyzer. ***Sampling*** is the part of the process related to the timing between individual digital pieces of the time history. ***Quantization*** is the part of the process related to describing analog amplitude as a digital value. Primarily, sampling considerations

alone affect the frequency accuracy while both sampling and quantization considerations affect magnitude and phase accuracy.

3.2.1 Sampling

Sampling is the process of recording the independent variables of an analog process. Sampling can be done in an absolute sense where the independent variable is in terms of time. The process of sampling arises from the need to describe analog time histories in a digital fashion. Sampling can be done, in general, by recording digitized amplitude and a reference time of measurement; or in the more common method of recording amplitudes at uniform increments of time (Δt). Since all analog to digital converters sample at constant sampling increments during each sample period, all further discussions will be restricted to this case.

Sampling Theory:

Two theories or principles apply to the process of digitizing analog signals and recovering valid frequency information. *Shannon's Sampling Theorem* states, the following in a very simple form:

$$F_{\text{sam}} \geq F_{\text{Nyq}} \times 2$$

Equation 3-1

$$F_{\text{Nyq}} \geq F_{\text{Max}}$$

Equation 3-2

Shannon' Sampling theorem describes the maximum frequency in an accurate way. The *Nyquist frequency* (F_{Nyq}) is the theoretical limit for the maximum frequency

and is defined as one half of the sampling frequency, which means that there will be at least two samples per period for any frequency below the Nyquist frequency.

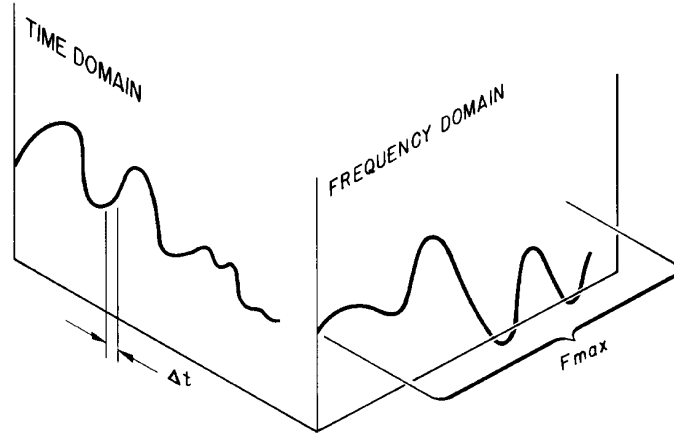


Figure 3-1 Shannon Sampling Theorem (Ewins, 1995)

In order to be certain that Equation 3-1, and measurement requirements **Hata! Başvuru kaynağı bulunamadı.** are always met, an analog, low pass filter (LPF) with a cutoff frequency below the Nyquist frequency must always be used when acquiring data. Generally, LPF is built into the digital signal analyzer. Due to practical limitations of the analog filters used prior to any digitization, the sampling frequency is normally chosen to be greater than two times the maximum frequency of interest. In this case, Equation 3-1 still applies as stated by the inequality. When a factor greater than two is used the resulting maximum frequency (F_{\max}) is less than the Nyquist frequency. F_{\max} being less than the Nyquist frequency may lead to some confusion when the data is recorded and/or displayed. Figure 3-2 shows the

common frequency relationship between the maximum frequency, the analog low pass filter cutoff frequency and Nyquist frequency.

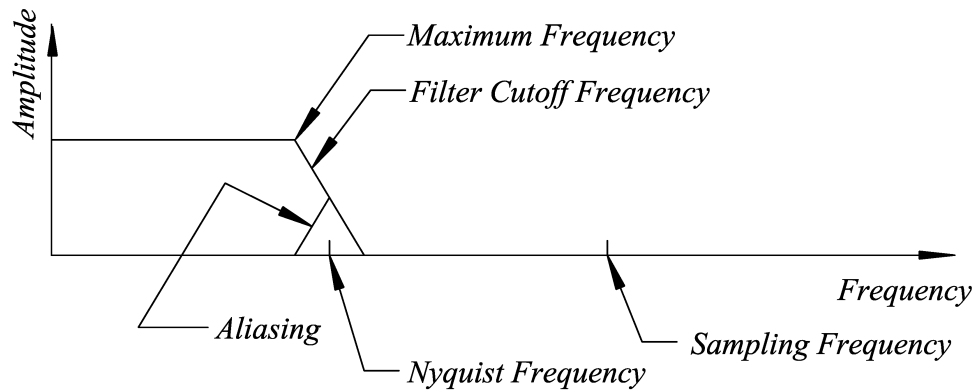


Figure 3-2 Basic Sampling Relationships

Rayleigh's criterion was first formulated in the field of optics and has to do with being able to resolve two closely related spaced frequency components. For a time record of T seconds, the lowest frequency component measurable is:

$$\Delta f = \frac{1}{T} \quad \text{Equation 3-3}$$

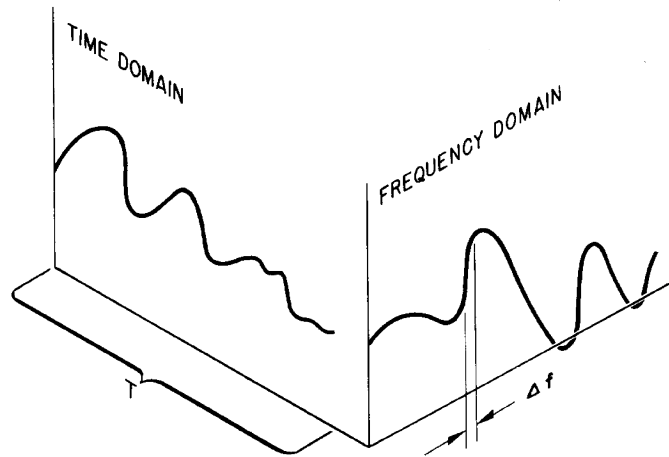


Figure 3-3 Rayleigh's Criterion

With Shannon's Sampling Theorem and Rayleigh's criterion in mind, the selection of sampling parameters are summarized as shown in Table 3-1 (Allemang, 1998).

Note that for this case, the equality Equation 3-1 has been used ($F_{max} = F_{Nyq}$).

Table 3-1 Digitization Equations ($F_{max} = F_{Nyq}$)

Sampling Relations		
Sampling Parameter	Automatically determines	BlockSize Determines
Δt	$F_{max} = \frac{1}{2\Delta t}$	$T = N \Delta t$ $\Delta f = \frac{1}{N \Delta t}$
F_{max}	$\Delta t = \frac{1}{2F_{max}}$	$T = N \Delta t$ $\Delta f = \frac{1}{N \Delta t}$
Δf	$T = \frac{1}{\Delta f}$	$\Delta t = \frac{T}{N}$ $F_{max} = \frac{N}{2} \Delta f$
T	$\Delta f = \frac{1}{\Delta t}$	$\Delta t = \frac{T}{N}$ $F_{max} = \frac{N}{2} \Delta f$

3.2.2 Quantization

Quantization is the conversion of a specific analog value of amplitude to the nearest discrete value available in the (analog to digital) converter. The process of conversion involves representing a range of voltage by a fixed number of integer steps. Normally, the range of voltage is chosen to be between positive and negative

limits for a given voltage limit. The number of discrete levels is a function of the number of bits in the analog to digital conversion.

3.2.3 ADC Errors

Most modern data acquisition systems minimize errors associated with the analog to digital conversion of data to the extent that the average user does not need to be concerned with the ADC errors. The primary ADC errors are **aliasing** and **quantization** errors.

3.2.3.1 Aliasing

If frequency components are larger than one half the sampling frequency present in the analog time history, amplitude and frequency errors will occur. These errors are a result of the inability of the Fourier transform to decide which frequencies are within the analysis band and which frequencies are outside the analysis band. This problem is explained graphically in Figure 3-4 from a time domain point of view.

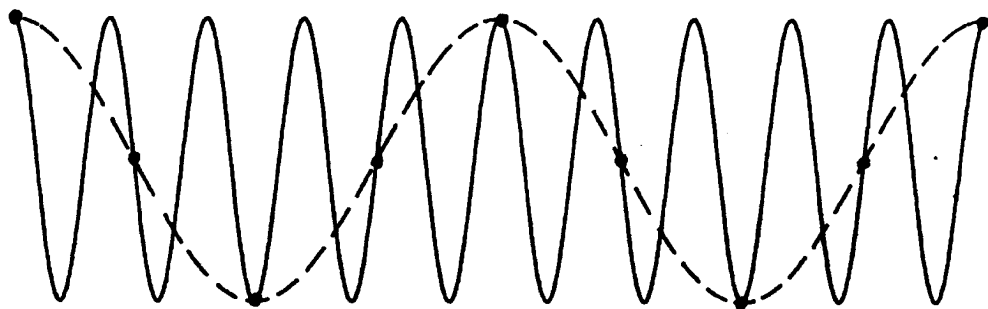


Figure 3-4 Aliasing Example

3.2.3.2 Quantization Error

Quantization Error is the difference between the actual analog signal and the measured digitized value. Since this error is a random event, averaging will minimize the effect on the resulting measurements. Note that, when measuring transient events that cannot be averaged, this error limits the achievable magnitude accuracy.

3.2.4 Discrete Fourier Transform

The Fourier series concept explains that a signal can be uniquely separated into a summation of sine and cosine terms at appropriate frequencies. This will generate a unique set of sine and cosine terms due to the orthogonal nature of sine functions at different frequencies, the orthogonal nature of cosine functions at different frequencies and the orthogonal nature of sine functions compared to cosine functions. If the choice of frequencies is limited to a discrete set of frequencies, the discrete Fourier transform will describe the amount of each sine and cosine term at each discrete frequency. The real part of the discrete Fourier transform describes the amount of each cosine term; the imaginary part of the discrete Fourier transform describes the amount of each sine term. Figure 3-5 (Allemang, 1998) is a graphical representation of this concept for a signal that can be represented by a summation of sinusoids.

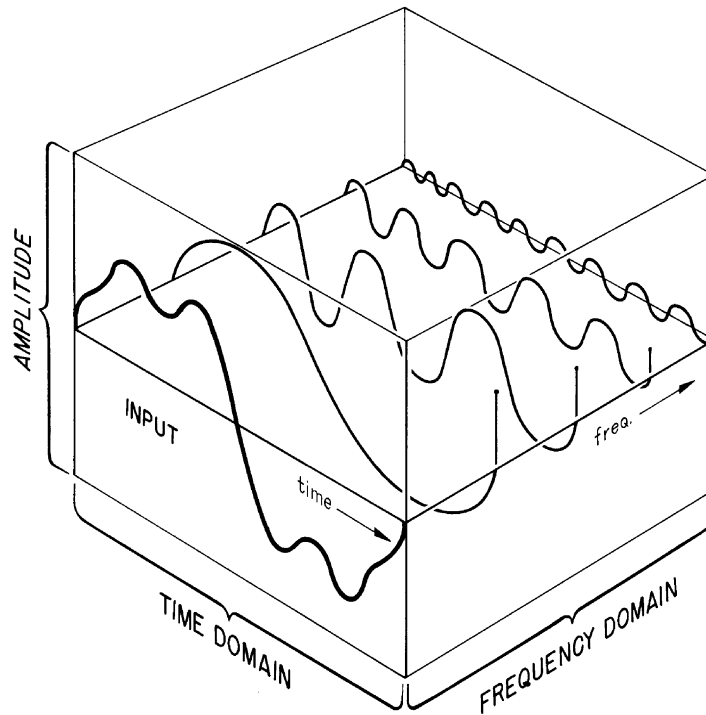


Figure 3-5 Discrete Fourier Transform Concept

The discrete Fourier transform algorithm is the basis for the formulation of any frequency domain function in modern data acquisition systems. In terms of an integral Fourier transform, the function must exist for all time in a continuous sense in order to be evaluated. For the realistic measurement situation, data is available in a discrete sense over a limited time period. The discrete Fourier transform, therefore, is based upon a set of assumptions concerning this discrete sequence of values. The assumptions can be reduced to two situations that must be met by every signal processed by the discrete Fourier transform algorithm. The first assumption is that the signal must be a ***totally observed transient*** with respect to the time period of observation. If this is not true, then the signal must be composed only of

harmonics of the time period of observation. If one of these two assumptions is not met by any discrete history processed by the discrete Fourier transform algorithm, then the resulting spectrum will contain bias errors accordingly. Much of the data processing that is considered with respect to acquisition of data and the formulation of a modal model revolves around an attempt to assure that the input and response histories match one of these two assumptions. For a more complete understanding of the discrete Fourier transform algorithm and the associated problems refer to Richardson, (1978), Chopra, (1995), and Meirovitch, (1996).

3.2.4.1 Discrete Fourier Transform Errors

The primary digital signal processing error involved with making measurements is an error associated with the discrete Fourier transform which is used to transform the digital time data to digital frequency data. This error is a bias error that is known as leakage or truncation error. Actually, it is not really an error but is a limitation of discrete Fourier transform. The discrete Fourier transform is expected to give the same answer as the integral Fourier transform, which is true when only certain conditions are met concerning the time domain data.

3.2.4.1.1 Leakage Error

Leakage error is basically due to a violation of an assumption of the Discrete Fourier transform algorithm. This assumption is that the true signal is periodic within the sample period used to observe the sample function. In the cases where both input and output are totally observable (transient input with completely observed decay output within the sample period) or are harmonic functions of the

time period of observation (T), there will be no contribution to the bias error. But if these assumptions are violated, due to the truncation that occurs in the time domain (T) there will be error which is referred as leakage.

Leakage is probably the most common and, therefore, the most serious digital signal processing error. Unlike aliasing and many other errors, the effects of leakage can only be reduced, not completely eliminated.

Discrete Fourier transform algorithm assumes that the data to be transformed is periodic with respect to the frequency resolution of the sampling period. Since, in general, the real world does not operate on the basis of multiples of some arbitrary frequency resolution; this introduces an error known as leakage.

The concept of multiplication and convolution represents a transform pair with respect to Fourier and Laplace transforms. More specifically, if two functions are multiplied in one domain, the result is the convolution of the two transformed functions in the other domain. Conversely, if two functions are convolved in one domain, the result is the multiplication of the two transformed functions in the other domain. When a signal is observed in the time domain with respect to a limited observation period, T , the signal that is observed can be viewed as the multiplication of two infinite time functions as shown in Figure 3-6 and Figure 3-7. The resulting time domain function is, in the limit, the signal that is processed by the Fourier transform which is shown in Figure 3-8. Therefore, by this act of multiplication, the corresponding frequency domain functions of Figure 3-6 and

Figure 3-7 will be convolved to give the result equivalent to the Fourier transform of Figure 3-6. In this way, the difference between the infinite and the truncated signal can be evaluated theoretically.

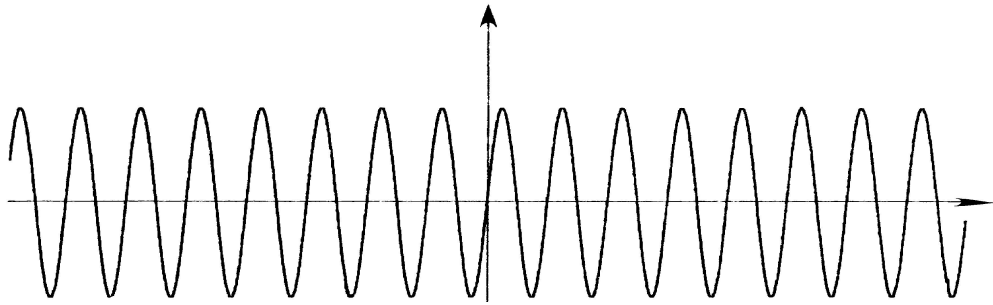


Figure 3-6 Time Domain Function: Theoretical Harmonic

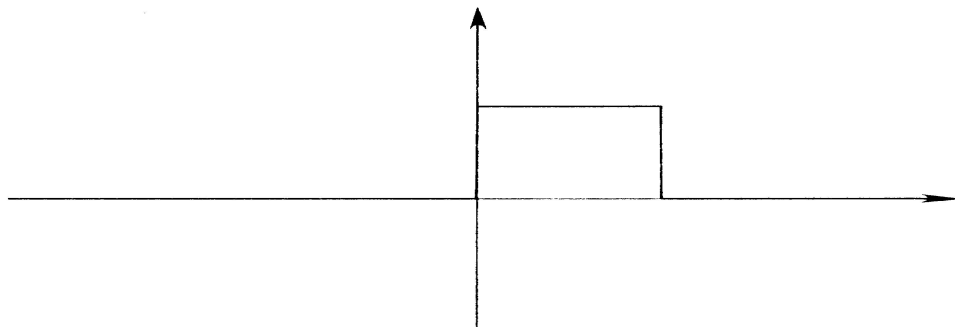


Figure 3-7 Time Domain Function: Theoretical Window

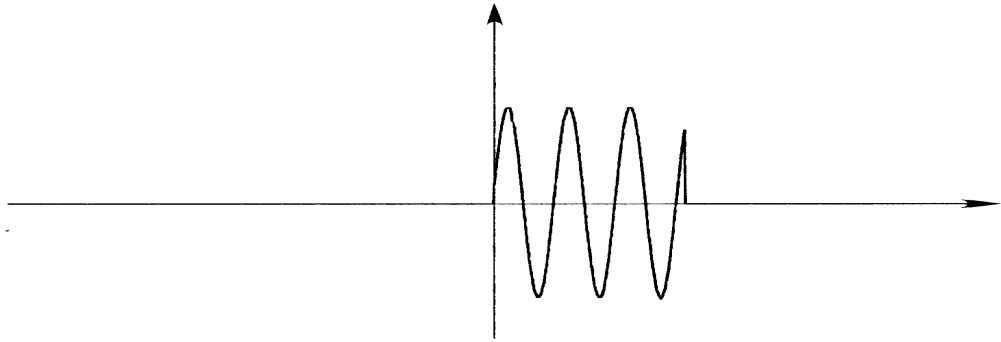


Figure 3-8 Time Domain Function: Multiplication of Signals

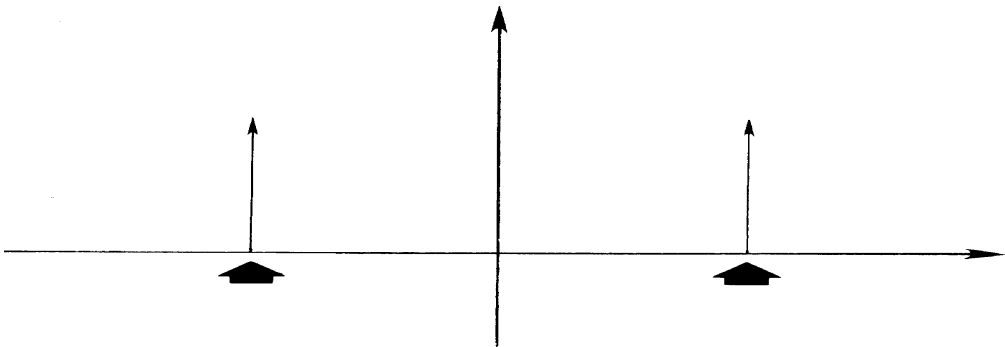


Figure 3-9 Frequency Domain: Theoretical Harmonic

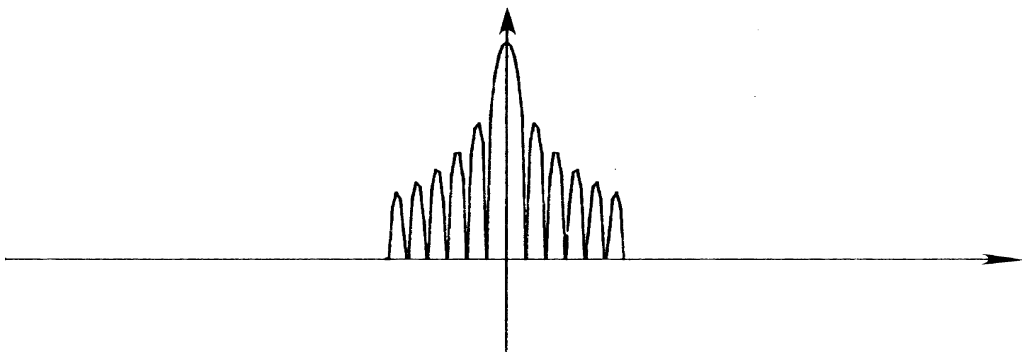


Figure 3-10 Frequency Domain: Theoretical Window

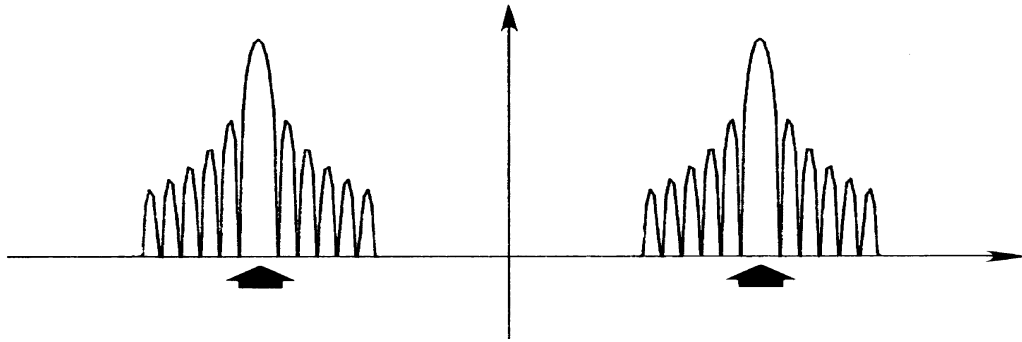


Figure 3-11 Frequency Domain: Convolved Signals

Therefore, when an analog signal is digitized in a Fourier analyzer, the analog signal has been multiplied by a function of unity (for a period of time T) in the time domain. This results in a convolution of the two signals in the frequency domain. Figure 3-9 and Figure 3-10 are the Fourier transform of Figure 3-6 and Figure 3-7 respectively. Where Figure 3-11 is the convolution of Figure 3-9 and Figure 3-10. This process of multiplying an analog signal by some sort of weighting function is referred to as "windowing". Whenever a time function is sampled, the transform relationship between multiplication and convolution must be considered. Likewise, whenever an additional weighting function such as a Hanning window is utilized, the effects of such a window can be evaluated in the same fashion. The concept of "windowing" is well explained in Aitavale, (1999), Ewins, (1995).

3.2.5 Transducer Considerations

The transducer considerations are often the most overlooked aspect of the experimental modal analysis process. Considerations involving the actual type and specifications of the transducers, mounting of the transducers, and calibration of the

transducers are often be some of the largest sources of error. Transducer specifications are concerned with the magnitude and frequency limitations that the transducer is designed to meet. Transducer specifications involves the measured calibration at the time that the transducer was manufactured, the frequency range over which this calibration is valid, and the magnitude and phase distortion of the transducer, compared to the calibration constant over the range of interest. The specifications of any transducer signal conditioning must be evaluated. Transducer mounting involves evaluation of the mounting system to make sure whether the mounting system has compromised any of the transducers specifications. The evaluation normally involves the possibility of relative motion between the structure under test and the transducer. Very often, the mounting systems, which are convenient to use and allow ease of alignment with orthogonal reference axes, are subject to mounting resonances which result in substantial relative motion between the transducer and the structure under test in the frequency range of interest.

Therefore, the mounting system that should be used depends heavily on the frequency range of interest and the test conditions. Test conditions include factors such as temperature, roving or fixed transducers, and surface irregularity. A brief review of many common transducer mounting methods is given in Table 3-2 (Allemang, 1998).

Table 3-2 Transducer Mounting Methods

Transducer Mounting Methods			
Method	Frequency Range (Hz)	Main Advantages	Main Disadvantages
Hand-held	20-1000	Quick look	Poor measurement quality for long sample periods
Putty	0-200	Good axis alignment, ease of mounting	Low frequency range, creep problems during measurement
Wax	0-2000	Ease of application	Temperature limitations, frequency range limited by wax thickness, axis alignment limitations
Hot glue	0-2000	Quick setting time, good axis alignment	Temperature sensitive transducers (during cure)
Magnet	0-2000	Quick setup	Requires magnetic material, axis alignment limitations, bounce problem with impact excitation, surface preparation
Adhesive film	0-2000	Quick setup	Axis alignment limitations, requires flat surface
Epoxy cement	0-5000	Mount on irregular surface, good axis alignment	Long curing time
Dental cement	0-5000	Mount on irregular surface, good axis alignment	Medium curing time, brittle
Stud mount	0-1000	Accurate alignment if carefully machined	Difficult setup, requires drill and tap

3.3 Experimental Modal Analysis Methods

Categorizing different methods of Experimental Modal Analysis is helpful when reviewing the literature in the area of Experimental Modal Analysis,

These methods are grouped according to:

1. Type of measured data that is acquired
 - a. Sinusoidal Input-Output Model
 - b. Frequency Response Function Model
 - c. Damped Complex Exponential Response Model
 - d. General Input-Output Model
2. Type of model used in modal parameter estimation stage
 - a. Parametric Model
 - i. Modal Model
 - ii. $[M]$, $[K]$, $[C]$ Model
 - b. Non-Parametric Model
3. According to the domain of the modal parameter estimation model
 - a. Time Domain
 - b. Frequency Domain
 - c. Spatial Domain

In this Section, Experimental Modal Analysis method of **Frequency Response Function** is explained in detail only. Frequency Response Function is a commonly used method in Experimental Modal Analysis. (Richardson, 1986, Shye *et al.*, 1987,

Richardson, 2000). In the following sections Frequency Response Function Model and Frequency Response Function Method are explained.

3.3.1 Frequency Response Function Model

The frequency response function method of experimental modal analysis is the most commonly used approach to the estimation of modal parameters. This method originated as a testing technique as a result of the use of frequency response functions to determine natural frequencies for effective number of degrees of freedom. In this method, frequency response functions are measured using excitation at single or multiple points. The relationships between the input $F(\omega)$ and the response $X(\omega)$ for both single and multiple inputs are shown in Equation 3-4 through Equation 3-6.

Single Input Relationship:

$$X_p = H_{pq} F_q \quad \text{Equation 3-4}$$

$$\begin{Bmatrix} X_1 \\ X_2 \\ \cdot \\ \cdot \\ X_p \end{Bmatrix} = \begin{Bmatrix} H_{1q} \\ H_{2q} \\ \cdot \\ \cdot \\ H_{pq} \end{Bmatrix} F_q \quad \text{Equation 3-5}$$

Multiple Input Relationship:

$$\begin{Bmatrix} X_1 \\ X_2 \\ \vdots \\ X_p \end{Bmatrix}_{N_o \times 1} = \begin{bmatrix} H_{11} & \cdot & \cdot & \cdot & \cdot & \cdot & \cdot & \cdot & H_{1q} \\ H_{21} & & & & & & & & H_{2q} \\ \cdot & & & & & & & & \cdot \\ \cdot & & & & & & & & \cdot \\ H_{pq} & & & & & & & & H_{pq} \end{bmatrix}_{N_o \times N_i} \begin{Bmatrix} F_1 \\ F_2 \\ \vdots \\ F_q \end{Bmatrix}_{N_i \times 1} \quad \text{Equation 3-6}$$

The frequency response functions are used as input data to modal parameter estimation algorithms that estimate modal parameters using a frequency domain model and spatial domain model. Through the use of the Fast Fourier Transform, the Fourier transform of the frequency response function, and the impulse response function can be calculated for use in modal parameter estimation algorithms involving time domain models.

3.3.2 Frequency Response Function Testing Method

For current approaches to Experimental Modal Analysis, the frequency response function is the most important measurement to be made. When estimating frequency response functions, a measurement model is needed that will allow the frequency response function to be estimated from measured input and output data in the presence of noise and errors. Some of the errors are:

- Leakage (FFT error)
- Aliasing (FFT error)
- Noise
 - Equipment problem (Power supply noise)
 - Cabling problems (Shield problem)

- Rattles, cable motion
- Calibration (operator error)
 - Complete system calibration
 - Transducer calibration

Several important points to be remembered before attempting to estimate frequency response functions are:

- The system (with the boundary conditions for that test) determines the frequency response functions for the given input/output locations.
- It is important to eliminate or at least minimize all errors (aliasing, leakage, noise, calibration, etc.) when collecting data.
- Since modal parameters are computed from estimated frequency response functions, the modal parameters are only as accurate as the estimated frequency response functions.

There are number of different Frequency Response Function testing configurations (Avalable, 2002). These different testing configurations are function of acquisition channels or excitation sources. These testing configurations are;

- Single input/single output. (SISO)
 - Only option with 2 channel data acquisition system.
 - Longest testing time. Roving inputs. Roving outputs.
 - Time invariance problems between measurements.

- Single input/multiple output. (SIMO)
 - Multiple channel system (3 or more). (One ADC channel for each response signal to be measured plus one ADC channel for an input signal.)
 - Shorter testing time than SISO. Transducers not necessarily moved.
 - Consistent frequency and damping for data acquired simultaneously.
 - Time invariance problems between measurements from different inputs.

- Multiple input/single output. (MISO)
 - Multiple channel system required (3 or more.). (One ADC channel for each input signal to be measured plus one ADC channel for a response signal.)
 - Long testing time. Roving response transducer.
 - More than one input location per measurement cycle.
 - Detects repeated roots. Maxwell reciprocity checks.
 - Time invariance problems between measurements from different responses.

- Multiple input/multiple output. (MIMO)
 - Multiple channel system (up to 512 channels). Increased set-up time.
 - Large amount of data to be stored and organized.
 - Shortest testing time.

- Consistent frequency and damping for all data acquired simultaneously.
- Detects repeated roots. Maxwell reciprocity checks.
- Best overall testing scheme.

3.3.3 Excitation

Excitation is any form of input that is used to create a response in a structural system. This can include environmental or operational inputs as well as the controlled force input(s) that are used in Experimental Modal Analysis. The following section is limited to the force inputs that can be controlled.

The primary assumption concerning the excitation of a linear structure is that the excitation is observable. Whenever the excitation is measured, this assumption simply implies that the measured characteristic properly describes the actual input characteristics.

If the excitation is not measured, modal scaling parameters (modal mass, modal A, residues, etc.) cannot be estimated. Even when the estimation of modal scaling parameters are not required still an assumption must be made, concerning the characteristics of the excitation of the system.

3.3.3.1 Classification of Excitation

Inputs which can be used to excite a system in order to determine frequency response functions belong to one of the two classifications (Aitavale, 1998,

Avaitable 1999). a) Random signals, b) Deterministic signals. Random signals are defined by their statistical properties over some time period and no mathematical relationship can be formulated to describe the signal whereas deterministic signals can be represented in an explicit mathematical relationship. Deterministic signals are further divided into “periodic” and “non-periodic” classifications. The most common inputs in the periodic deterministic signal designation are sinusoidal while the most common inputs in the non-periodic deterministic designation are transient in form. Mostly periodic input signals are generated by using shaker. Figure 3-12 shows shaker used in experimental modal analysis.

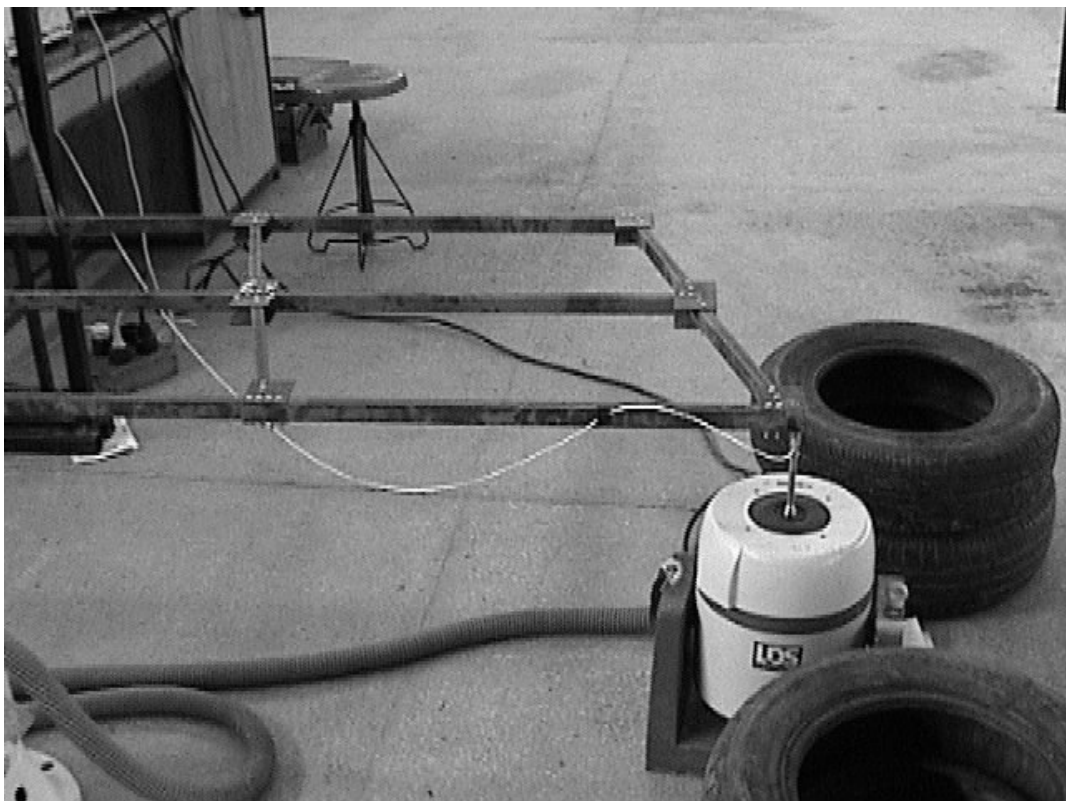


Figure 3-12 General view of test Configuration: Shaker

Swept sine periodic deterministic signals are used in this study for frequency response function estimation. The swept sine signal is a periodic deterministic signal with a frequency that is an integer multiple of the FFT frequency increment. Sufficient time is allowed in the measurement procedure for any transient response (due to change in frequency) to decay so that the resultant output response is periodic with respect to the sample period. Therefore, the total time needed to compute an entire frequency response function are functions of the number of frequency increments required and time allowed for transient responses to decay.

The following paragraphs summarize the terminology used in swept sine excitation method.

- **Delay Blocks:** The number of continuous blocks of excitation that take place without the associated input and output data being acquired are referred as Delay Blocks. Delay Blocks are needed in order to give the transient response to decay out of the response signal. Transient responses are occurred due to start or change in the periodic excitation. So both input and output responses will be periodic within the observation period (T). This is why swept sine excitation method is time consuming. The length of each delay block is equal to the length of the observation period (T). Number of delay blocks is normally chosen as integer. The delay blocks are not recorded and are not used in FRF estimation.

- **Capture Blocks:** The number of capture blocks refers to the number of continuous blocks of time data (input and output) that are recorded (captured). Number of capture blocks is also the number of cyclic averages that will be used to estimate FRF measurement.

There are several periodic and non-periodic deterministic signals and also several non-deterministic signals. Since the details of signal type properties are out of the scope this study they are not explained here. The following table shows a general list of most commonly used for frequency response function estimation (Allemang, 1998).

Table 3-3 Various signals used in Frequency Response Estimation

<i>Name</i>	<i>Signal Type</i>
Swept Sine	Periodic Deterministic
Periodic Chirp	Periodic Deterministic
Impact (Impulse)	Non periodic(transient) Deterministic
Step Relaxation	Non periodic(transient) Deterministic
Pure Random	Ergodic, stationary random
Pseudo Random	Ergodic, stationary random
Periodic Random	Ergodic, stationary random
Burst Random	Both , transient deterministic and Ergodic stationary random

CHAPTER 4

MODAL PARAMETER ESTIMATION

4.1 Introduction

Modal parameter estimation is a special case of system identification where the *a priori* model of the system is known to be in the form of modal parameters. Therefore, regardless of the form of measured input-output data, the form of the model used to represent the experimental data can be stated in a modal model using temporal (time or frequency) and spatial (input DOF and output DOF) information (Awaitable, 1999). There exist several modal parameter estimation algorithms that are being used privately or being sold as a part of commercial software. Modal parameter estimation algorithms are grouped according to the data domain that they are being used (Michael *et al.*, 1992). For the purpose of this study, a second order frequency domain algorithm is examined and used.

4.2 Modal Parameters:

Modal identification involves estimation of the modal parameters of a structural system from measured input-output data. Most current modal parameter estimation methods use measured data in the form of frequency response functions (FRF) or an

equivalent impulse response function (IRF), which is typically found by taking inverse Fourier transform of the frequency response function. Modal parameters include the complex-valued modal frequencies (λ_r), modal vectors ($\{\psi_r\}$) and modal scaling (modal mass or modal A). Additionally, modal participation vectors $\{L_r\}$ and residue vectors $\{A_r\}$ are used. Modal participation vectors are a result of multiple reference modal parameter estimation algorithms and relate how well each modal vector is excited from each of the excitation reference locations included in the measured data. The combination of the modal participation vector and the modal vector for a given mode give the residues for that mode. In general, these two vectors represent portions of the right and left eigenvectors associated with the structural system for a specific mode of vibration.

Modal parameters are considered to be global properties of a system. The concept of “global modal parameters” simply means that there is only one answer for each modal parameter and that the modal parameter estimation solution procedure enforces this constraint (Richardson 1986). Every frequency response or impulse response function measurement theoretically contains the information that is represented by the characteristic equation, the modal frequencies and damping. If individual measurements are treated in the solution procedure independent of one another, there is nothing to guarantee that a single set of modal frequencies and damping will be generated. Most of the current modal parameter estimation algorithms estimate the modal frequencies and damping in a global sense.

4.3 Complex Mode Indication Function (CMIF)

Complex Mode Indication Function is an algorithm based on singular value decomposition (SVD), (Avalable 2001) methods applied to multiple or single reference FRF measurements. CMIF was first developed in order to identify the proper number of modal frequencies, particularly when there are closely spaced or repeated modal frequencies (Shih *et al.* 1989). CMIF is capable to indicates the existence of real normal or complex modes and the relative magnitudes of each mode. Furthermore, CMIF yields the corresponding mode shape and modal participation vector.

CMIF is defined as the singular values, solved from a FRF matrix, at each spectral line. The CMIF plot is the plot of these Eigenvalues on a log magnitude scale as a function of frequency. The peaks detected on the CMIF plot indicate the existence of modes, and the corresponding frequencies of these peaks give the damped natural frequencies for each mode. The number of modes detected in CMIF determines the minimum number of degrees-of-freedom of the analytical system and the order of the system equation used in the algorithm.

4.3.1 Theory of SVD and CMIF

For multi degree of freedom systems Frequency Response Function formulation is given in Equation 2-38 and modified here to represent discrete input output relations.

$$[H(\omega)]_{N_o \times N_i} = \sum_{r=1}^N \frac{[A_r]}{j\omega - \lambda_r} + \frac{[A_r^*]}{j\omega - \lambda_r^*} = \sum_{r=1}^{2N} \frac{[A_r]}{j\omega - \lambda_r} = \sum_{r=1}^{2N} \frac{Q_r \{\phi\}_r \{L\}_r^H}{j\omega - \lambda_r}$$

Equation 4-1

Where

N_o is the number of response point(output)

N_i is the number of excitation point (input)

$[H(\omega)]$ is the FRF matrix of size N_o by N_i

$[A_r]$ is the residue matrix of size N_o by N_i

$\{\phi\}_r$ is r^{th} the mode shape of size N_o by 1

$\{L\}_r$ is the r^{th} modal participation factor of size N_i by 1

Q_r is the scaling factor for the r^{th}

λ_r is the system pole value of r^{th} mode

Since Q_r is a complex valued scalar Equation 4-1 can be rewritten as;

$$[H(\omega)]_{N_o \times N_i} = \sum_{r=1}^{2N} \{\phi\}_r \frac{Q_r}{j\omega - \lambda_r} \{L\}_r^H$$

Equation 4-2

Thus the contribution of the r^{th} mode is $\{\phi\}_r \frac{Q_r}{j\omega - \lambda_r} \{L\}_r^H$.

By taking the singular value decomposition of the FRF matrix at **each** spectral line (say ω_k), a similar expression of Equation 4-2 is obtained. Frequency Response Function at each spectral line is represented with matrix A

$$[A] = [H(\omega_k)]_{N_o \times N_i}$$

$$SVD([A]) = [U(\omega_k)] [\Sigma(\omega_k)] [V(\omega_k)]^H$$

Equation 4-3

Where

$[U(\omega_k)]$ is the left singular matrix of size $N_o \times N_e$ which is an unitary matrix

$[\Sigma(\omega_k)]$ is the singular value matrix of size $N_e \times N_e$, which is a diagonal matrix..

$[V(\omega_k)]$ is the right singular matrix of size $N_e \times N_i$ which is also an unitary matrix.

N_e is the number of dominant modes. The dominant modes are the modes that contribute to the response of the structure at this particular frequency ω .

As stated above $[U(\omega_k)]$ and $[V(\omega_k)]$ are unitary matrices. Thus

$$[U(\omega_k)]^* U(\omega_k)^H = V(\omega_k)^* V(\omega_k)^H = I$$

Also due to the nature of the SVD $U(\omega_k)$ and $V(\omega_k)$ matrices have orthogonal columns.

At this point it is easy to see that Equation 4-2 and Equation 4-3 are identical. If the number of effective modes (N_e) is less than or equal to the smaller dimension of the FRF matrix, ie. $N_e \leq N_i$ or $N_e \leq N_o$, the singular value decomposition leads to mode shapes (left singular vectors) and modal participation factors (right singular vectors). The singular value is then equivalent to the scaling factor Q_r divided by the difference between the discrete frequency and the modal frequency $j\omega - \lambda_r$. Since for a given mode, the scaling factor is a constant, the closer the modal frequency is to the discrete frequency, the larger the singular value will be. Therefore, the damped natural frequency is the frequency at which the maximum magnitude of the singular value occurs. Since the CMIF plot is defined as the plot of the diagonal elements of singular value matrix ($[\Sigma(\omega_k)]$) solved from FRF matrix ($[A]$) at each spectral line on a log magnitude scale. Thus the peaks in CMIF plot indicate the existence of modes. A typical CMIF plot is given in Figure 4-2.

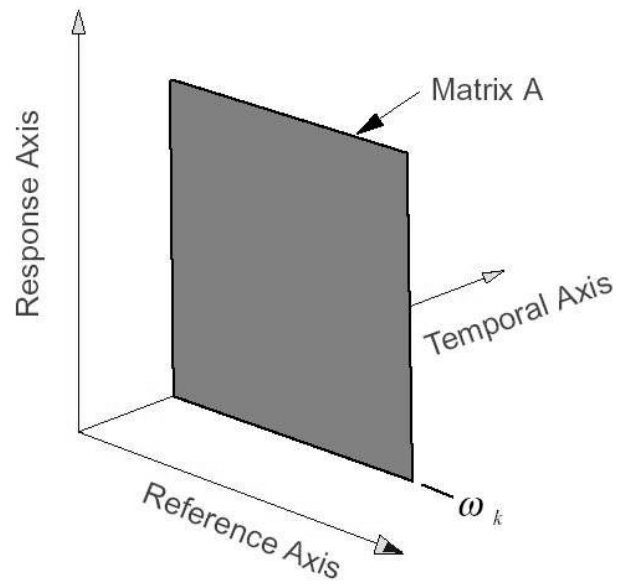


Figure 4-1 FRF matrix [A] for spectral line ω_k

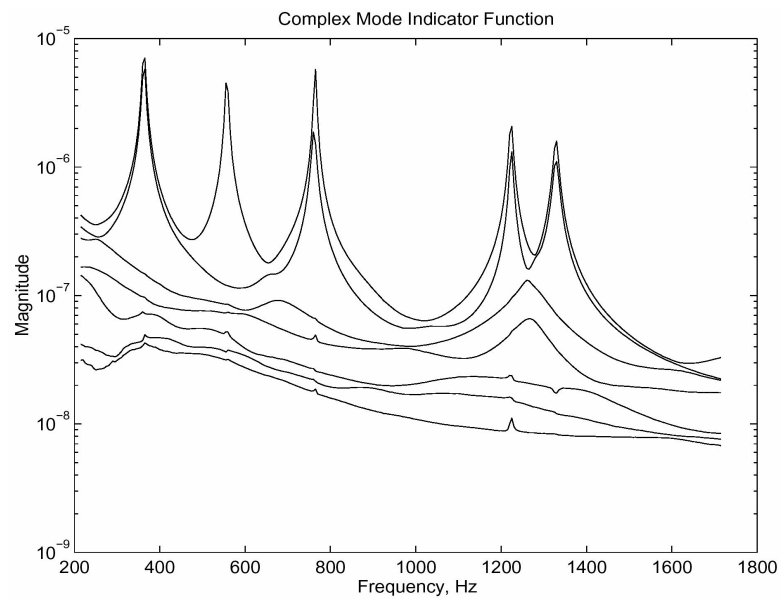


Figure 4-2 CMIF Plot

4.4 Enhanced Frequency Response Function (eFRF)

Enhanced Frequency Response Function is a weighted average of all of the measured frequency response functions. The singular vectors obtained from SVD (mode shapes and modal participation factor) are used as weighting functions. eFRF isolates a single mode so that a simple single degree of freedom parameter estimation algorithm is used to estimate the Eigenvalues and modal scale factors for the enhanced mode.

Thus for the r^{th} mode at spectral line k

$$eFRF(\omega_k)_r = \{U(\omega_r)\}^H H(\omega_k) \{V(\omega_r)\} \quad \text{Equation 4-4}$$

Where

$\{U(\omega_r)\}$ is unitary vector of size $N_o \times 1$

$\{V(\omega_r)\}$ is unitary vector of size $N_i \times 1$

$[H(\omega_k)]$ is the FRF matrix of size N_o by N_i

Thus for the r^{th} mode at spectral line k $eFRF(\omega_k)_r$ is complex valued scalar

Enhance frequency response function plot is drawn by calculating $eFRF(\omega_k)_r$ at each spectral line.

Since the mode shapes and modal participation factors from singular value decomposition are unitary vectors, by substituting Equation 4-2 into Equation 4-4, the enhanced FRF is actually the decoupled single mode response function:

Therefore for the r^{th} mode

$$eFRF(\omega_k)_r \equiv \frac{Q_r}{j\omega_k - \lambda_r} \quad \text{Equation 4-5}$$

That is why it is said that “eFRF isolates a single mode”. Looking to the Equation 4-5 is easy to see that for the r^{th} mode the eFRF is only related with the modal scaling factor and pole of the r^{th} mode.

4.5 Pole Estimation

As stated in Section 4.3, the peaks in CMIF plot indicate the existence of Modes. The corresponding frequencies of a peak in CMIF plot is damped natural frequencies. Poles of the measured data are estimated from eFRF plots. **Second Order Frequency Domain UMPA** model is used for pole estimation. Additional B terms are used for the modes that are out of frequency range (residual effect). The general form of UMPA model is given in Equation 4-6. The Second Order Frequency Domain UMPA model is given in Equation 4-7. The second order formulation is analogous to the MCK model formulation (See Section 2.2.1.2). The second order equation of motion for a single degree of freedom MCK system in frequency domain is given in Equation 4-8 :

$$\sum_{n=0}^N (j\omega)^n [A_n] \{eH(\omega)\} = \sum_{m=0}^M (j\omega)^m [B_m] \{R(\omega)\} \quad \text{Equation 4-6}$$

$$\left[(j\omega)^2 [A_2] + (j\omega)^1 [A_1] + [A_0] \right] \{eH(\omega)\} = \sum_{m=0}^M (j\omega)^m [B_m] \{R(\omega)\} \quad \text{Equation 4-7}$$

$$\left[(j\omega)^2 [M] + (j\omega)^1 [C] + [K] \right] \{eH(\omega)\} = \{R(\omega)\} \quad \text{Equation 4-8}$$

In Equation 4-7, the enhanced frequency response $\{eH\}$ (or sometimes $\{eH\}$) is known for the frequency band of interest, whereas the index matrix $[R]$ is unity load vector. The A's and B's in Equation 4-7 are the unknowns. A least squares solution is formulated for the solution of A&B. Least square solution is formulated by assuming $[A_2] = [I]$, thus the multiplier of $[A_1]$ is taken to the right side, whereas $[B_n]$ and R are taken to the left.

$$\begin{bmatrix} A_1 & A_0 & B_0 & \cdots & B_m \end{bmatrix} \begin{bmatrix} (j\omega)H(\omega) \\ H(\omega) \\ -R(\omega) \\ \vdots \\ -(j\omega)^m R(\omega) \end{bmatrix} = -(j\omega)^2 H(\omega) \quad \text{Equation 4-9}$$

Thus;

$$\begin{bmatrix} A_1 & A_0 & B_0 & \cdots & B_m \end{bmatrix} = -(j\omega)^2 H(\omega) \begin{bmatrix} (j\omega)H(\omega) \\ H(\omega) \\ -R(\omega) \\ \vdots \\ -(j\omega)^m R(\omega) \end{bmatrix}^+ \quad \text{Equation 4-10}$$

Where $(^+)$ indicates generalized inverse operation (pseudo inverse)

Since the second order UMPA formulation is analogous to the MKC model formulation, the poles of UMPA model is exactly same as for MKC model.

For MCK model the state space formulation is as follow;

$$M \ddot{x}(t) + C \dot{x}(t) + Kx(t) = 0 \quad \text{Equation 4-11}$$

Define

$$x_1(t) = x(t) \quad \text{Equation 4-12}$$

$$x_2(t) = \dot{x}(t) \quad \text{Equation 4-13}$$

Substituting Equation 4-12 and Equation 4-13 to Equation 4-11 gives;

$$M \dot{x}_2(t) + C x_2(t) + Kx_1(t) = 0 \quad \text{Equation 4-14}$$

Thus in state space formulation (Kashani, www.deicon.com) there exist two sets of equation which are;

$$M \dot{x}_2(t) = -C x_2(t) - Kx_1(t)$$

and

$$\dot{x}_1(t) = x_2(t)$$

The two set of equations in matrix form is given in Equation 4-15.

$$\begin{Bmatrix} \dot{x}_1 \\ \dot{x}_2 \end{Bmatrix} = \begin{bmatrix} 0 & 1 \\ -\frac{K}{M} & -\frac{C}{M} \end{bmatrix} \begin{Bmatrix} x_1 \\ x_2 \end{Bmatrix} \quad \text{Equation 4-15}$$

Letting

$$a = \begin{bmatrix} 0 & 1 \\ -\frac{K}{M} & -\frac{C}{M} \end{bmatrix} \quad \text{Equation 4-16}$$

Thus, the poles of the MCK model is equivalent to the eigen values of the coefficient matrix(companion matrix) given in Equation 4-15. Since second order UMPA formulation is analogous to the MKC model formulation, the poles of UMPA model is also equivalent to the eigenvalues of the coefficient matrix. Thus for second order UMPA formulation companion matrix becomes

$$a = \begin{bmatrix} 0 & 1 \\ -\frac{A_o}{A_2} & -\frac{A_1}{A_2} \end{bmatrix}$$

Keeping in mind that $[A2] = [I]$

$$a = \begin{bmatrix} 0 & 1 \\ -A_o & -A_1 \end{bmatrix}$$

Thus the poles of the UMPA model is calculated as shown in Equation 4-17

$$\begin{Bmatrix} \lambda \\ \lambda^* \end{Bmatrix} = eig(a) \quad \text{Equation 4-17}$$

One important point in companion matrix formulation is that, terms in Companion matrix can be rearranged so that the poles are calculated by taking the eigenvalues of the negative companion matrix. In that case the companion matrix becomes

$$a = \begin{bmatrix} A_1 & A_0 \\ -1 & 0 \end{bmatrix}$$

Where the poles are calculated as in Equation 4-18

$$\begin{Bmatrix} \lambda \\ \lambda^* \end{Bmatrix} = eig(-a) \quad \text{Equation 4-18}$$

4.6 Scaling Computation

Once the modal frequencies (poles) and mode shapes are estimated, the associated modal scaling factor and corresponding modal A, and residues can be calculated by using Equation 4-5.

Keeping Equation 2-43 in mind;

For Mode r;

$$M_{Ar} = \frac{pinv(efrf)}{\{j\omega - \lambda_r\}}$$

Where;

$$Q_r = \frac{1}{M_{Ar}}$$

Since the mode shapes and modal A are calculated, it is now possible to calculate residue terms, by Equation 4-19.

$$A_{pqr} = \frac{\phi_{pr}\phi_{qr}}{M_{Ar}} \quad \text{Equation 4-19}$$

Since residual terms are calculated. The frequency response functions can be re-synthesized by using Equation 2-37

CHAPTER 5

MODAL DATA PRESENTATION/VALIDATION

5.1 Introduction

The measured modal model data and constructed modal model needs to be validated against completeness, orthogonality, consistency and similar criteria.

After the modal parameters are determined, several procedures can be used for modal data (model) presentation/validation. Some of the procedures that may be used are:

- Measurement Synthesis
- Visual Verification (Animation)
- Finite Element Analysis
- Modal Vector Orthogonality
- Modal Vector Consistency (Modal Assurance Criterion)
- Modal Modification Prediction
- Modal Complexity
- Modal Phase Co linearity and Mean Phase Deviation

All of these methods depend upon the evaluation of an assumption concerning the modal model. Unfortunately, the success of a validation method only defines the validity of the assumptions; the failure of a modal validation does not generally define what the cause of the problem is. For the purpose of this study four modal data presentation /validation procedures are studied.

5.2 Measurement Synthesis

The simplest validation procedure is to compare the data synthesized from the modal model with the measured data. This comparison is particularly effective if the measured data was not part of the data used to estimate the modal parameters. Comparison of generated data against measured data serves as an independent check of the calculated modal parameter estimation variables.

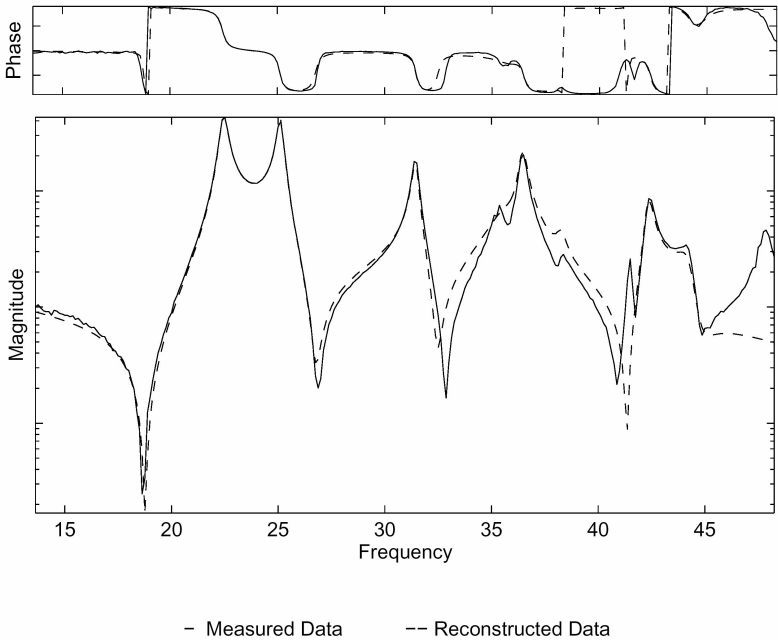


Figure 5-1 Typical FRF Synthesis

5.3 Visual Verification (Animation)

Another relatively simple method of modal model validation is to evaluate the modal vectors visually. While visualization of mode shapes can be accomplished using plotted modal vectors superimposed over the undeformed geometry, the modal vectors are normally animated (superimposed upon the undeformed geometry) in order to quickly assess the modal vector.

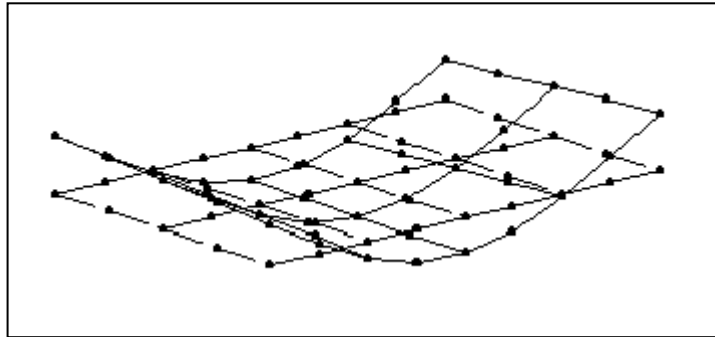


Figure 5-2 Visual Verification of Modal Vectors

5.4 Finite Element Analysis

The mode shapes obtained from the finite element model of a structural system can also be used for modal model validation. While the problem of matching the number of analytical degrees of freedom N_a to the number of experimental degrees of freedom N_e causes some difficulty, the modal frequencies and modal vectors can be compared visually or by consistency checks. Unfortunately, when the comparison is not sufficiently acceptable, the question of error in the experimental model versus error in the analytical model cannot be easily resolved. Generally,

reasonable agreement can be found in the first ten deformable modal vectors but agreement for higher modal vectors is more difficult. Some of the analytical modes may not be measured during test, especially if the accelerometers are placed in one direction only (i.e. lateral modes will be missed if no accelerometers are placed in lateral direction). Also modal frequency differences between the measured and modeled systems are expected due to variation in the assumed variables.

5.5 Modal Assurance Criterion

Modal Assurance Criterion (**MAC**) provides a measure of consistency between estimated modal vectors. This measure (MAC) provides an additional confidence factor in the evaluation of a modal vector when different excitation locations are used. The modal assurance criterion (MAC) also provides a method of determining the degree of causality between estimates of different modal vectors of the same system.

MAC also provides a method of easily comparing estimates of modal vectors originating from different sources. The modal vectors from a finite element analysis can be compared against with those determined experimentally as well as modal vectors determined by way of different experiments or modal parameter estimation methods. In this way, effect of different methods can be compared in order to evaluate the mutual consistency of different procedures, on the estimation of modal vectors.

MAC is defined as a scalar constant (between zero and one) relating the portion of the auto moment of the modal vector that is linearly related to the reference modal vector as follows:

$$MAC_{cdr} = \frac{|\{\psi_{cr}\}^H \{\psi_{dr}\}|^2}{\{\psi_{cr}\}^H \{\psi_{cr}\} \{\psi_{dr}\}^H \{\psi_{dr}\}} = \frac{(\{\psi_{cr}\}^H \{\psi_{dr}\})(\{\psi_{dr}\}^H \{\psi_{cr}\})}{\{\psi_{cr}\}^H \{\psi_{cr}\} \{\psi_{dr}\}^H \{\psi_{dr}\}} \quad \text{Equation 5-1}$$

The constant takes values from zero, representing no consistent correspondence at all, to one, representing exact duplicate. In this manner, if the modal vectors under consideration truly exhibit a consistent relationship, the modal assurance criterion should approach to unity.

CHAPTER 6

EXPERIMENTAL MODAL ANALYSIS SOFTWARE

6.1 Introduction

Today modal analysis softwares are available in markets with prices starting from 500 Euro. Examples are X Modal, FemTool and SDT. Since these software packages were not available in Structural Mechanics Lab, this enforced us to write Experimental Modal Analysis software. Matlab platform is chosen for programming due to its rather simple architecture and ease of use for matrix manipulations. There are many advantages of Matlab platform: Firstly most of the required functions are readily available within Matlab (such as matrix inverse, eigenvalue solution, matrix manipulations). Secondly the written software can be converted to a stand-alone application where the end-user does not require Matlab in order to run the written software (Marchand 1999). The short name of the written software is (Experimental Modal Analysis Software) **EMAS**.

6.2 Structure of EMAS

EMAS is a user friendly graphical user interfaced software. It consists of several parts which are explained in the following Sections. In addition to EMAS, two more programs were prepared that can be either executed within EMAS or executed separately These programs are;

- a) Finite Element Updating Software (Calibration Software): The theory and software will be explained in Chapter 9.
- b) Frequency Response Function Generator Software: Generates FRFs according to the given M C K matrices, which is used to generate synthetic FRFs to verify EMAS results.

The appearance of EMAS is given in Figure 6-1.

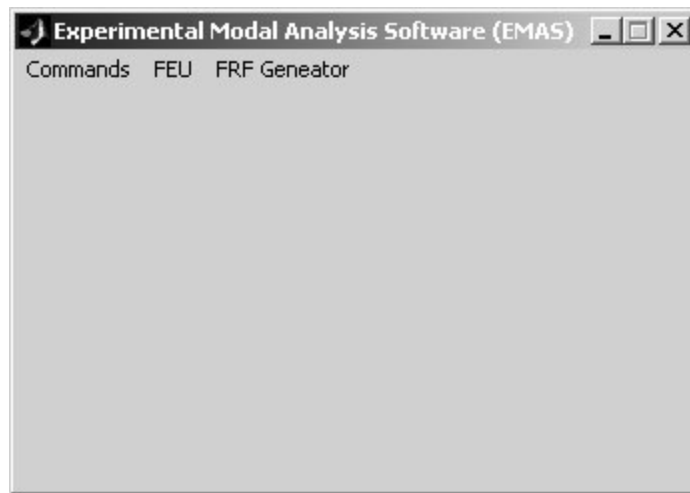


Figure 6-1 Appearance of EMAS

EMAS consists of 3 menu items. These are:

- **Commands,**
- **FEU, and**
- **FRF Generator.**

Each menu item is explained in detail in the following Sections.

6.2.1 Commands

“Commands” is the first menu item of EMAS. It consists of four sub menu items.

These sub menu items are:

- Input File Editor
- Frequency Response Function Loader
- Modal Parameter Estimator.
- Exit

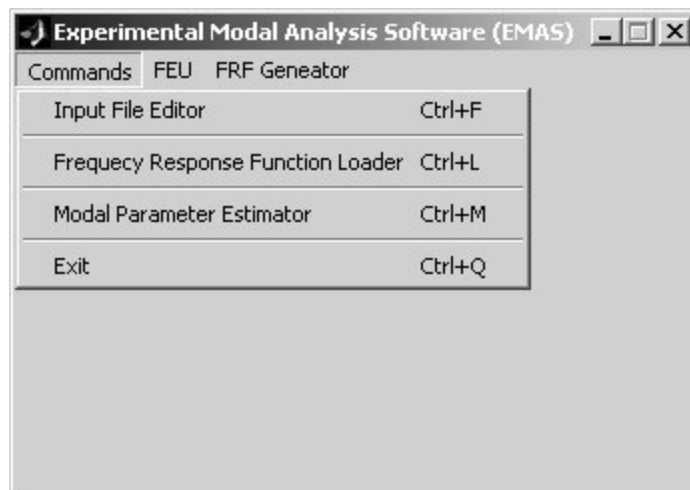


Figure 6-2 Items under Command pull down menu

These sub-menu items are further explained below.

6.2.1.1 Input File Editor

“**Input File Editor**” menu item is at the beginning of EMAS software, at which the general model geometry used in Experimental Modal Analysis is defined. Clicking on “Input File Editor” activates Input File Editor program. The usage of the Input File Editor program is rather simple. Nodes, Elements, Constraints, and Masters are defined in this part. Input files can be prepared in Input File Editor program or in any word-processor. The extension of input files created by Input File Editor program is fea as in the form of “*.fea”. Fea is the abbreviated form of **Finite Element Analysis**. The appearance of Input File Editor program is given in Figure 6-3. Once input file is prepared by clicking **Load File** button the commands displayed in the Input File Editor program is executed Figure 6-3.

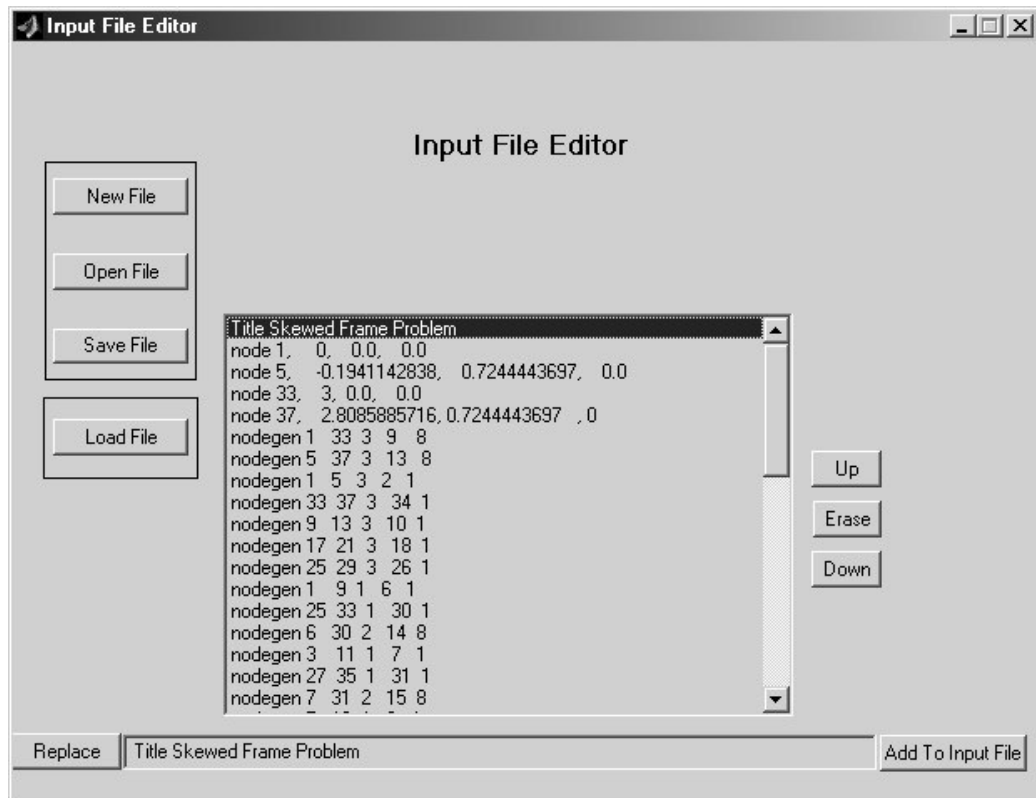


Figure 6-3 Input File Editor Program

There are several commands used in input files that define the model. These commands are briefly explained below.

6.2.1.1.1 NODE

Usage: **Node id, x, y, z**

This Command specifies the location and number of a node in three-dimensional (3D) Cartesian coordinates. "id" is the node number, and it is a positive integer. Every node has a unique node number. Variables x, y, z are the real coordinates of the node id in 3D space.

An example illustrating the use of the command “node” is given below.

Node 1, 0, 0, 0

- Specifies node number 1 with coordinates x =0, y =0, z=0.

6.2.1.1.2 NODEGEN

Usage: **NODEGEN n1, n2, (num, start, offset)**

This command generates additional nodes linearly between two previously defined nodes. The new nodes are spaced evenly between n1 and n2, where **n1, n2** are the two end node numbers (n1 must be less than n2). **num** (optional) is the total number of nodes to be generated. Num defaults to the difference between the node numbers n1 and n2. **start** (optional) is the start node number of the new nodes to be generated. Start defaults to n1+1. **offset** (optional) is the difference in node number between each newly generated node. Offset defaults to +1. Offset can also be negative.

Examples:

Nodegen 1, 11

- Generates 9 nodes numbered 2,3,...,10 located on a straight line with equal spacing between nodes 1 and 11.

Nodegen 1, 11, 9, 100

- Generates 9 nodes numbered 100, 101,..., 109 located on a straight line with equal spacing between nodes 1 and 11.

Nodegen 1, 11, 3, 100, 10

- Generates 3 nodes numbered 100, 110, 120 located on a straight line with equal spacing between nodes 1 and 11.

6.2.1.1.3 ELEMTYPE

Usage: **ELEMTYPE elemname**

This command specifies the type of element that will be generated by subsequent Elem and Elemgen commands. The latest Elemtype command becomes valid and replaces the previously defined ones. Elemname is the name of the particular element type.

Available element types are

- a) 2 dimensional frame element (Beam2d)
- b) 3 dimensional frame element (Beam3d)
- c) 1 dimensional spring element (Spring)
- d) 2 dimensional mass element (Mass2d)
- e) 3 dimensional mass element (Mass3d)
- f) 2 dimensional truss element (Truss)
- g) 3 dimensional spring element (Spring3d)

Example:

Elemtype beam3d

- Subsequent elements are 3-dimensional beam elements.

6.2.1.1.4 ELEM

Usage: **ELEM id, n1, (n2, n3,...)**

This command creates an element between two previously defined nodes. The type of element must have been previously specified by an Elemtyp command. Different elements require different number of nodes, but they all require at least one node. Available elements are given in Section 6.2.1.1.3. Although elements requiring more than 2 nodes (Shell elements, plate elements etc) are not prepared, elem command supports this type of elements also. **id** is the element number, which is a positive integer. Every element must have a unique element number. **n1, n2, ...** are the node numbers that define an element. The number of nodes required depends on the type of the element to be generated. All of the nodes must have been previously defined.

Example:

Elem 100, 1, 2

- Generates element number 100 of type previously specified in last Elemtyp command, between nodes 1 and 2.

6.2.1.1.5 ELEMGEN

Usage: **ELEMGEN elemid, num, (elemstart, eleminc, nodeinc)**

This command generates multiple elements based on the nodes of a template element. The new elements are generated by adding a node number increment (nodeinc) to each of the nodes of the template element. The generation is done for a

specified number of times. Note that every node to be used in the element generation process must already be defined, and every element number to be generated must not be previously defined. Also, the current element type must be the same as the element type of the template element. Variable **elemid** is the element number of the template element. **num** is the number of elements to be generated. **elemstart** (optional) is the start element number of the elements to be generated. Elemstart defaults to elemid+1. Variable **eleminc** (optional) is the increment of the the generated element numbers. Variable **eleminc** can be also negative and defaults to 1. Variable **nodeinc** (optional) is the increment of the node numbers of the template element which can also be negative. The default value of **nodeinc** is 1.

Examples:

Elem 100, 1, 2

Elemgen 100, 3

- Generates the three elements:

Elem 101, 2, 3

Elem 102, 3, 4

Elem 103, 4, 5

Elem 100, 1, 2, 5

Elemgen 100, 4, 200, 10, 2

- Generates the four elements:

Elem 200, 3, 4, 7

Elem 210, 5, 6, 9

Elem 220, 7, 8, 11

Elem 230, 9, 10, 13

6.2.1.1.6 CONSTNODE

Usage: **CONSTNODE nodeid, (num, inc)**

This command constrains (grounds) one or more nodes, by fixing all six degrees of freedom of the nodes. Variable **nodeid** is the node number of the first node to be constrained. Variable **num** (optional) is the total number of nodes to be constrained. Default value of **num** is 1. Variable **inc** (optional) is the increment between every node number that is constrained. Default value of **inc** is 1.

Examples:

Constnode 50

- Constrains node number 50

Constnode 50, 4

- Constrains nodes number 50, 51, 52, 53

Constnode 50, 4, 2

- Constrains nodes number 50, 52, 54, 56

6.2.1.1.7 CONSTDOF

Usage: **CONSTDOF nodeid, dof, (num, inc)**

This command constrains specified degrees of freedom of one or more nodes.

Degrees of freedom are numbered as follows:

1. Translation along the X-axis
2. Translation along the Y-axis
3. Translation along the Z-axis
4. Rotation about the X-axis
5. Rotation about the Y-axis
6. Rotation about the Z-axis

Variable nodeid is the node number of the first node with a DOF to be constrained.

Variable **dof** is the number of the DOF to be constrained, and takes a value between 1 and 6. Variable **num** (optional) is the total number of DOFs to be constrained. The default value for **num** is 1. Variable **inc** (optional) is the increment between nodes which defaults to 1.

Examples:

Constnode 50, 3

- Constrains Z-translation for node number 50

Constnode 50, 5, 4, 10

- Constrains Y-rotation for node numbers 50, 60, 70, 80

6.2.1.1.8 MASTERNODE

Usage: **MASTERNODE nodeid, (num, inc)**

The format of Masternode command is almost identical as Constnode command.

The only difference is that degrees of freedom of the selected nodes are not constrained but chosen as masters.

6.2.1.1.9 MASTERDOF

Usage: **MASTERDOF nodeid, dof, (num, inc)**

The format of Masterdof command is almost same as Constdof command. The only difference is that the selected degrees of freedom are not constrained but chosen as master degrees of freedom.

6.2.1.1.10 ALLMASTERDOF

Usage: **ALLMASTERDOF (dof)**

This command is used to easily select types of degrees of freedom as masters. If the number **dof** is given, between 1 and 6, then every degree of freedom of that type in the model is selected as a master dof. If **Allmasterdof** is executed without a number following the command then every degrees of freedom is selected as a master dof. Variable **dof** (optional) is the degrees of freedom number type to be select as master dof. Master degrees of freedoms are used in Frequency Response Function Loader (FRFL) which is explained in the following Section. If a degrees of freedom is not defined as a master degrees of freedom, it is not possible to assign the acquired (measured) modal data to that degrees of freedom.

Examples:

Allmasterdof

- All degrees of Freedoms are selected as masters.

Allmasterdof 1

- All X-translation degrees of freedom are selected as masters.

6.2.1.2 Frequency Response Function Loader

Frequency Response Function Loader (FRFL) is a menu item defined under the **Commands** item (see Figure 6-2). This is the part of EMAS where acquired (measured) modal data is imported into the program. Clicking on FRFL menu item activates the FRFL program. The usage of FRFL is quite simple and further described in Section 6.2.1.2.1. The appearance of FRFL program is given in Figure 6-4 for a cantilever beam model.

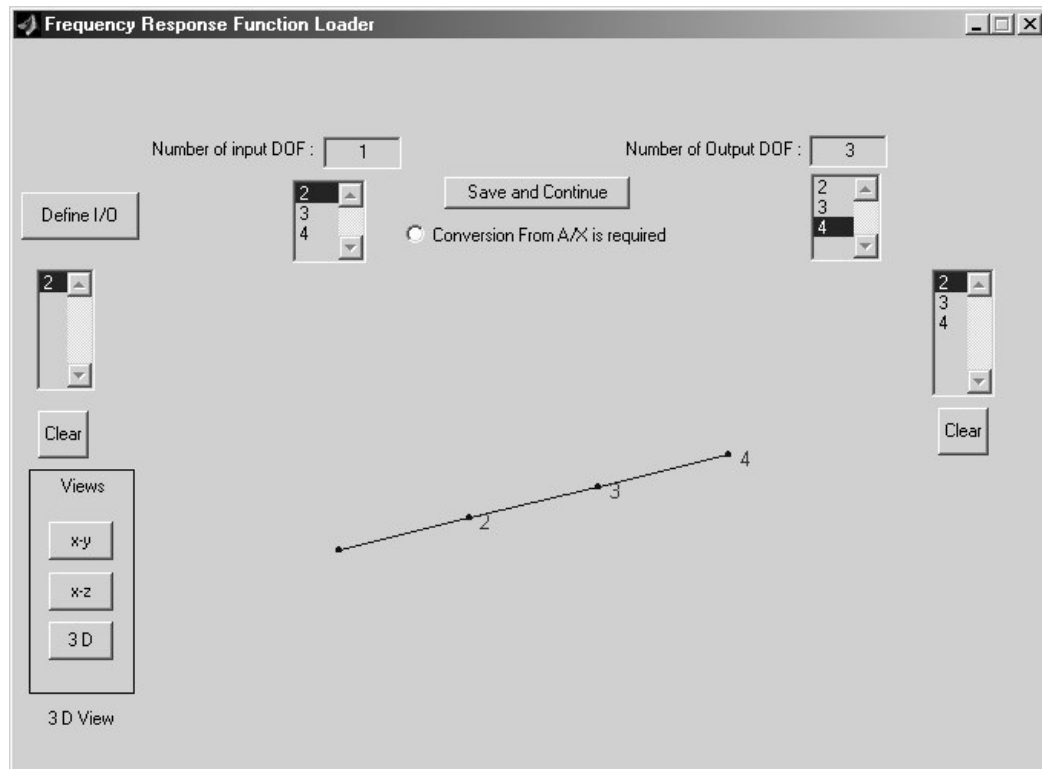


Figure 6-4 Appearance of FRFL Program

6.2.1.2.1 How Does FRFL Program Work

First step to do in FRFL is to define **Number of Input DOF** and **Number of Output DOF**. These argument should be less than or equal to number of masters degrees of freedom. Note that master degrees of freedom are defined in Input File Editor program, as explained in Sections 6.2.1.1.8, 6.2.1.1.9, and 6.2.1.1.10. After entering these arguments, by clicking **Define I/O** the number of input and output degrees of freedom is stored in the program. Then for each input-output degrees of freedom pair, a data file obtained from modal data acquisition is imported. If the data obtained from modal data acquisition is the form of accelerance (A/F), this is converted into receptance (X/F) by the help of a radio button named **Conversion**

from A/X is required. After importing data (obtained from modal data acquisition) for all input-output d.o.f pairs, clicking **Save and Continue** button ends FRFL program. After clicking **Save and Continue** button, a question dialog box appears asking if saving the FRF Data is required. If **YES** is selected FRF data file is saved to a file (which its name is defined by the user), otherwise without saving the FRF data to a file the program is ended.

Saving the FRF data to a file is useful for further use. Next time running EMAS the user can directly jump to MPE part of EMAS without executing FRFL program. Keeping in mind that when FRFL menu item was first clicked, a question dialog box was appeared asking whether loading FRF data from file is required or not.

6.2.1.3 Modal Parameter Estimation

Modal Parameter Estimation (MPE) is a menu item defined under the **Commands** item (see Figure 6-2). As a part of EMAS, MPE is used to extract modal parameters from the measured data obtained by modal data acquisition. The general appearance of MPE program is given in Figure 6-4 for an example FRF data generated from 3 dof cantilever beam model.

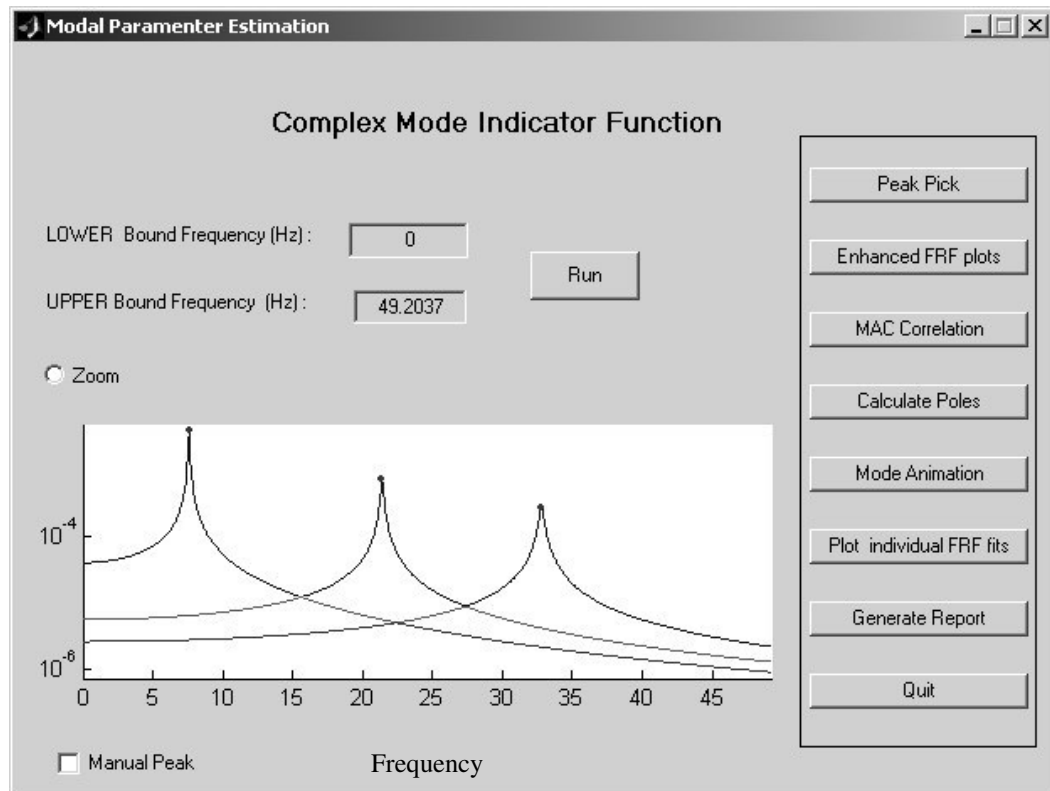


Figure 6-5 MPE Program

6.2.1.3.1 How Does MPE Program Work

First step in MPE is to define the frequency range of interest. This is achieved by defining the **Lower Bound Frequency** and **Upper Bound Frequency**. After the **Run** button is clicked the CMIF plot is drawn. As stated in Chapter 4, Section 4.3, the picks in CMIF plot indicates the existence of a mode. The peaks in CMIF plot are selected with **Peak Pick** button. After clicking Peak Pick Button, it is required to click a point on the Plot. The peak pick algorithm automatically moves towards uphill, locates, and picks the peak. Alternatively the peaks can also be selected manually. This is achieved by checking the **Manual Peak** check box. When the

Manual Peak check is on, it is required to select the peak manually. This procedure is repeated until all peaks are selected. Clicking the **Enhanced FRF** button displays the eFRF plots for selected peaks (modes). The theory of eFRF is explained in Chapter 4, Section 4.4. The appearance of Enhanced FRF plot is given in Figure 6-6.

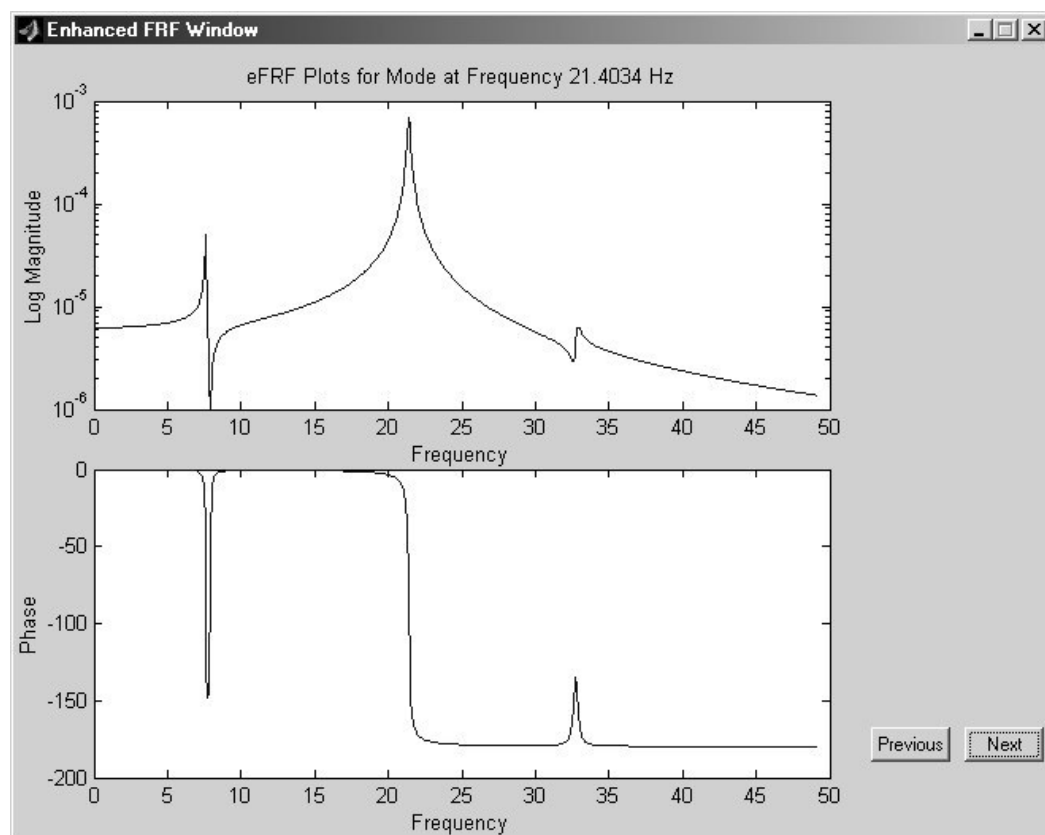


Figure 6-6 Enhanced FRF Window

The **MAC Correlation** button in Figure 6-4 displays a bar chart of the MAC values of selected peaks (modes). The theory of MAC is explained in Chapter 5, Section 5.5. The appearance of MAC Correlation windows is given in Figure 6-7

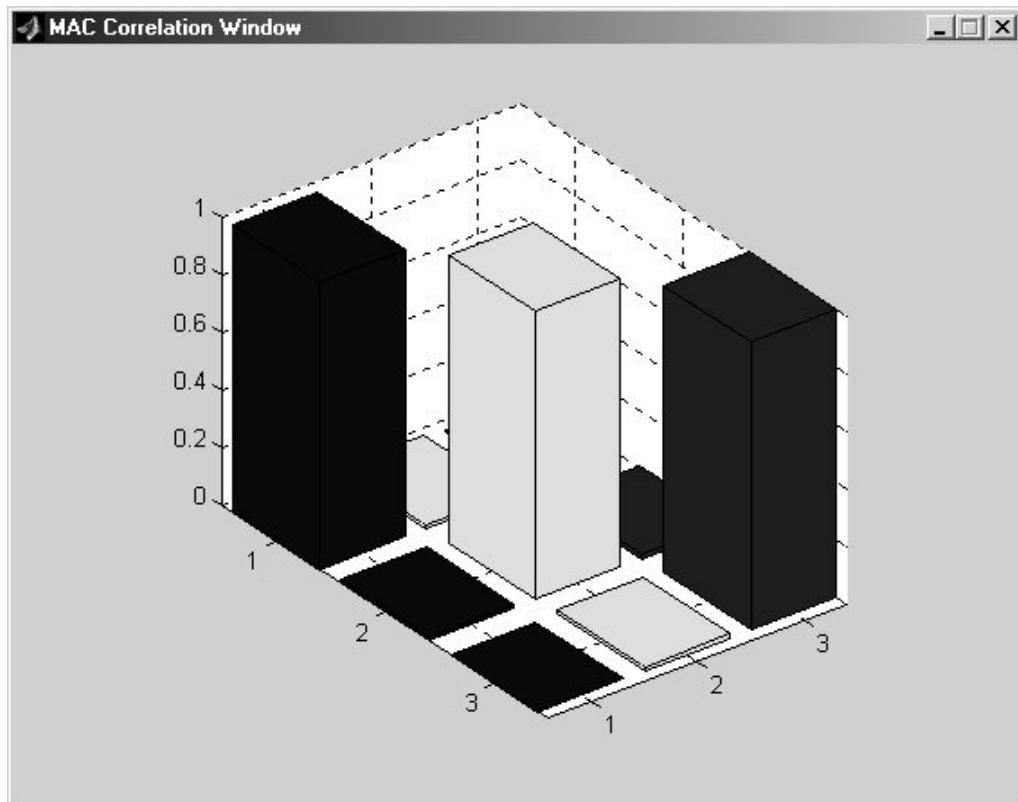


Figure 6-7 MAC Correlation Window

The **Calculate Poles** Button calculates the Poles of the selected peaks. The theory of Pole calculation is explained in Chapter 4, Section 4.4.

Mode Animation button animates modal vector of selected modes. Mode animation is a method of modal model validation which is explained in Chapter 5, Section 5.3. Mode Shape Animation Window is shown in Figure 6-8 displaying the third mode of vibration of a cantilever example beam. The modal frequency and percent damping ratios are also displayed in the same window. The speed of

animation and the magnitude of modal vectors are adjusted using the vertical sliding bar displayed at the left and right side of the window, respectively (Figure 6-9). While mode shapes are animated, it is not possible to adjust sliding bars.

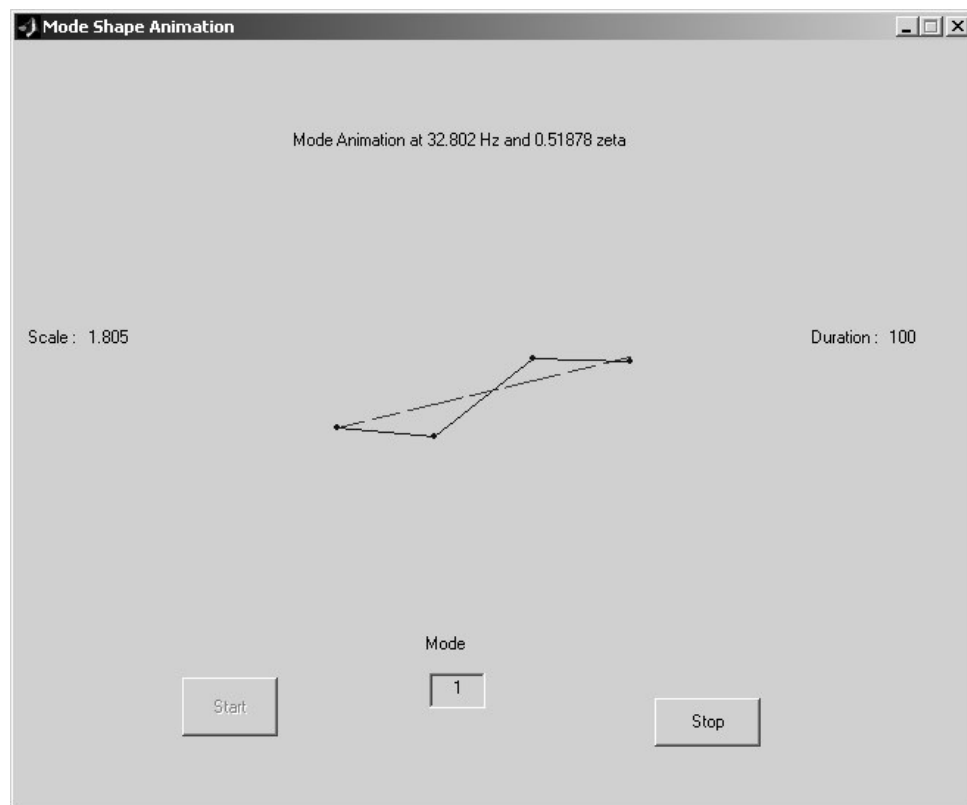


Figure 6-8 Mode Shape Animation Window

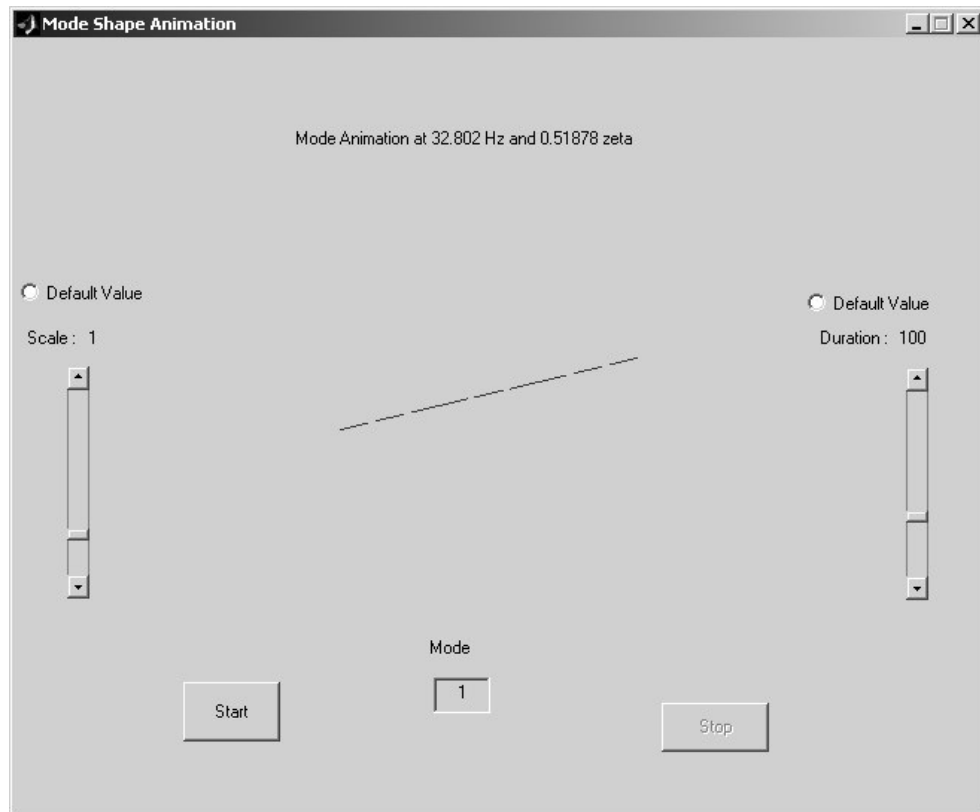


Figure 6-9 Vertical sliding bars used for adjusting the speed and magnitude of the mode shapes

Plot Individual FRF Fits Button plots regenerated FRF on top of the measured FRF. This is a method of modal model validation which is explained in Chapter 5, Section 5.2 as Measurement Synthesis. The appearance of Individual FRF Fit Windows is given in Figure 6-10. The top figure displays the magnitude of regenerated and measured FRF while the bottom part displays the phase information for changing frequency.

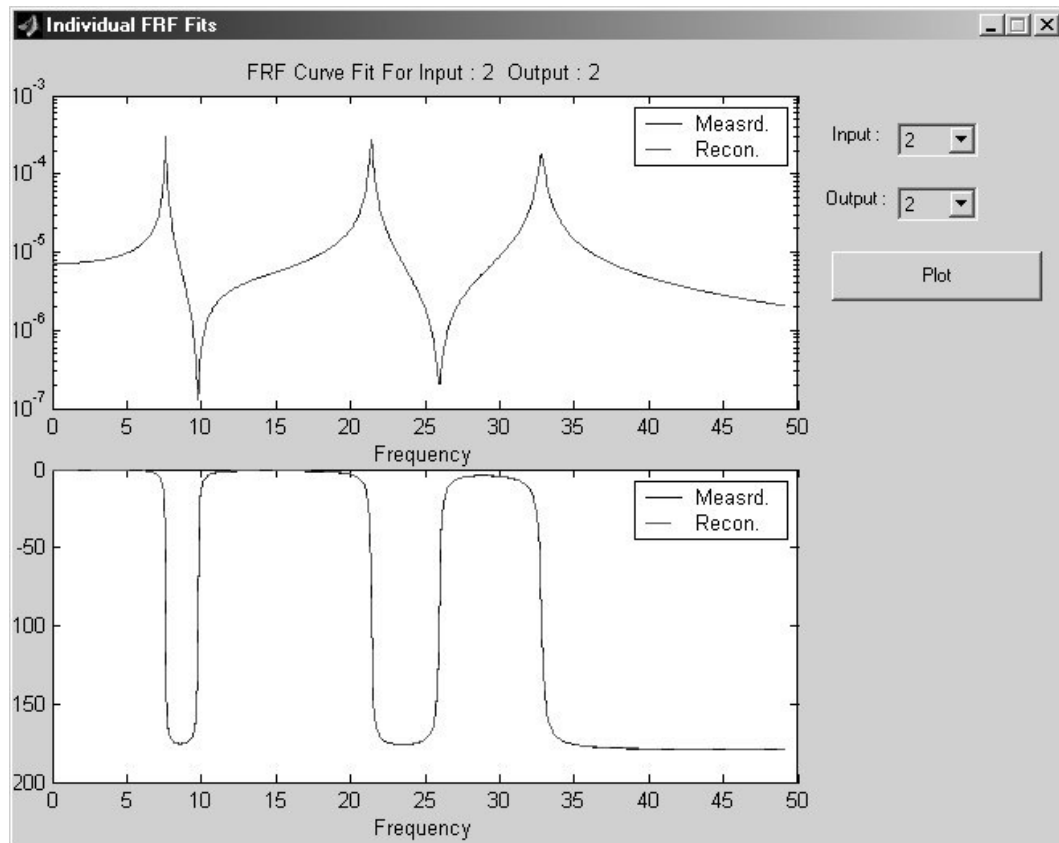


Figure 6-10 Individual FRF Fit Window

Generate Report Button (Figure 6-5) creates a text file which contains information about the Nodes, element connection, constraints, masters, and modal parameters (natural frequencies, damping, mode shapes). The appearance of Generate Report screen is given Figure 6-11

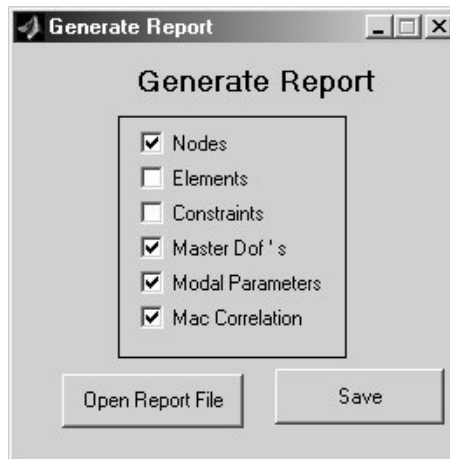
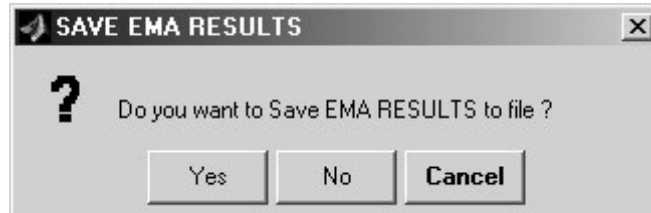


Figure 6-11 Generate Report

The last button in MPE program is **Quit** Button (Figure 6-5). The following screen appears by clicking the **Quit** button.



Clicking the **Yes button** causes the MPE results to be saved in a MATLAB data file with MAT extension.. The data file name is defined by user.As the MPE program ends, it returns to the main program, EMAS. Clicking **No** button ends MPE program without saving, and returns to the main program EMAS. Clicking **Cancel** button cancels the “Quit” command and returns back to the MPE program without quitting.

6.2.1.4 FRF Generator

Clicking **FRF Generator** (see Figure 6-1) activates FRF Generator part of EMAS.

FRF can be generated if the mass (M), stiffness (K), damping(C) matrices of a system are known. Equation used for FRF generation is given in Equation 6-1.

$$H(\omega_k)_{N_i \times N_o} = \frac{1}{(j\omega_k)^2 M + (j\omega_k) C + K} \quad \text{Equation 6-1}$$

Where ω_k is a frequency variable that can take any value within the range of interest.

Appearance of FRF Generator is shown in Figure 6-12.

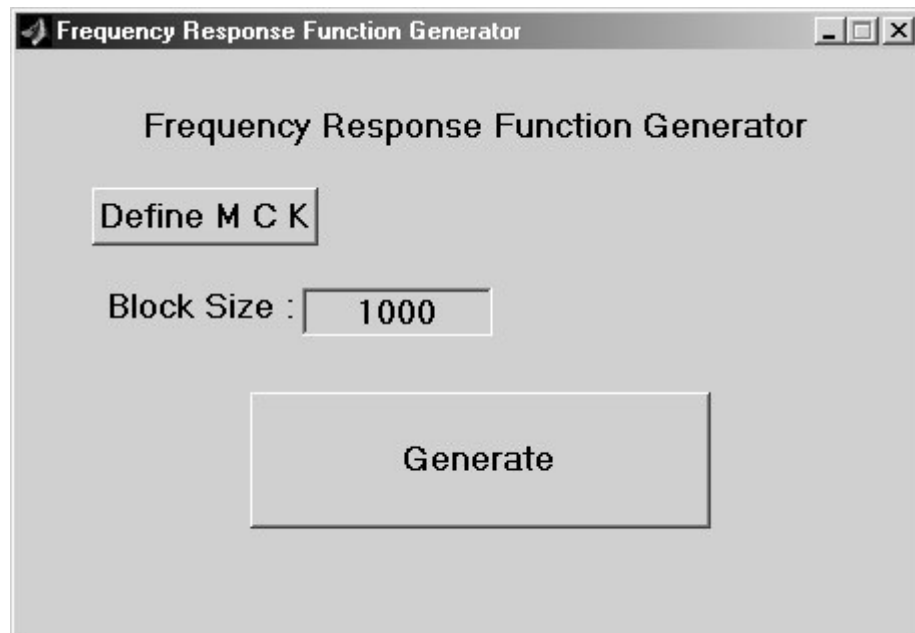


Figure 6-12 FRF Generator

By Clicking **DEFINE M C K**, Figure 6-13 appears which allows user to import binary texts files containing MCK matrices. Block size is used to define the number of data points to be generated between minimum and maximum frequencies.

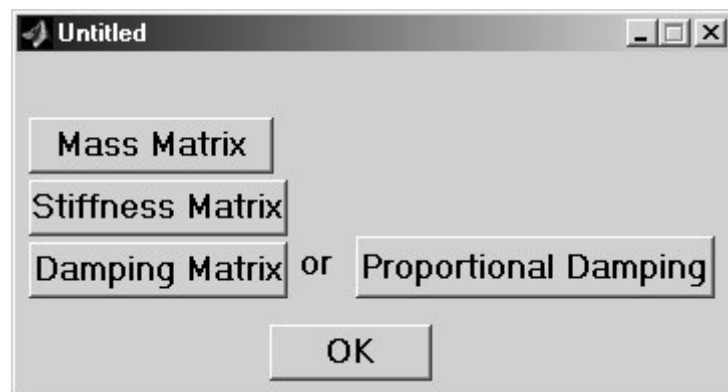


Figure 6-13 DEFINE M C K

Damping matrix can be defined to be proportional as stated in Equation 2-46.

Proportional damping is defined by clicking **Proportional Damping** button. As shown in Figure 6-14.

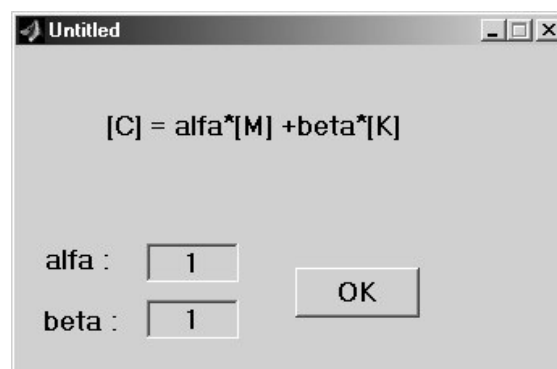


Figure 6-14 Proportional Damping

FRF Generator calculates the Eigenvalue solution of $M C K$ system by using state space formulation. The state space formulation of $M C K$ system is explained in Chapter 4, Section 4.5. The range of frequency is automatically defined to be 1.5 times of the highest natural frequency. The frequency step size is defined as frequency range divided by **Block Size**.

By FRF generator program any FRF with known $M C K$ matrices can be generated and printed to binary files. By default the name of all binary FRF files starts with the letter “a”. Each FRF file consists of 3 columns of data. These columns are Frequency (Hz), real part of FRF and imaginary part of FRF.

For example for a 10 d.o.f system with known $M C K$ matrices, 100 binary FRF files will be created. These files are shown in Table 6-1

Table 6-1 FRF Table

Name of File	Input Number	Output Number
A1.txt	1	1
A2.txt	1	2
A3.txt	1	3
A4.txt	1	4
.	.	.
.	.	.
.	.	.
A10.txt	1	10
A11.txt	2	10
.	.	.
.	.	.
.	.	.
A100.txt	10	10

CHAPTER 7

VERIFICATION OF EMAS

7.1 Introduction

Experimental Modal Analysis Software (EMAS) is written and explained in Chapter 6. Before using this software in measured experimental data, it is compulsory to verify that the software is working properly and yields correct results. For this purpose, Frequency Response Functions are generated by using FRF Generator part of EMAS and analyzed by using Modal Parameter Estimation part of EMAS. Modal Parameters obtained From EMAS are compared against theoretical values.

7.2 Verification of EMAS using 3. d.o.f Model

A 3-dof model with proportional damping M C K matrices; are defined as below.

$$M = \begin{bmatrix} 8 & 0 & 0 \\ 0 & 10 & 0 \\ 0 & 0 & 12 \end{bmatrix} \quad C = \begin{bmatrix} 13 & -6 & 0 \\ -6 & 11 & -5 \\ 0 & -5 & 5 \end{bmatrix}$$

$$K = 10000 \times \begin{bmatrix} 26 & -12 & 0 \\ -12 & 22 & -10 \\ 0 & -10 & 10 \end{bmatrix}$$

Nine binary FRF files are generated by FRF Generator part of EMAS and loaded to EMAS using FRFL program. The M C K matrices are assumed to belong to a cantilever beam (for animation purposes) and node location, element connection information are prepared accordingly. The input file is given in Table 7-1. The Input file is loaded to EMAS using Input File Editor program. Figure 7-1 shows the CMIF plot for the generate FRF data including selected peaks.

Table 7-1 Input File for 3 D. o. f. system

```

title 3 d.o.f cantilever beam (Units Length: N Force: m)

node 1,  0.0,  0.0,  0.0
node 2,  1,  0.0,  0.0
node 3,  2  0  0
node 4   3  0  0

elemtype beam3d

elem  1, 1, 2
elem  2 2 3
elem  3 3 4

allmasterdof 3

constnode 1

```

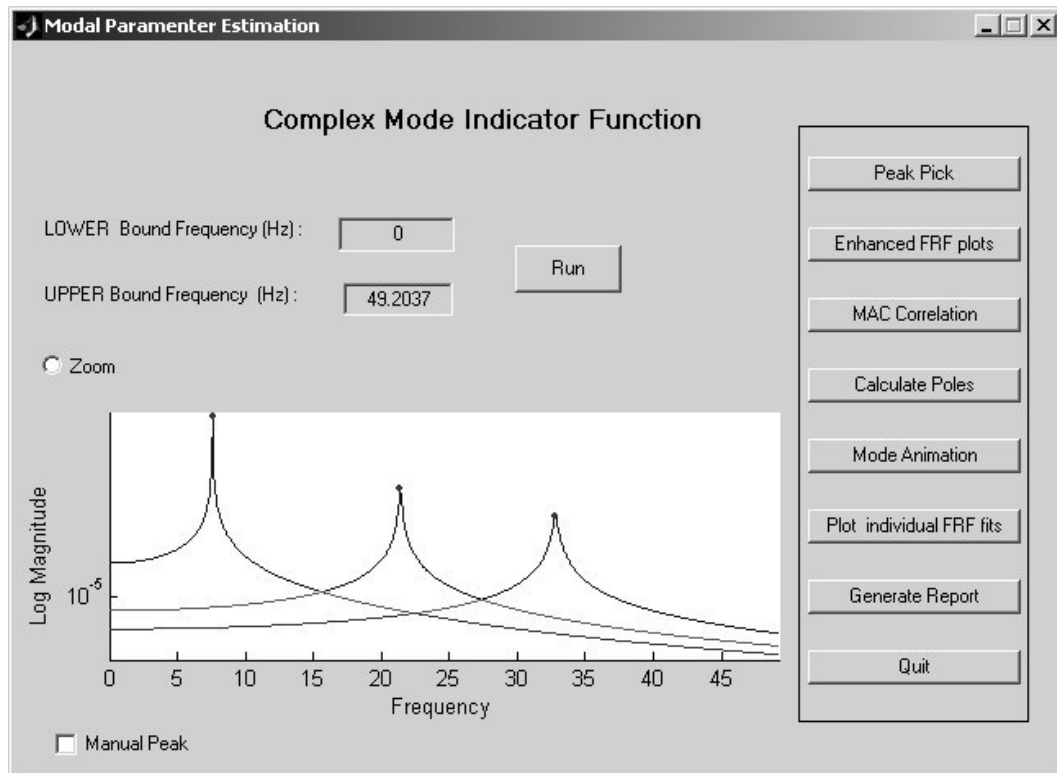


Figure 7-1 CMIF Plot for 3 d.o.f problem

7.2.1 Enhanced FRF Plots & eFRF Plots with Synthesized Peaks

The selected verification model has three degrees of freedom (d.o.f). Three Enhanced FRF (eFRF) plots exist for a three d.o.f. system, which are used for pole, modal scaling, and residue calculation. These plots are represented through Figure 7-2 to Figure 7-4. As it can be seen from these plots, each eFRF plot isolates a single mode so that a simple single degree of freedom parameter estimation algorithm can be used to estimate poles and modal scale factors for the enhanced mode. For each mode, 10 data points are used for before and after each peak. Number of B terms is selected as 3 (Selecting B value very high causes stability problems and thus causes numerical errors). Selecting B value very small causes an

under estimation of modal parameters). eFRF plots with synthesized peaks are represented through Figure 7-5 to Figure 7-7. The peaks are synthesized by using the modal parameters obtained from Modal Parameter Estimation (MPE) for the 20 data points for each mode.

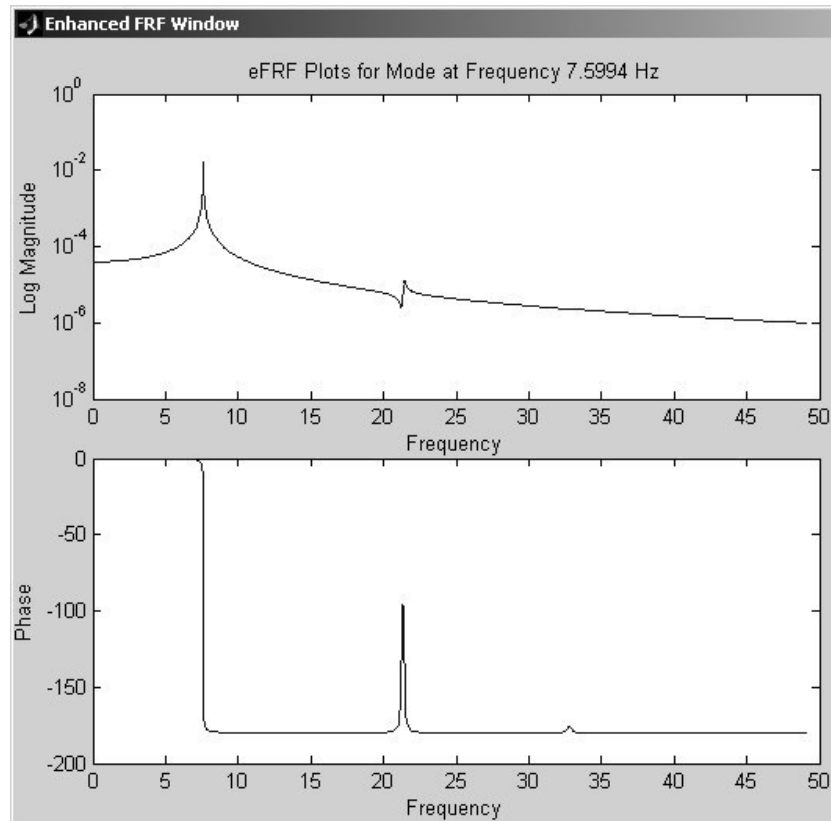


Figure 7-2 eFRF plot for 1st Mode

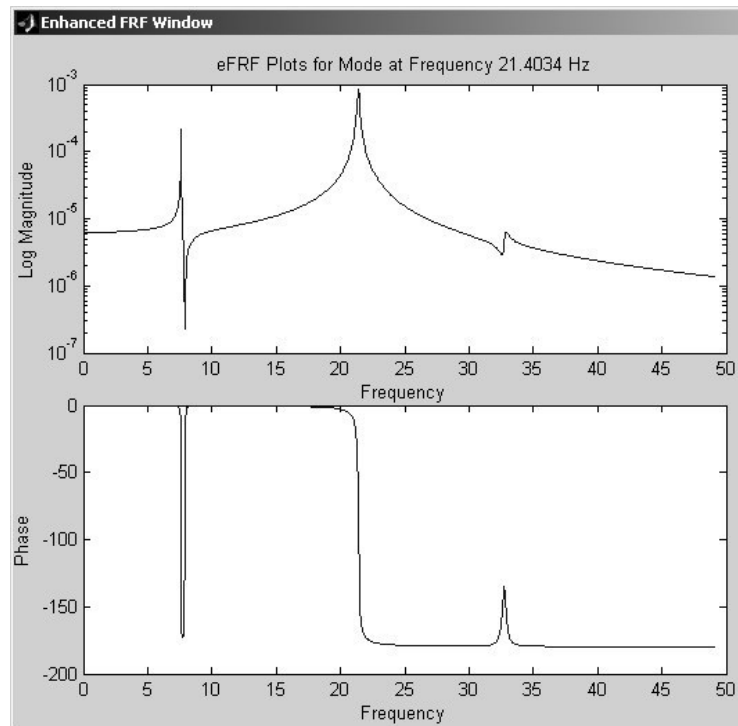


Figure 7-3 eFRF plot for 2nd Mode

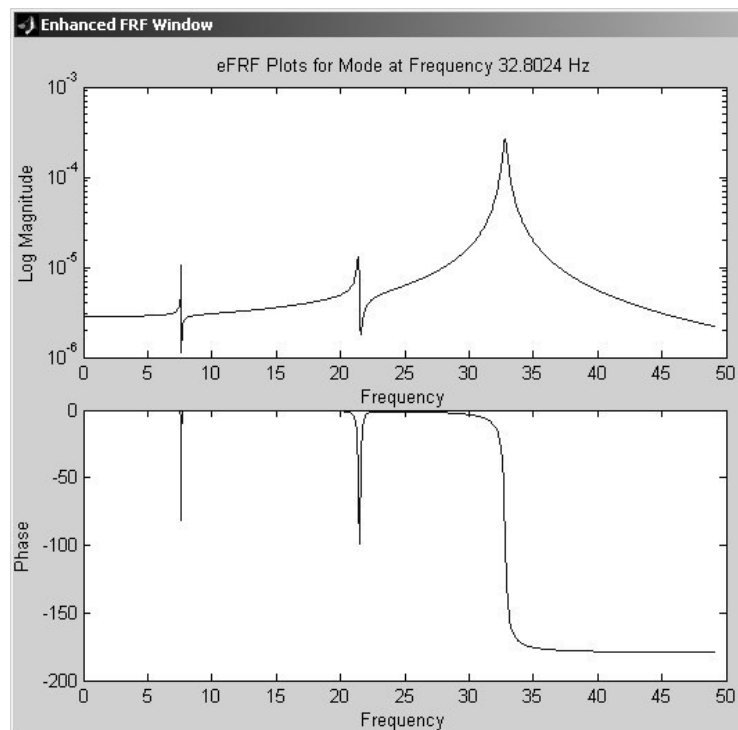


Figure 7-4 eFRF plot for 3rd Mode

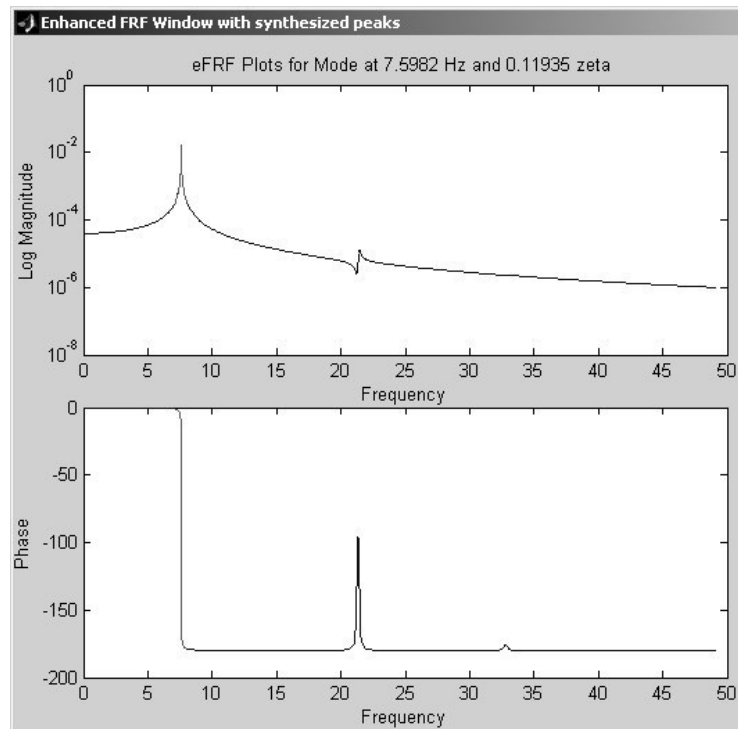


Figure 7-5 eFRF plot with synthesized peak for 1st Mode

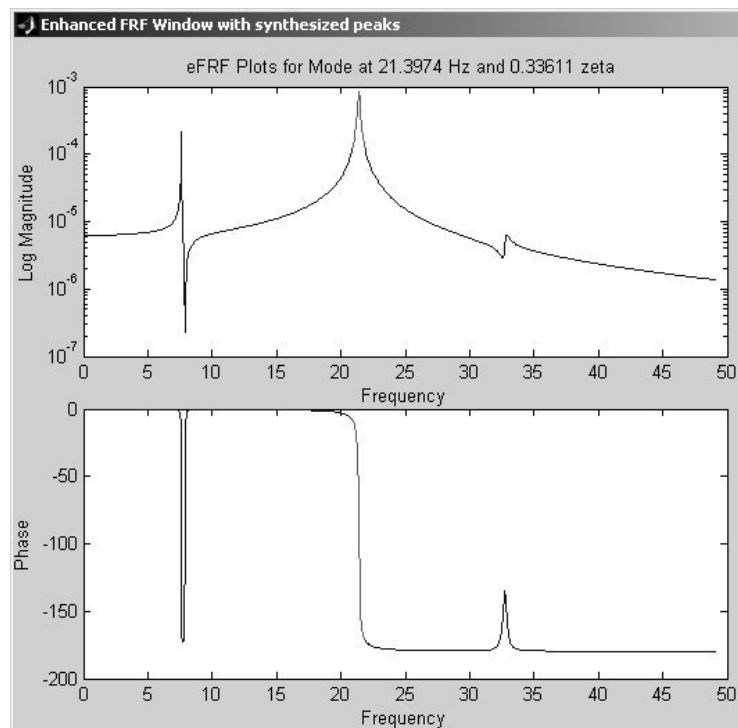


Figure 7-6 eFRF plot with synthesized peak for 2nd Mode

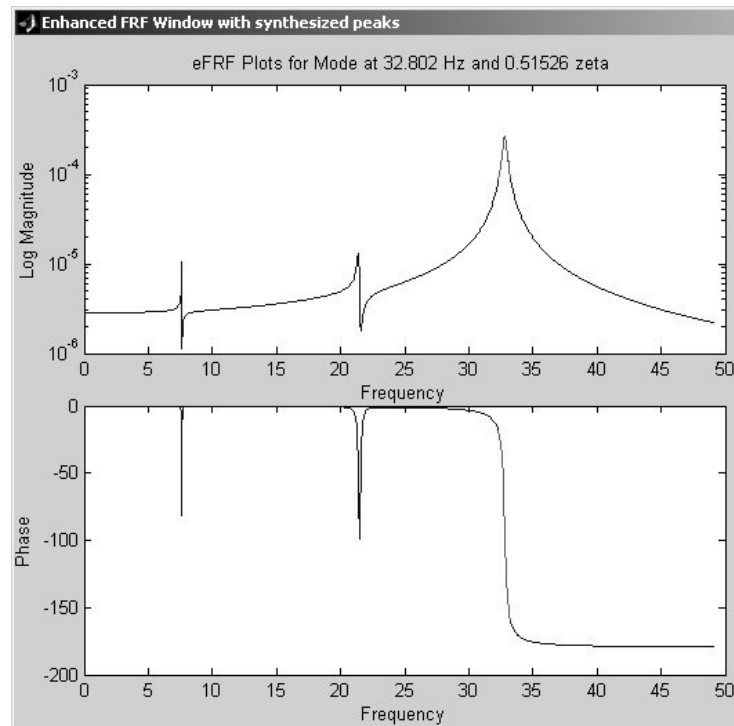


Figure 7-7 eFRF plot with synthesized peak for 3rd Mode

7.2.2 MPE Results

Modal parameters obtained from MPE part of EMAS are given in Table 7-2. In the following Sections the theoretical results are represented and compared against MPE results.

Table 7-2 Modes and corresponding Freq-damping (Experimental)

Mode	Natural Frequency (Hz)	Damping (%)
1	7.598	0.119
2	21.397	0.336
3	32.802	0.515

7.2.3 Measurement Synthesis

It is useful to compare the reconstructed FRFs with measured (original) FRFs (see Section 5.2 for further details). The reconstructed Frequency Response Functions for the selected 3 d.o.f. system are compared against the original data through Figure 7-8 to Figure 7-16. In general, the reconstructed FRF curves successfully match the original curves. Small differences between the curves are addressed to numerical and truncation errors.

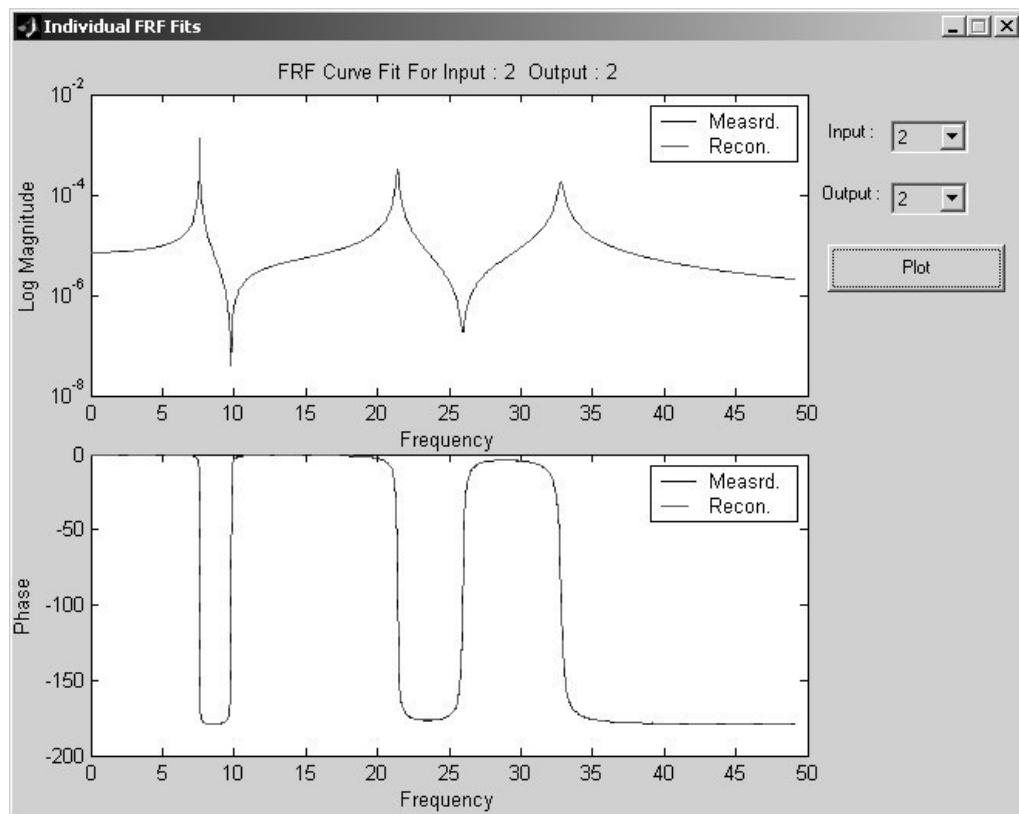


Figure 7-8 Actual FRF vs. Generated FRF for Input: 2 Output: 2

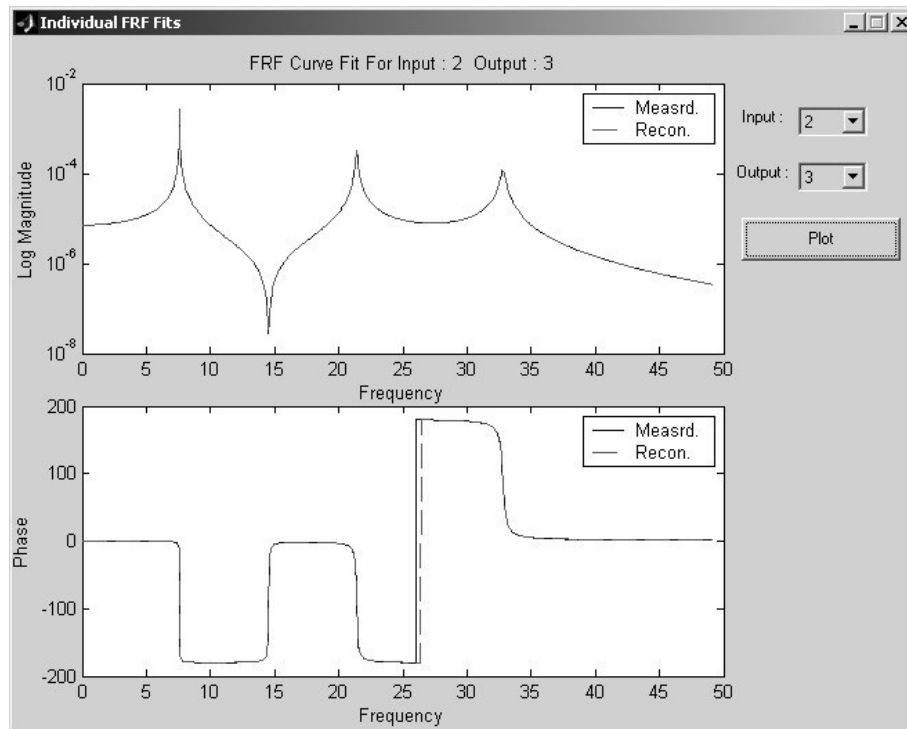


Figure 7-9 Actual FRF vs. Generated FRF for Input: 2 Output: 3

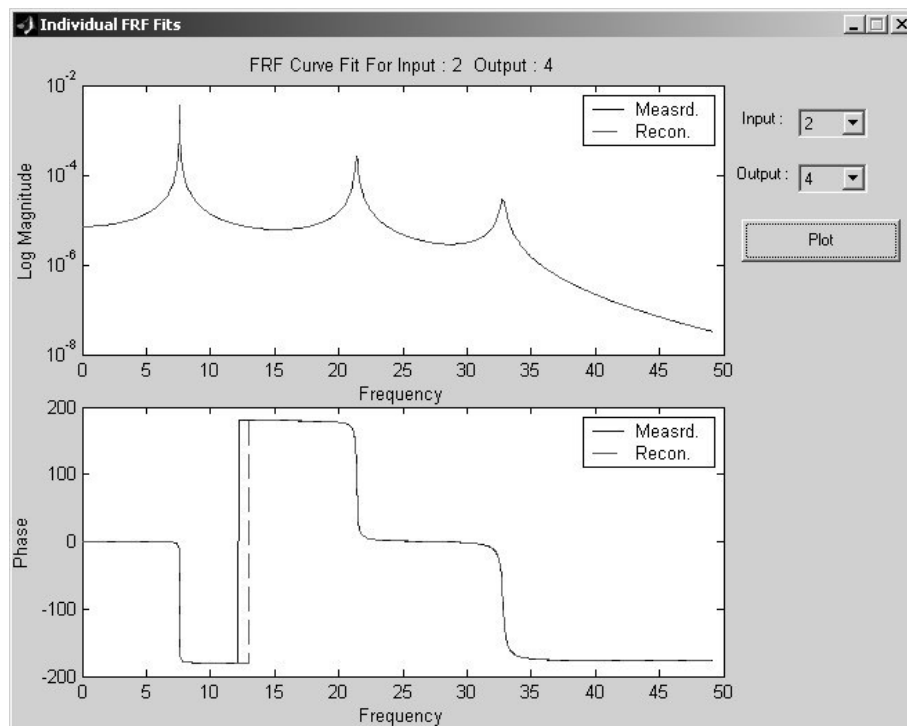


Figure 7-10 Actual FRF vs. Generated FRF for Input: 2 Output: 4

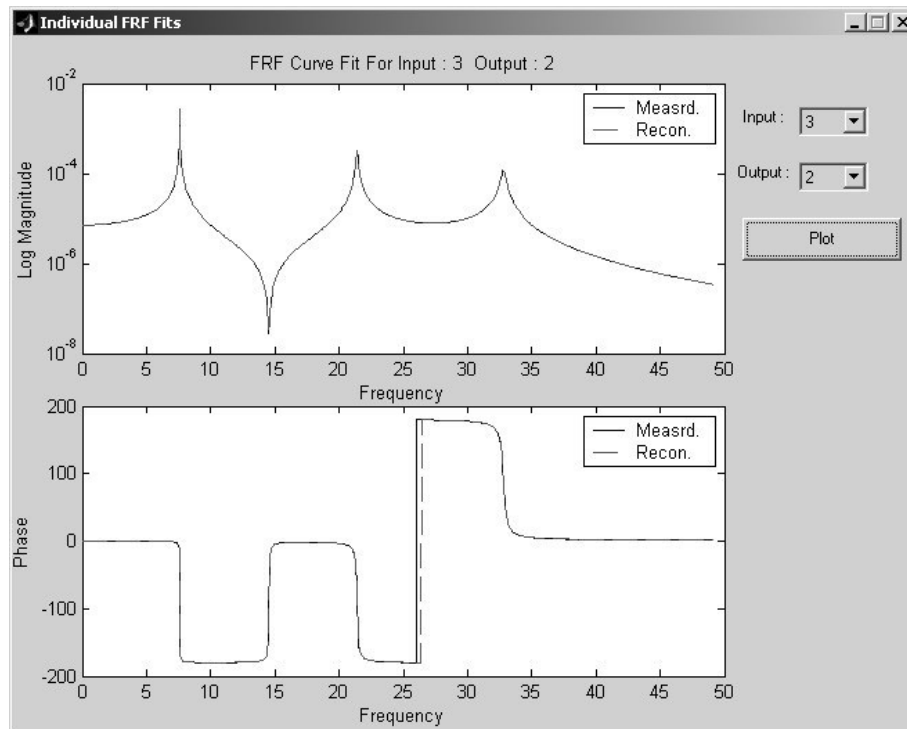


Figure 7-11 Actual FRF vs. Generated FRF for Input: 3 Output: 2

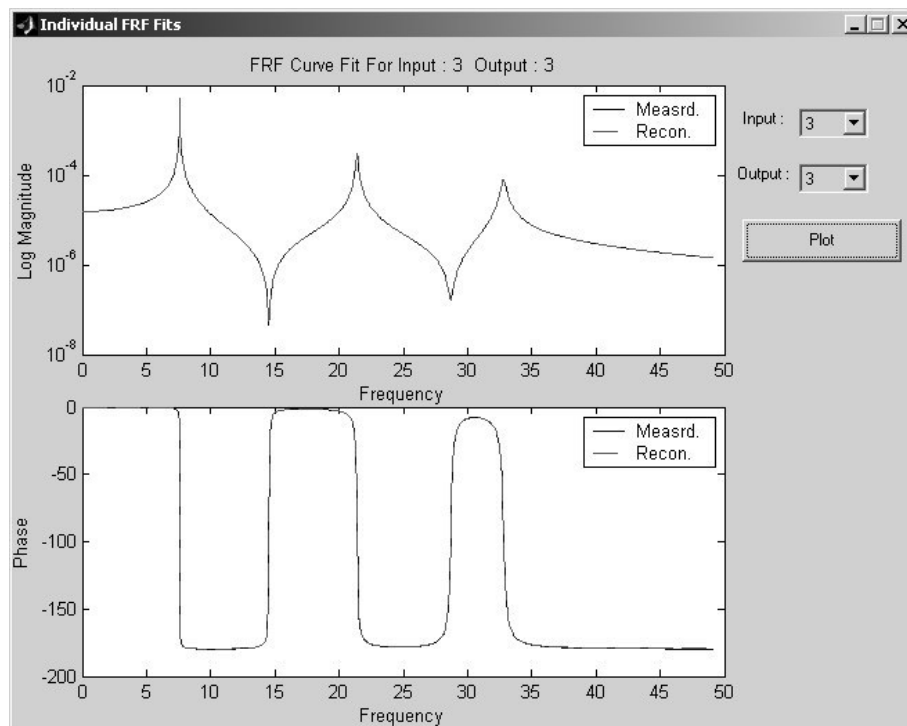


Figure 7-12 Actual FRF vs. Generated FRF for Input: 3 Output: 3

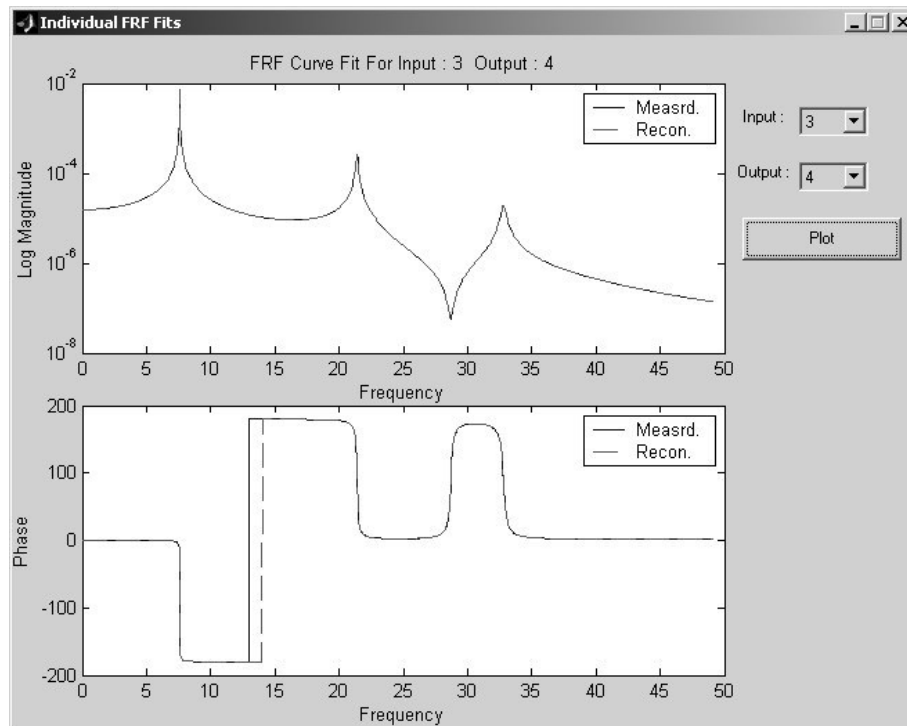


Figure 7-13 Actual FRF vs. Generated FRF for Input: 3 Output: 4

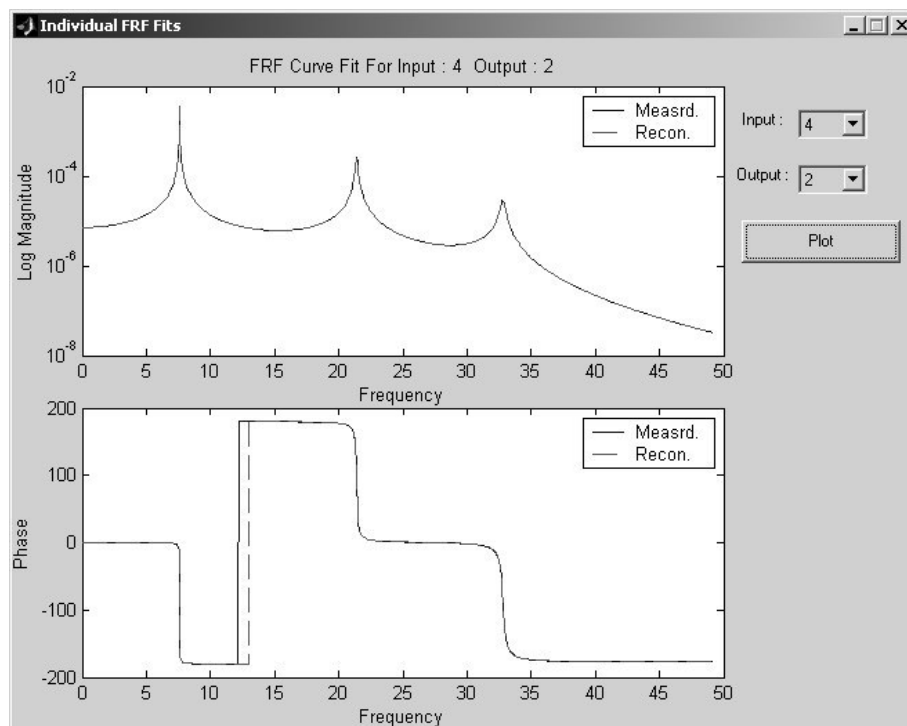


Figure 7-14 Actual FRF vs. Generated FRF for Input: 4 Output: 2

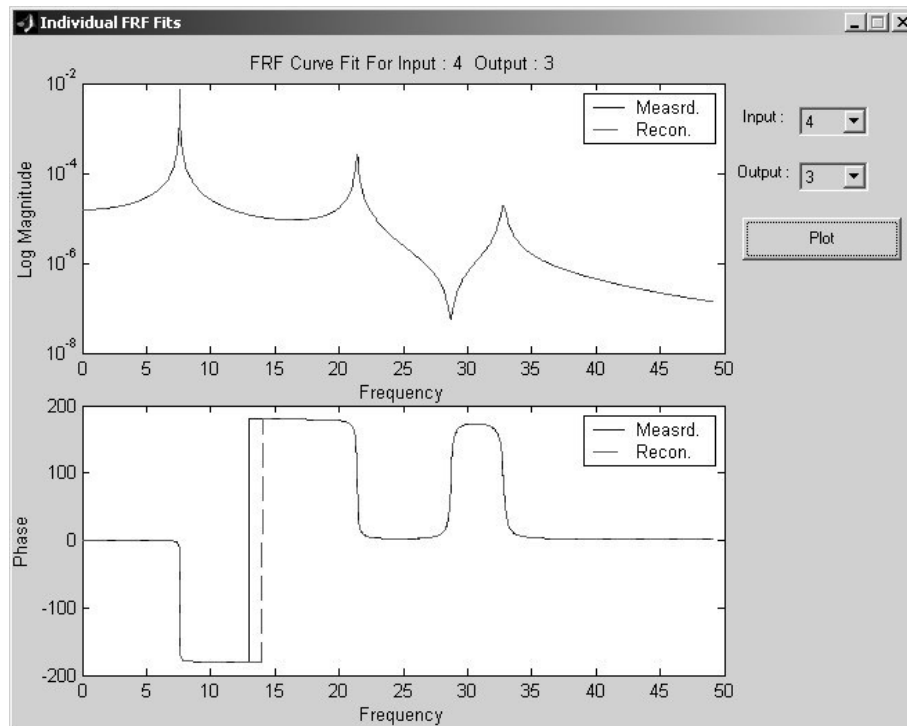


Figure 7-15 Actual FRF vs. Generated FRF for Input: 4 Output: 3

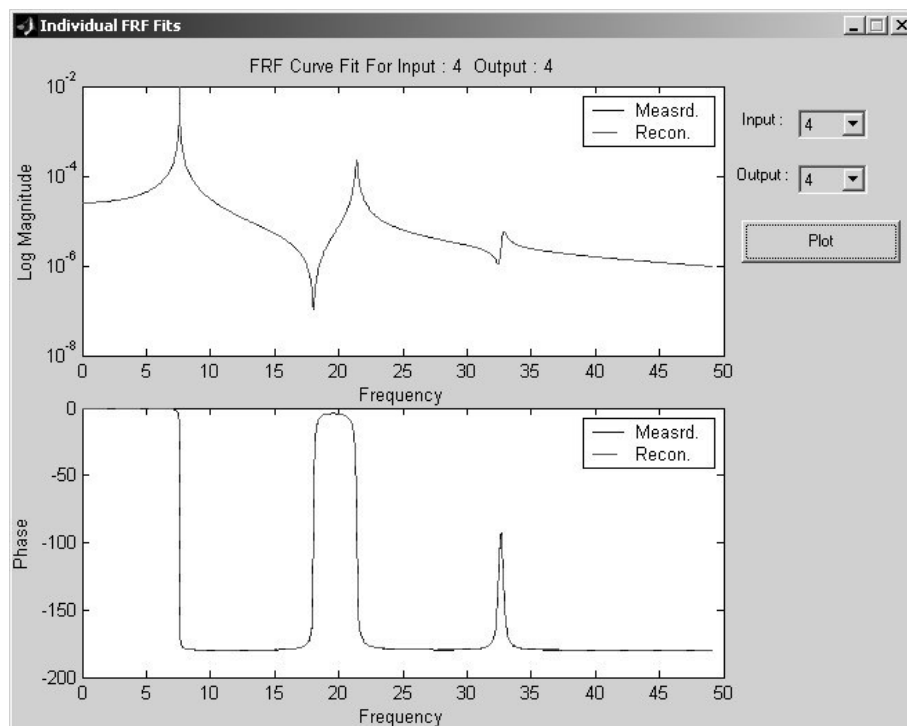


Figure 7-16 Actual FRF vs. Generated FRF for Input: 4 Output: 4

7.2.4 Visual Verification

The visual verifications are carried out using mode shape animations. The mode shape animation of the selected 3 d.o.f cantilever system is represented through Figure 7-17 to Figure 7-19.

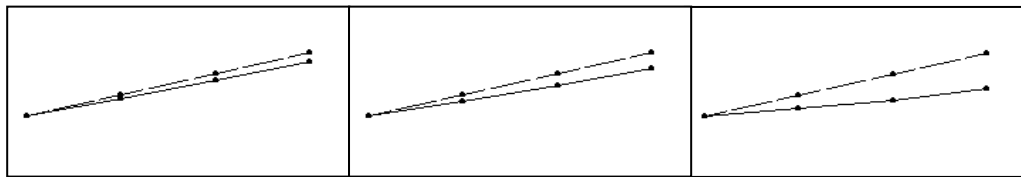


Figure 7-17 Animation of Mode 1

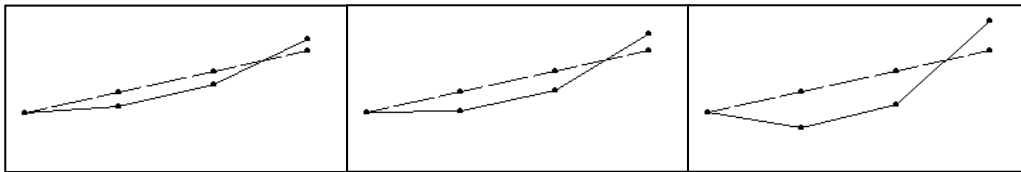


Figure 7-18 Animation of Mode 2

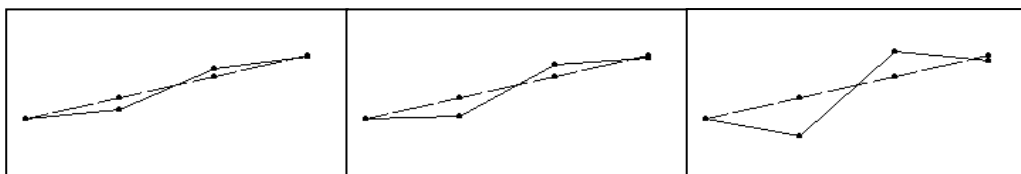


Figure 7-19 Animation of Mode 3

It is typical of the modes that 1st mode exhibit no sign change, 2nd mode exhibit one sign change, and 3rd mode exhibit two sign changes. Correspondingly, 1st mode does not have a point of zero displacement whereas the second and third modes have one and two points of zero displacement respectively.

The animated mode shapes shown, successfully represent the general behavior of the three vibration modes of a cantilever beam. The results pass the visual verification.

7.2.5 Modal Assurance Criterion (MAC) Correlation

MAC correlation gives us information about how well two modes correlate. Theoretically any two different modes of a structural system are orthogonal to each other. Therefore the MAC values of two different modes should theoretically be equal to zero, and MAC values of the same modes must be equal to one. The MAC comparison matrix of the three modes from the generated FRF data is presented in Figure 7-20. The obtained results shown in Figure 7-20 supports the theory by unity values across the diagonal and zero values on the off diagonals. MAC correlation of the modes also shows that the obtained modes are different and orthogonal.

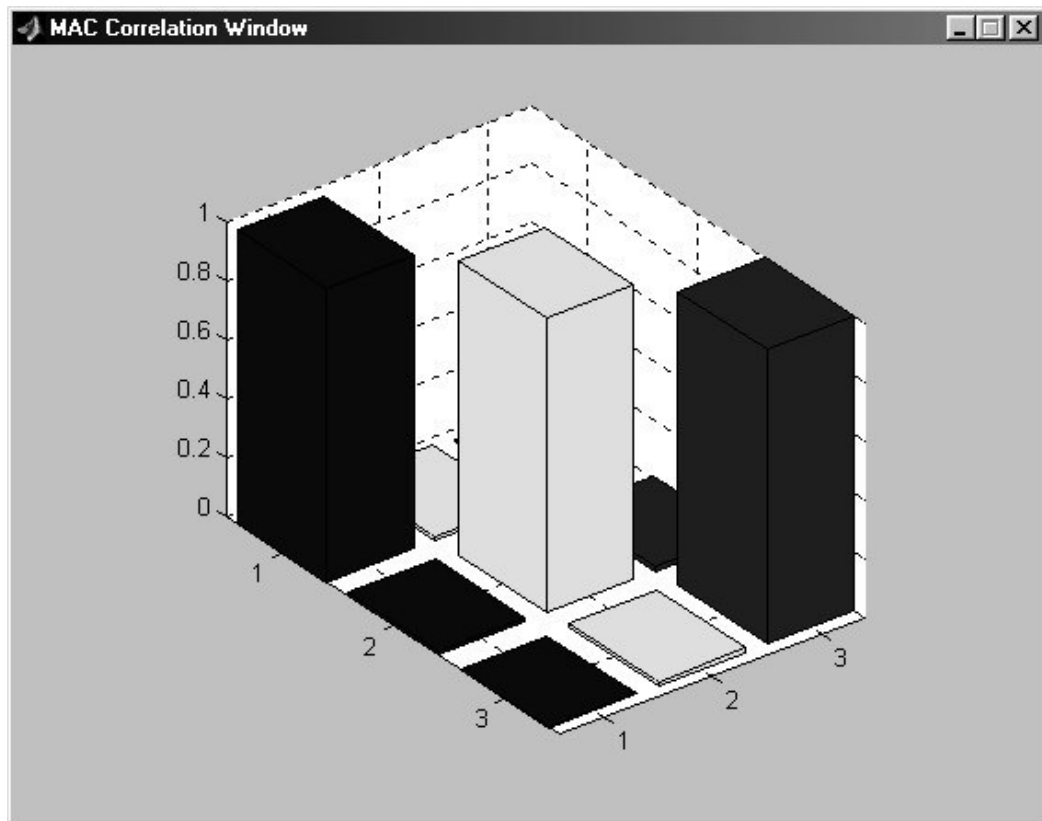


Figure 7-20 Bar Chart for MAC Correlation Matrix

7.2.6 Comparison of Results Obtained from MPE Part of EMAS Against Theoretical Results

In order to compare the results obtained with MPE part of EMAS, the selected 3 d.o.f. system is analyzed by using state-space formulation. The state space formulation of $M \ C \ K$ system is explained in Chapter 4, Section 4.5. Results obtained from state-space formulation are presented in Table 7-3. Percentage error between results obtained from MPE part of EMAS against theoretical results and theoretical results are shown in Table 7-4.

Table 7-3 Modes and corresponding Freq-damping (Theoretical)

Mode	Natural Frequency (Hz)	Damping (%)
1	7.598	0.119
2	21.397	0.336
3	32.802	0.515

Table 7-4 Percentage error between experimental and theoretical results

Mode	Natural Frequency (%)	Damping (%)
1	2.469e-8	-1.572e-4
2	1.02e-8	-6.631e-4
3	5.120e-8	-4.532e-5

As it is shown in the above table (Table 7-4) the error between the results obtained from MPE part of EMAS and theoretical results are negligible. The highest percent error is $6.63\text{e-}4$. The above figures, plots, and tables verify that that EMAS is working properly and yields correct results. Also it is verified that FRF Generator part of EMAS is working properly. The report generated by the **Generate Report** part of EMAS for the selected 3 d.o.f. system is given in Appendix A.

CHAPTER 8

EXPERIMENTAL STUDY

8.1 Introduction

Modal parameter estimation using EMAS software was verified in Chapter 7. Therefore, the EMAS software is used with real experimental data. For the experimental modal analysis part a steel grid model is constructed in Structural Mechanics Laboratory. Testing and modal data acquisition was conducted in Vibration and Acoustic Laboratory of Mechanical Engineering Department because of the availability of proper measurement tools.

8.2 Specifications of Model

The constructed model is four bay single span skewed steel grid frame. The dimensions of the model are given in Figure 8-1. The members of model are hollow tube steel sections. The grid model had a skew angle of 15° . Joint details are given in Figure 8-2 through Figure 8-4. The joints are designed to transmit bending moments using two cover plates at the top and bottom surface. Each member is connected using two bolts. The longitudinal members kept continuous and transverse members were cut from the original material.

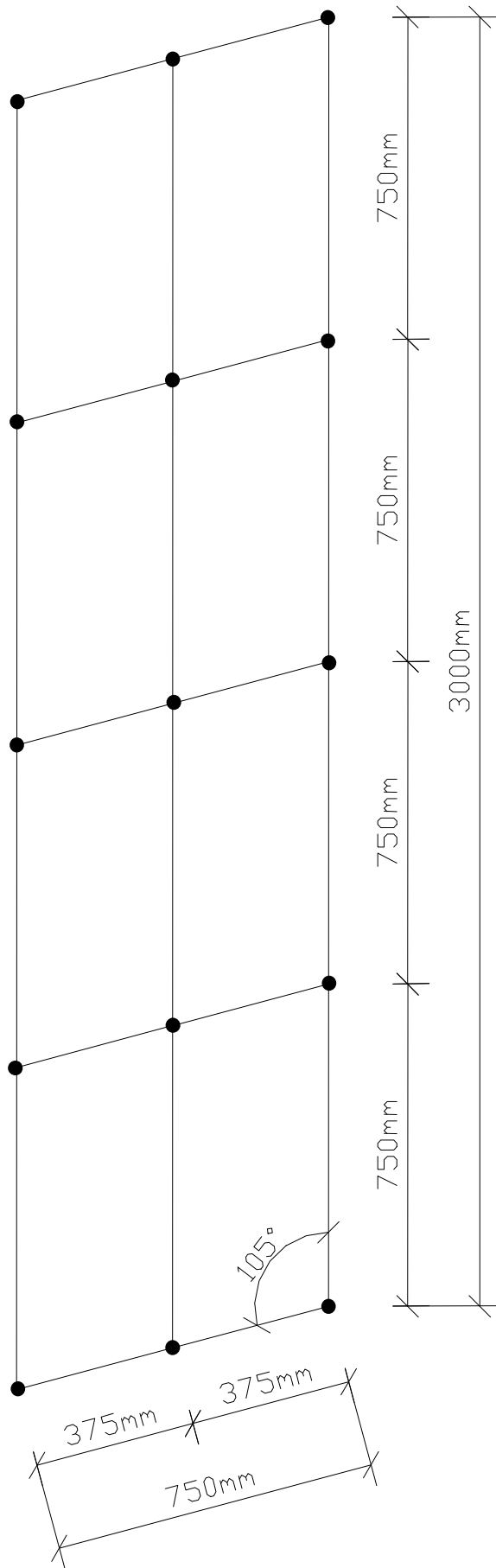


Figure 8-1 Dimensions of 4 bay single span skewed steel grid frame

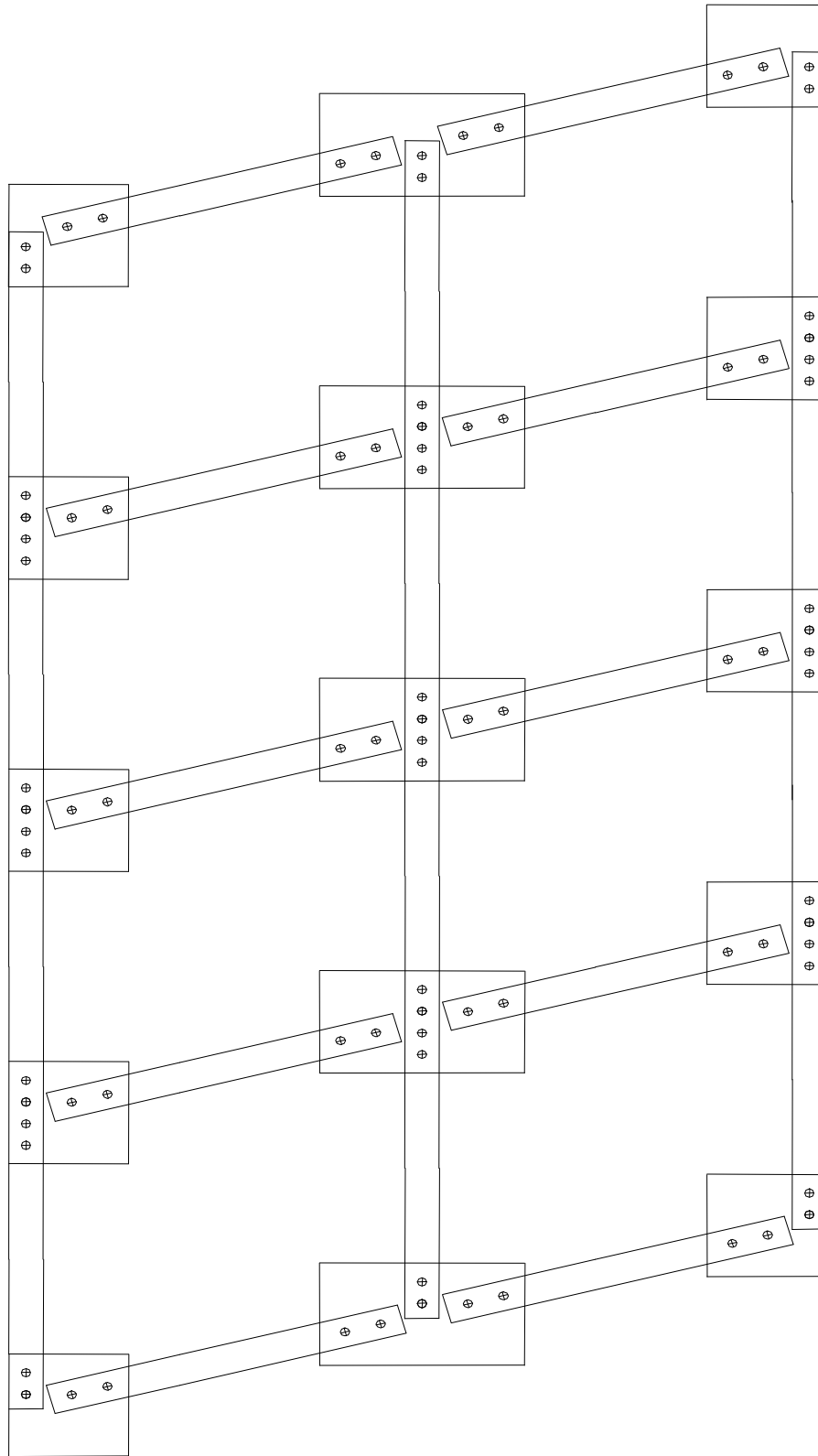


Figure 8-2 Joints details of all connections

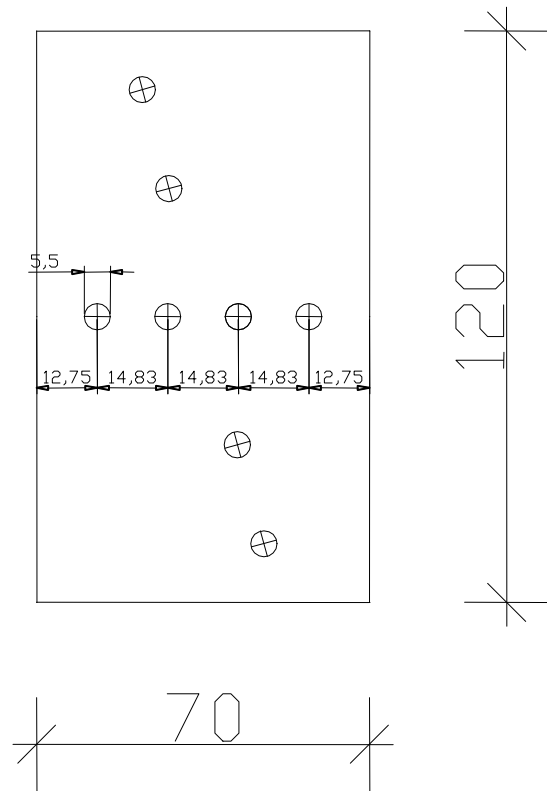


Figure 8-3 Joint detail for a mid joint (dimensions in mm)

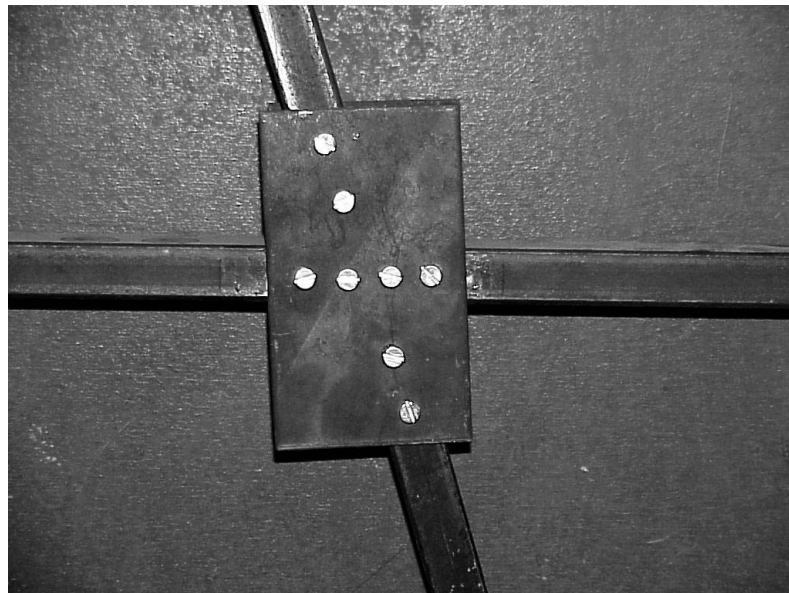


Figure 8-4 Joint detail of a mid joint

8.3 Boundary Conditions

The model was tested in free-free boundary conditions. It is not exactly possible to simulate free-free boundary conditions in an actual experiment. The only way to simulate free-free boundary conditions is to hang the model from several points to a fixed place using elastic/rubber bands.

For this purpose the model is suspended from a steel frame by low stiffness elastic bands. The stiffness difference between the elastic bands and the steel grid is very large. Therefore, the dynamic response of the test model became close to a free-free support condition. Elastic rods and steel frame are shown in Figure 8-5 and Figure 8-6. Theoretically, the rigid body modes exist at 0 Hz frequency for free-free boundary conditions. The rubber bands have a certain amount of stiffness causing the rigid body mode frequencies to slightly shift from zero (0) Hz. The existence of rubber bands over the actual modes and higher modal frequencies were minimal and it is not possible to simulate free-free boundary conditions in real life without using elastic rods to hang up the model. Furthermore, hanging the model in air using elastic bands is a common practice in modal testing practice.

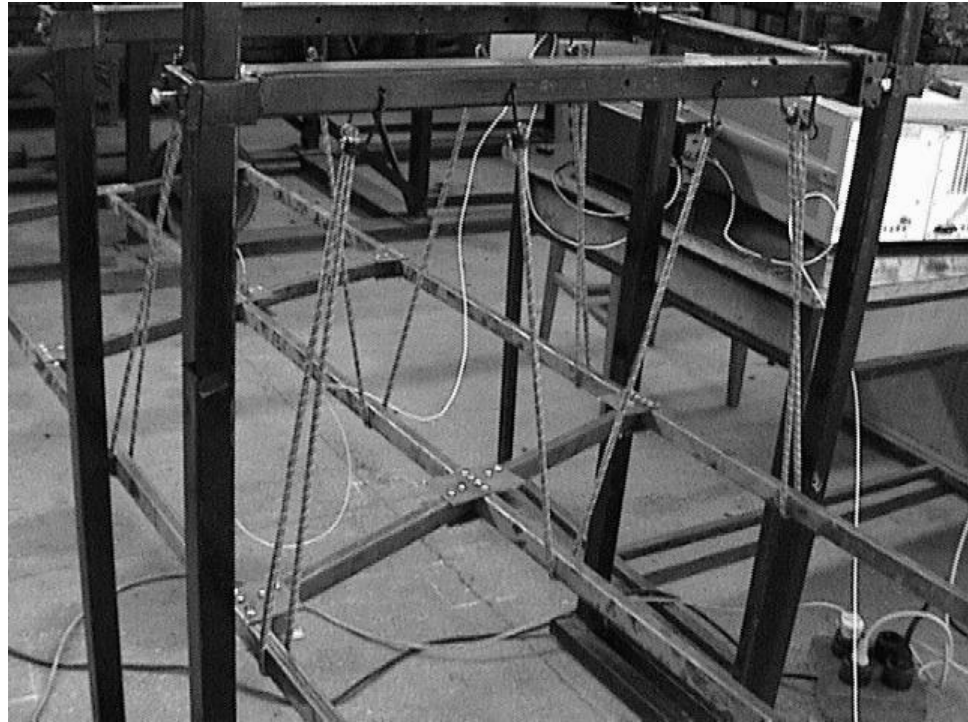


Figure 8-5 Steel Frame and elastic bands

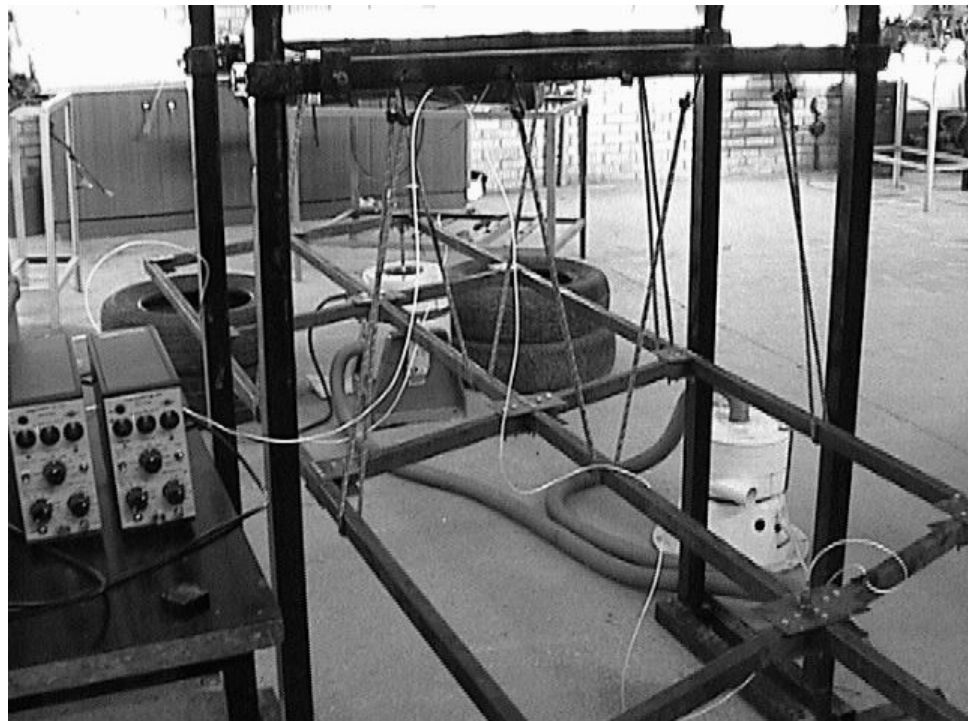


Figure 8-6 Steel Frame and elastic bands

8.4 Excitation

Swept sine periodic deterministic signals are used for frequency response function estimation. In order to generate signals a LDS shaker system is used. LDS shaker system consists of 3 parts. These are

1. Shaker
2. Cooling system
3. Signal Generator.

These parts are shown in Figure 8-7 and Figure 8-8.



Figure 8-7 LDS Signal Generator

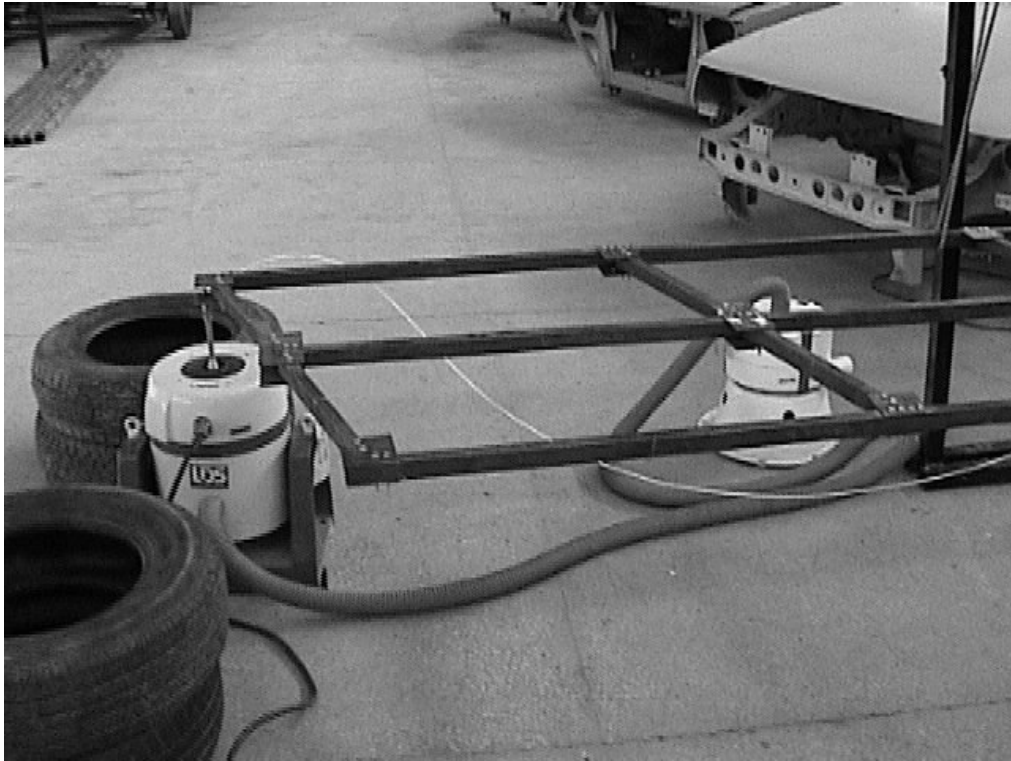


Figure 8-8 LDS Shaker and LDS Cooling System

The shaker system supplied excitation to the structural system and the response is measured using accelerometers.

8.5 Sensors

The response of the system is acquired by an accelerometer and the input (force) is acquired by a force transducer located at the tip of the shaker system. Bruel& Kjaer force transducer and accelerometer are used in the experiments. Figure 8-9 shows accelerometer and Figure 8-10 shows force transducer. Since accurate measurement of the force transmitted to model is crucial, the force transducer is placed at the top of the shaker rod. In this way, actual force applied to the structure is measured.

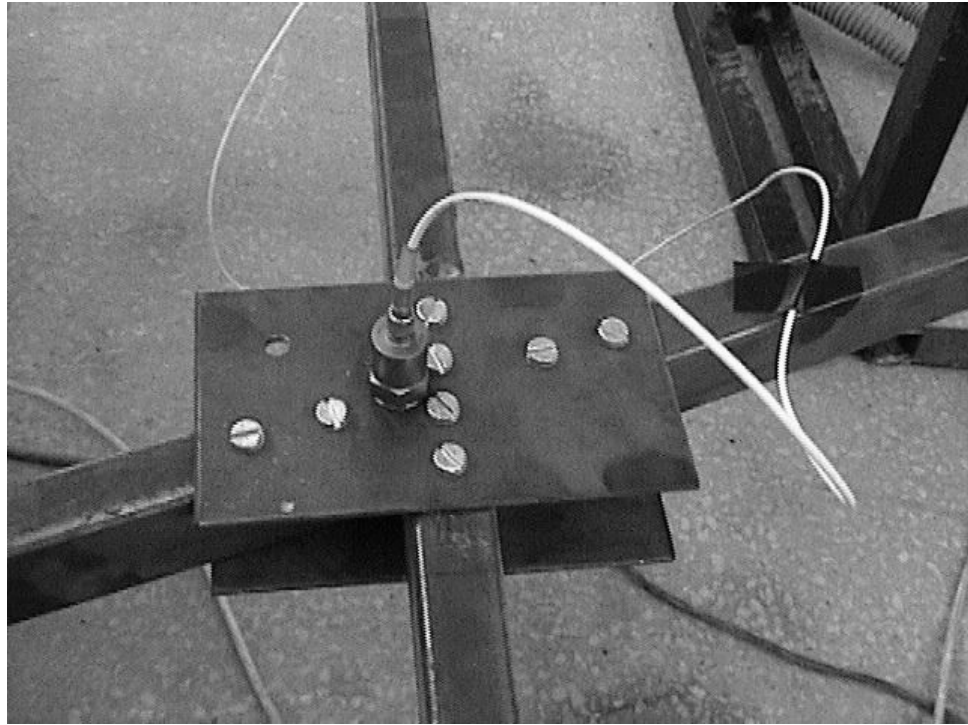


Figure 8-9 Accelerometer

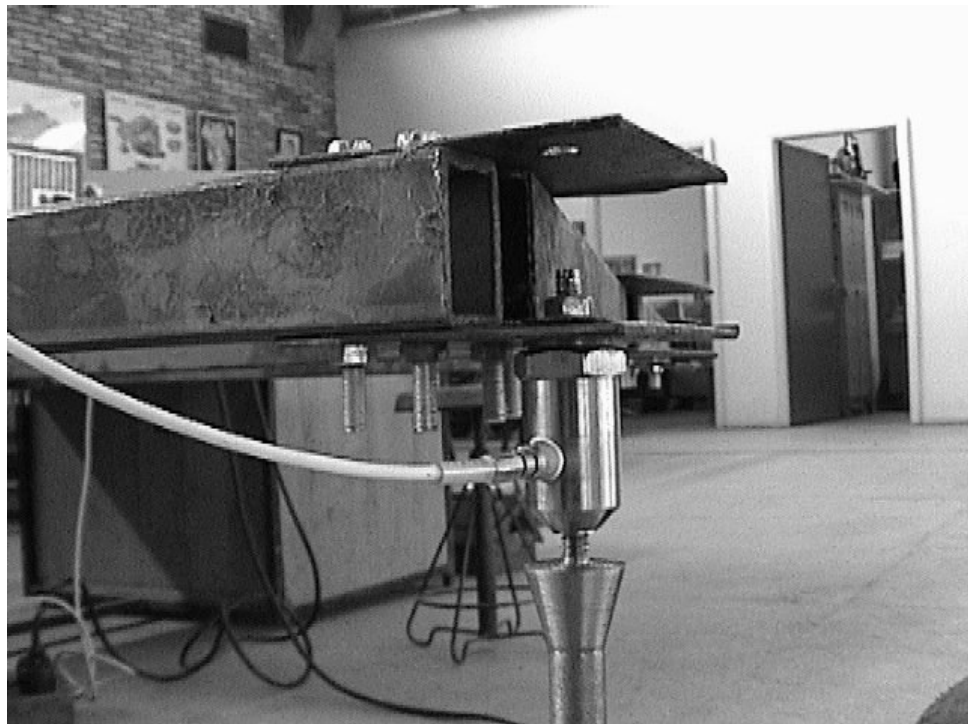


Figure 8-10 Force Transducer

8.6 Dynamic Signal Analyzer

The data acquired from accelerometer and force transducer are first amplified and then sent to Dynamic signal analyzer for frequency response calculations. Hp 35665A dynamic signal analyzer is used for the measurement. Hp 35665A dynamic signal analyzer is shown in Figure 8-11. The amplifiers used to condition and increase the signal level are used between the transducers and acquisition system as shown in Figure 8-12. The signal analyzer has a built in macro to measure the response at each frequency to obtain frequency response function (FRF). An example FRF obtained during testing is seen in the display of the dynamic signal analyzer Figure 8-13.

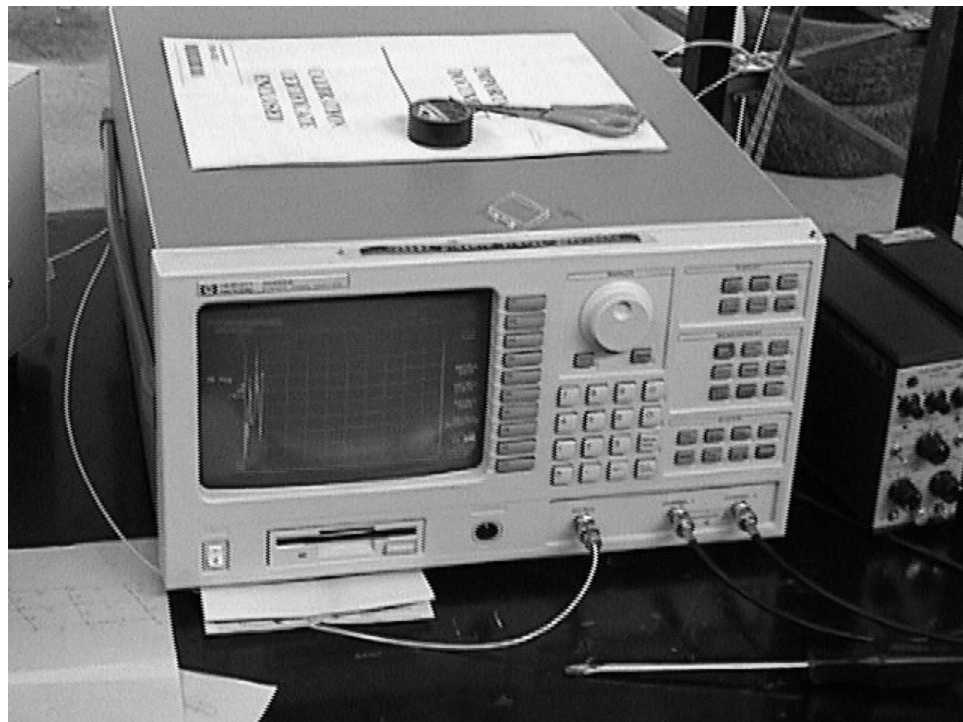


Figure 8-11 Hp 35665A Dynamic Signal Analyzer



Figure 8-12 Bruel & Kjaer Amplifiers

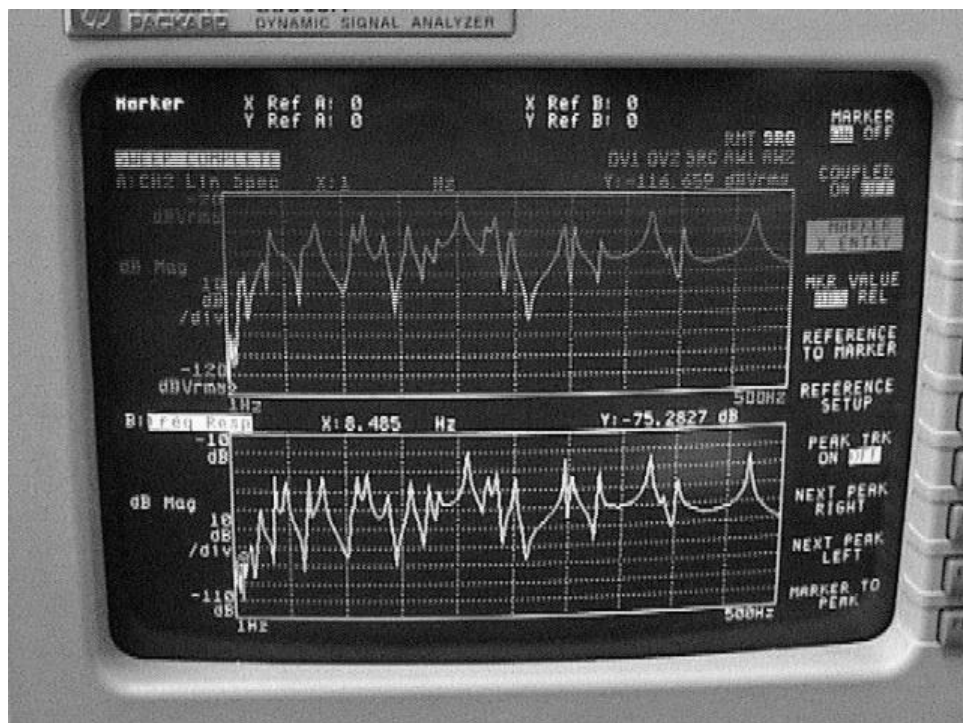


Figure 8-13 Display of Dynamic Signal Analyzer

8.7 Modal Data Acquisition & Parameters

In this experiment 2 input and 37 output d.o.f are used. Two different tests are conducted by relocating the excitation location. The model is excited in vertical direction at node 1 and node 33 separately. The responses in vertical direction are measured one by one at each nodal location. Node numbers are shown in Figure 8-14. For the first experiment, frequency range of 1-500 Hz is scanned with a frequency interval of 1.2475 Hz where 401 data points are used. For the second experiment frequency range of 1-260 Hz is scanned with a frequency interval of 0.6475 Hz where again 401 data points are obtained. It is realized from the first experiment that using a frequency range of 1-500 with 401 data points will lead coarse results since frequency interval is high. Therefore in the second experiment the frequency range is reduced to 1-260 and therefore the sensitivity of the experiment is almost doubled. In both experiments a delay block of 10 cycles and capture block of 10 cycles are used for each one of the 401 measurement frequencies.

The first experiment took about 10-12 minutes to obtain one FRF for a single node (one input-output pair). The second experiment took about 6-8 minutes to complete a single node FRF measurement. The measured frequency response functions (FRF) are recorded to 3½ Floppy diskette at the end of each test. This procedure is repeated for all nodes (37 times) for each experiment. The files recorded to diskette are in special DAT file format which are only accessible using Hp 35665A dynamic signal analyzer's own program. The name of the program is SDFTOASC.EXE. By the help of this program DAT files that are originally in BINARY format are

converted to ASCII files which can be easily read by and word processor. The program works in MS-DOS Prompt where the command line is as follows:

```
SDFTOASC  DATFILE.dat  ASCIIFILE.txt  /x/a
```

Where;

DATFILE.dat is converted to an ASCII file with extension txt. The structure of these ASCII files are the same as FRF files generated by FRFGEN software (refer to Section 6.1.2.4).

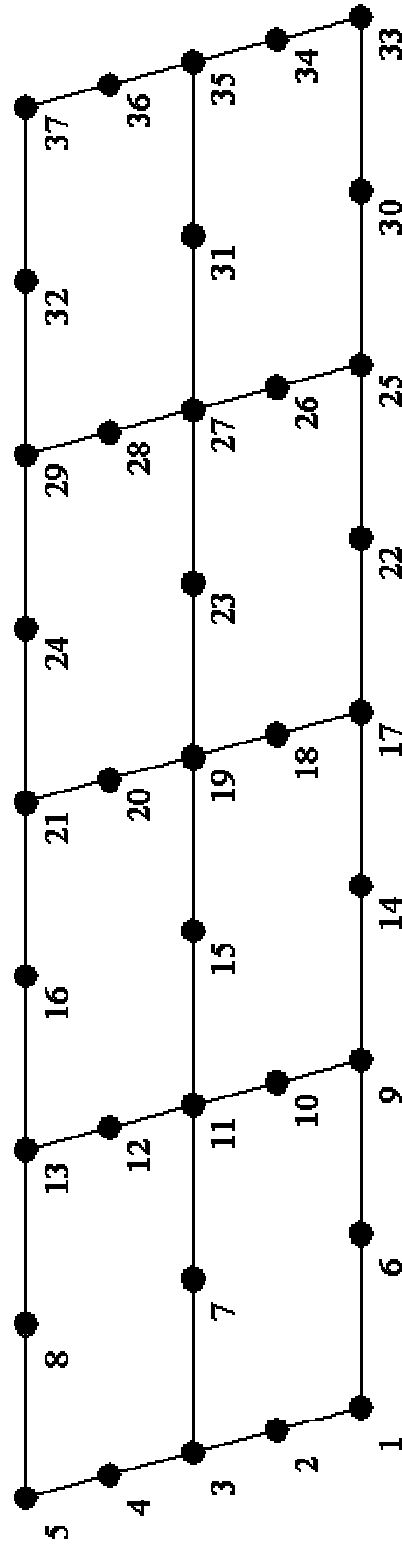


Figure 8-14 Node Numbering of the Model

8.8 Input File of Model

The model input file prepared for the EMAS software is given in Table 8-1.

Commands used in this input file are explained in Chapter 6.

Table 8-1 Input File for model

```
title skewed frame Problem
node 1, 0, 0.0, 0.0
node 5, -0.1941142838, 0.7244443697, 0.0
node 33, 3, 0.0, 0.0
node 37, 2.8085885716, 0.7244443697, 0
nodegen 1 33 3 9 8
nodegen 5 37 3 13 8
nodegen 1 5 3 2 1
nodegen 33 37 3 34 1
nodegen 9 13 3 10 1
nodegen 17 21 3 18 1
nodegen 25 29 3 26 1
nodegen 1 9 1 6 1
nodegen 25 33 1 30 1
nodegen 6 30 2 14 8
nodegen 3 11 1 7 1
nodegen 27 35 1 31 1
nodegen 7 31 2 15 8
nodegen 5 13 1 8 1
nodegen 29 37 1 32 1
nodegen 8 32 2 16 8
elemtype beam3d
elem 1, 1, 6
elem 2 6 9
elem 25 1 2
elem 9 3 7
elem 10 7 11
elem 17 5 8
elem 18 8 13
elemgen 1 3 3 2 8
elemgen 2 3 4 2 8
elemgen 25 4 29 4 8
elemgen 25 3 26 1 1
elemgen 26 4 30 4 8
elemgen 27 4 31 4 8
elemgen 28 4 32 4 8
elemgen 9 3 11 2 8
elemgen 10 3 12 2 8
elemgen 17 3 19 2 8
elemgen 18 3 20 2 8
allmasterdof 3
```

8.9 Data Loading

Frequency response functions (FRFs) obtained from the testing of experimental model using modal data acquisition system is loaded in to EMAS software with the help of FRFL program. The FRFs obtained from the tests are in accelerance type (acceleration/force). Thus, FRFs are converted from accelerance to receptance (displacement/force) in FRFL program. FRFL program is explained in Chapter 6.

8.10 Modal Parameter Estimation

MPE part of EMAS is used to estimate modal parameters from estimated Frequency Response Functions. MPE is used twice to obtain modal parameters from the first and second experiments respectively (see Section 8.7 for the explanation of the experiments).

8.10.1 First Experiment (Excitation at Node 1)

The CMIF plot with selected peaks for the first experiment is shown in Figure 8-15. The x-axis is used for Frequency (Hz) and y-axis plots Singular Values (dB) for each frequency. As previously stated in Chapter 4, the peaks in a CMIF plot indicate the existence of modes.

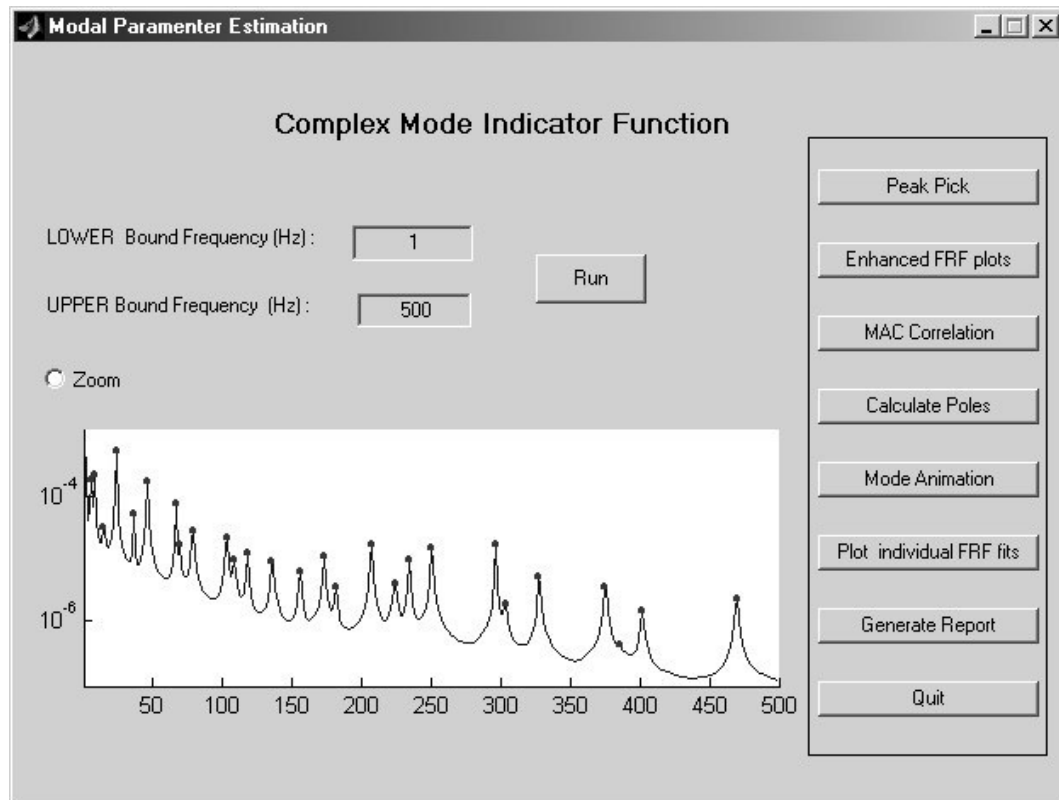


Figure 8-15 CMIF plot with selected peaks for the first experiment

MAC correlation of selected peaks (modes) is given in Figure 8-16. MAC correlates two selected modes and takes a value between 0 and 1. One refers to perfect correlation and zero refers to orthogonal vectors. The estimated experimental modes are correlated against each other. The diagonal values of the comparison matrix are equal to one since comparison of a mode by itself would be a perfect correlation. Similarly, off-diagonal values of the MAC matrix are expected to be zero. Examination of Figure 8-16 reveals that although off-diagonal terms are very small, they are not exactly equal to zero.

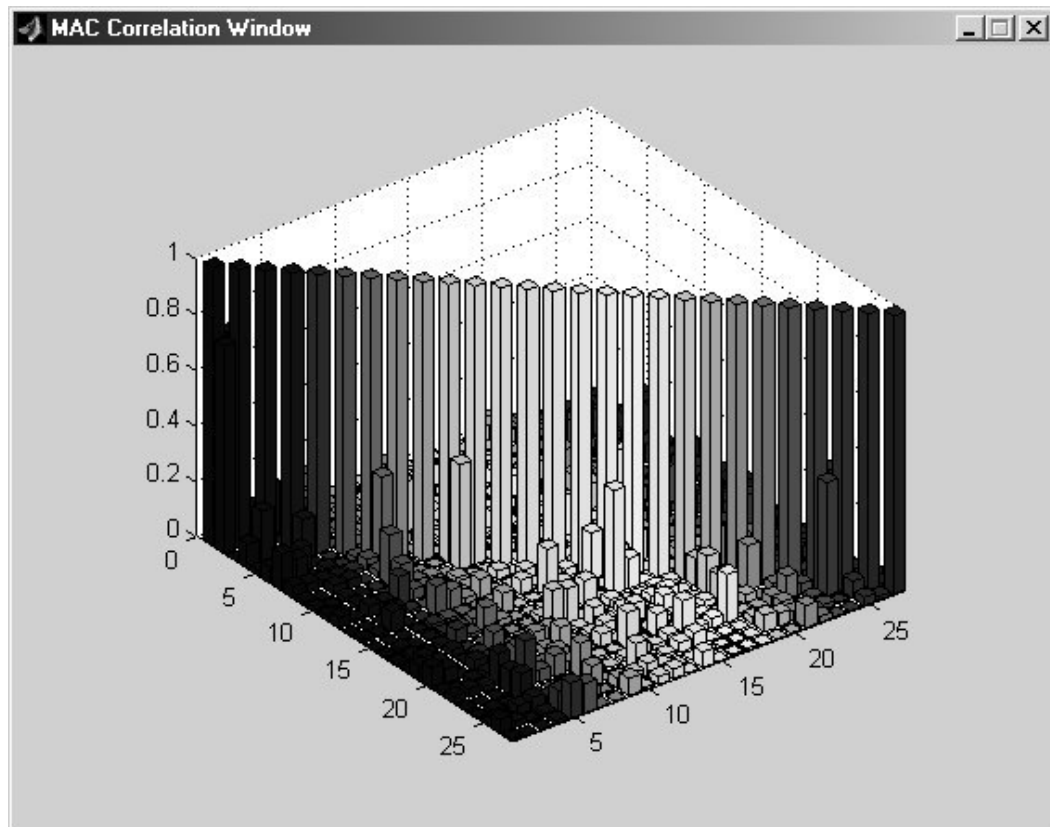


Figure 8-16 MAC correlation of the selected peaks

The post processing of experimentally obtained FRFs also reveal natural frequencies of the tested structural system. The natural frequencies and corresponding damping factors obtained from the post-processing are given in Table 8-2.

Table 8-2 Results of MPE for the first experiment

Mode	Natural Frequency (Hz)	Damping (%)
1	6.2325	1.6516
2	14.9984	0.62407
3	24.6408	0.11188
4	37.2949	0.17752
5	47.1186	0.07784
6	67.2184	0.045684
7	79.0423	0.51138
8	104.066	0.48815
9	109.891	0.6834
10	118.218	0.02049
11	136.269	0.38227
12	156.695	0.02718
13	172.872	0.25466
14	182.002	0.31377
15	207.665	0.13437
16	223.905	0.19216
17	234.085	0.07861
18	250.922	0.11491
19	296.531	0.03747
20	304.296	0.28217
21	328.367	0.10738
22	375.774	0.13905
23	401.75	0.1742
24	469.608	0.11824

8.10.2 Second Experiment (Excitation at Node 33)

The CMIF plot with selected peaks for the second experiment is shown in Figure 8-17. The x-axis is used for Frequency (Hz) and y-axis plots Singular Values (dB) for each frequency. As previously stated in Chapter 4, the peaks in a CMIF plot indicate the existence of modes.

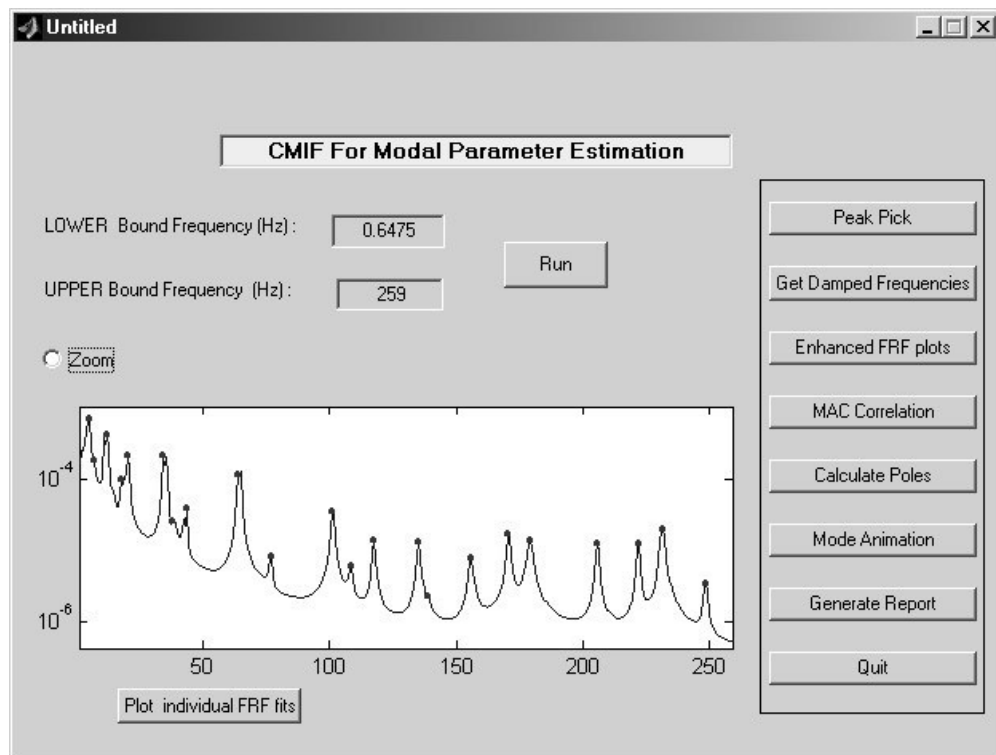


Figure 8-17 CMIF plot with the selected peaks

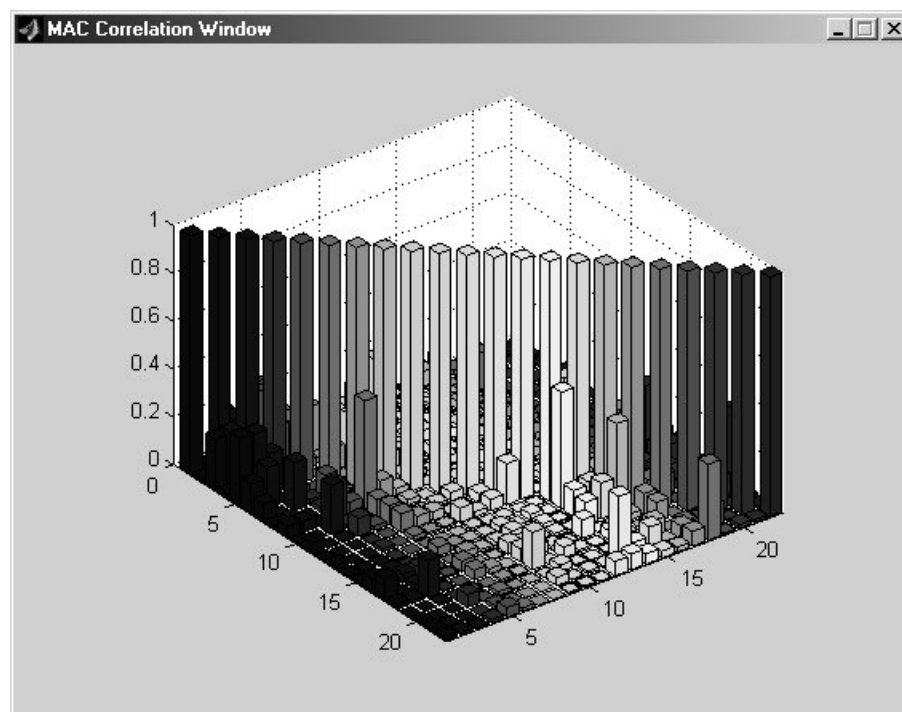


Figure 8-18 Mac correlation of selected peaks

Table 8-3 Natural Frequencies and corresponding damping factors obtained from experiment2

Mode	Natural Frequency (Hz)	Damping (%)
1	6.1892	1.5296
2	13.3584	0.87568
3	18.5315	0.7652
4	21.2636	0.54843
5	35.4435	0.26963
6	39.9946	0.3804
7	44.2785	0.1378
8	64.8885	0.1208
9	77.9366	0.6726
10	102.3701	0.21234
11	110.0407	0.67488
12	118.1387	0.085589
13	136.1027	0.26334
14	139.4138	0.52862
15	156.9301	0.35899
16	171.6848	0.29686
17	179.8252	0.34772
18	206.5501	0.10027
19	222.6988	0.14811
20	232.8387	0.03099
21	249.4215	0.22493

CHAPTER 9

FE UPDATING

9.1 Introduction

Modifying FE model in order to bring the FE model prediction into better agreement with the experimental results is referred as **FE Updating (FEU)**. There are several applications of FE Updating in literature (Examples: Ventura *et al.*, 2001, Dascotte, 2001 Haapaniemi *et al.*, 2002 Chen *et al.*, 2000, and Ewins *et al.*, 2001)

Fist step in FE Updating is to compare nominal FE model results with EMA results. If the difference between is within acceptable limits, then there is no need for FE Updating.

FE Updating Procedure can be divided into 3 parts. These are;

- a) Comparison of FEA results with EMA results (Objective Function Calculation).
- b) Modification of FE model in order to correlate FEM and EMA results (FEU Strategy)

- c) Analysis of modified FE model (FEA)

The above procedure is repeated until a convergence criterion is achieved. Each item in the above procedure is explained in detail below, not in the order above but in the order of the study.

9.2 Finite Element Analysis

For FE Updating purposes a Finite Element Analysis (FEA) code is developed and programmed in Matlab. The reason of using Matlab platform for programming is explained in Chapter 5. Since static analysis is out of scope of this study, FEA code is developed for **Free Vibration Analysis** only. Currently FEA code is capable to handle different type of elements. These are;

- a) 2D Frame Element
- b) 3D Space Frame Element
- c) 2D Mass Element
- d) 3D Mass Element
- e) 1D Spring Element

For all of the above Element types, literature survey is carried out, and Mass, Stiffness, and Transformation matrices are extracted /formulated. These informations are not given here but explained in detail in most of the books related with finite element Analysis and Dynamics (Cook *et al.*, 1989, Kwon, 1982 Chandrupatla *et al.*, 1997)

In order to reduce the computational cost of programmed FEA code. The following points are taken into consideration;

- 1) Banded mass, stiffness, and transformation matrices are used in matrix formulation.
- 2) Built in functions for Eigenvalue/Eigenvector analysis of Matlab is used.
- 3) Guyan Reduction technique is implemented for the analysis of large Finite Element Models where only a few number of degrees of freedom are of interest. Guyan Reduction technique is explained in detail in Chandrupatla *et al.*, 1997

Taking into consideration of the above points, fast, reliable, and computationally cheap FEA software is programmed for Free Vibration analysis part of FEU.

9.3 Objective Function Calculation

Objective Function is a real number used for defining how well or bad the two set of data correlate. Where these the two sets of data are FEM and EMA results. Objective function is calculated by the Equation 9-1.

$$OF = \sum_{r=1}^N \left(\frac{|\omega_{Ar} - \omega_{Er}|}{\omega_{Er}} + (1 - Mac_{Ar,Er}) \right) \quad \text{Equation 9-1}$$

Where;

ω_{Ar} : Natural Frequency for Mode r obtained from analytical data

ω_{Er} : Natural Frequency for Mode r obtained from experimental model

$Mac_{Ar,Er}$: Mac values obtained from experimental data vs. analytical data.

N : Number of matched Modes.

9.4 Modification of FE model in order to Correlate FEM and EMA Results (FEU Strategy)

Modification of FE model is the most important part of FEU. Therefore there is a need of a strategy for modification. That is why the title of this Section is **FEU Strategy**. Actually repetition of the FE Updating procedure is nothing else but an optimization process. Thus “a robust global search and optimization technique” (Hasançebi, 2001) of **Simulated Annealing** is adapted for the “Modification of FE Model” part of the above procedure.

Since Simulated Annealing (SA) is only a tool to achieve the aim of this study, it is explained here briefly. But more detailed explanation and application are given in (Hasançebi, 2001). Hasançebi studied Simulated Annealing for shape, size, and topology optimization of structural systems. Unless not stated the sentences written below are quoted from his study and necessary modifications are done in order to adapt Simulated Annealing for Finite Element Updating Process.

9.4.1 Simulated Annealing

Simulated Annealing (SA) is a robust global search and optimization technique, which offers a heuristic approach to yield encouraging solutions even for the most difficult optimization problems. SA employs a simulative model of the annealing

process of physical systems, establishing a direct analogy to the elementary principles of thermodynamics and statistical mechanics.

9.4.1.1 Physical Origin of SA

In this process, the aim is to bring a physical system (either a solid, e.g., metal or a liquid) to a state of minimum energy level by rearranging its atomic configuration. For this reason, the physical system is first heated up to a sufficiently high temperature. The reason of this is; To disorder the existing state of its atomic structure leading to a non-minimum energy level; and to allow the atoms to move freely for such a target configuration. This is followed by a very slow cooling of the system, reducing the temperature monotonously towards a value at which the freezing or crystallization takes place, which is referred to *the frozen temperature*. At each temperature manipulated, as the cooling proceeds, the atoms experience different configurations repeatedly and attempt to order themselves in a way to pass to a lower energy level. By this way, the system is successively pushed to be more ordered, strong and stable under restricted mobility of its atoms. Finally, when the cooling reaches the frozen temperature, the atoms line themselves up to produce a perfectly regular crystal structure, and thus to minimize the energy level of the system, which is called *ground state*.

The idea that this process is simulated to solve optimization problems are rendered possible by defining a parallelism between minimizing the **energy level** of a physical system and lowering the **objective function**.

9.4.2 How Does SA Work?

First step in FEU is to group the elements used in the FE Model. The grouped elements are forced to have the same properties throughout the FEU process. The next step is the formation of an initial model to be used as the starting model and current solution of FEU. This is accomplished by specifying each variable of the grouped elements, a value of which is its original value. Next, following the choice of an appropriate annealing schedule, the current temperature is assigned the initial temperature to be used as the point from which the annealing is initiated. The initial temperature can be set as follows: it should be high enough (i) to allow a large number of model transitions for a thorough exploration of the design space at early stages; and (ii) to let the process cool down gradually to attain thermal equilibrium at each temperature as the cooling proceeds.

There exist two loops in FEU. These are outer loop and inner loop. **Outer loop** is used to proceed the algorithm at different temperatures during the cooling cycles and to control the termination criterion which is simply defined as the case when the current temperature falls below the final temperature which corresponds to the frozen temperature in the actual annealing analogue. When the current temperature is above the final temperature, iterations of the inner loop are performed. In a single iteration of the inner loop a number of candidate models which is equal to the number of model variables are created in the vicinity of the current model to be sampled. This is performed as follows: (i) each design variable in the current model is selected only once in a random order; (ii) the selected variable is then perturbed by assigning a new value to it; and (iii) finally, the candidate model is created by

using the new value of this variable and taking the values of other variables same as in the current model. **This implies that the current model differs from a candidate only in terms of its one design variable,** A competition then takes place between the current and each candidate models sampled. Whenever a candidate model provides a better solution (e.g., a lower value of the objective function, downhill move), it is immediately declared as to be the winner, and thus is authorized to replace the current model to provide data for the following candidates. However, in the opposite case (e.g., a higher value of the objective function, uphill move), the winner is determined in accordance with the Metropolis test (explained in Section 9.4.4), where either the candidate is accepted, or it is rejected and the current model maintains itself,. The underlying principle of inner loop is associated with the concept of thermal equilibrium in the actual annealing analogue. Hence, it is mimicked here by reducing the objective function to a reasonably low value correlated with the current temperature. After completing the whole iterations of inner loop at a particular temperature, the temperature of next cooling cycle is established by multiplying the current temperature with a cooling factor, the above process is repeated in the same way until the whole cooling cycles are iterated.

9.4.3 Formation of the Candidate Model

As stated in Section 9.4.2 the candidate model is obtained by perturbing only one design variable of the current model. The current model is designated as x^c and the candidate (alternative) model is designated as x^a ,

If the selected variable for perturbing is denoted as x_m^c and corresponding selected variable in current design is denoted as x_m^a then

$$x_m^a = x_m^c \cdot [1 + (r - 0.5) \cdot \delta] \quad \text{Equation 9-2}$$

Where;

r : Real valued random number in the range of $[0,1]$

δ : Perturbation limit parameter in the range of $[0, \infty]$

The perturbation limit parameter δ determines to which extent the vicinity of current design is taken into account while creating a candidate design,

For better understating the perturbation limit parameter the following example is given.

If the current value of variable in current model is x_m^c is 10 and the perturbation limit parameter is taken as 1. Then the candidate (alternate) variable x_m^a will have the following upper and lower limits

If the random variable (r) is 1 then the candidate variable x_m^a will be $x_m^c = 10 \cdot [1 + (1 - 0.5) \cdot 1] = 15$. If the random variable (r) is taken as 0 then the candidate variable x_m^a will be $x_m^c = 10 \cdot [1 + (0 - 0.5) \cdot 1] = 5$. Thus for a perturbation limit value of 1, candidate variable will have a range of plus and minus %50, less or more of the current variable respectively.

As will be stated in the programming part of FEU, the user has the chance of defining the perturbation parameter for varying temperatures. This is formulated in Equation 9-3

$$\delta = \delta^f + (\delta^f - \delta^i) \left(\frac{t - t^f}{t^f - t^i} \right) \quad \text{Equation 9-3}$$

Where

t^i : Initial temperature

t^f Final temperature

δ^i Value of perturbation limit parameter at initial temperature

δ^f Value of perturbation limit parameter at final temperature

The most important modification on simulated annealing is enforced at this point. (Hasançebi, 2001) formulated SA (for optimum structural design) as a discrete optimization method. For FEU purposes SA is reformulated as a continuous optimization method. Equation 9-2 is used for this purpose where the candidate variable is continuously perturbed. Also for FEU purposes, perturbation limit parameter is related with annealing schedule. Perturbation limit variable decreases as the temperature decreases which might be a good approach to fine tune the model at low temperatures.

9.4.4 Number of Iterations of the Inner Loop (I)

The number of iterations of the inner loop (I) is important for the efficiency of the algorithm. A high number of iterations may result in a very high degree of computational cost on the algorithm and a low number of iterations, on the other hand, may not be sufficient to bring the system to the thermal equilibrium at a particular temperature. For initial temperatures the number of iterations should be

kept low and it should gradually be increased as cooling proceeds. For a particular temperature (t), calculation of the number of iterations of the inner loop (I) is given in Equation 9-4

$$I = \text{round} \left[I^f + (I^f - I^i) \left(\frac{t - t^f}{t^f - t^i} \right) \right] \quad \text{Equation 9-4}$$

Where;

t^i : Initial temperature.

t^f : Final temperature.

I^i : Number of iterations of the inner Loop at initial temperature.

I^f : Number of iterations of the inner Loop at final temperature

9.4.5 Metropolis Test

As stated in Section 9.4.2, when competition takes place between the current and a candidate model sampled. If a candidate model provides a better solution (e.g., a lower value of the objective function, downhill move), it is immediately declared as to be the winner, and thus is authorized to replace the current model to provide data for the following candidates. However, in the opposite case (e.g., a higher value of the objective function, uphill move), the winner is determined in accordance with the Metropolis test.

For FEU purposes the metropolis test is formulated in two different ways (Hasançebi, 2001).

- a) Simplified Metropolis Test: The probability of accepting a poor candidate model is assigned to $P = e^{-\Delta W / t}$.
- b) Metropolis Test with Boltzman Parameter: The probability of accepting a poor candidate model is assigned to $P = e^{-\Delta W / Kt}$.

In the above equation K is defined as the Boltzman parameter. K is defined as the running average of the positive valued ΔW (note that positive ΔW indicates a poor candidate). Whenever a poor candidate model is sampled with respect to the current model ($\Delta W > 0$), this parameter is updated as shown in Equation 9-5 before its probability of acceptance is calculated in Metropolis test.

$$K^{(N_a+1)} = \frac{K^{(N_a)} N_a + \Delta W^{(N_a+1)}}{N_a + 1} \quad \text{Equation 9-5}$$

Where;

$K^{(N_a)}$: The value of the Boltzman parameter for the previous N_a number of poor candidates

$\Delta W^{(N_a+1)}$: The value of ΔW for the $(N_a + 1)$ -th poor candidate,

$K^{(N_a+1)}$: The updated parameter value, including $(N_a + 1)$ -th poor candidate.

It is advantageous to calculate Boltzman parameter in this fashion. Since this serves to normalize the ΔW values for the metropolis test, which in turn enables useful implementation of the algorithm regardless of the problem type. Also calculating Boltzman parameter in this fashion allows adaptive search experience, such that the

determination of a next candidate is correlated to the general formation of all the previous candidates.

There are several formations for Boltzman parameter. These are not used in FEU process. **Weighted Boltzman parameter** and **critical Boltzman parameter** approaches are formulated for SA structural design optimization in reference (Hasançebi, 2001).

9.5 Matlab Based FEU Software (FEUS)

For the application of FEU, Matlab based FEU Software (FEUS) is written. The reason of selecting Matlab for programming purposes is explained in Section 5,1. FEUS can be executed within EMAS (see Figure 6-1) or can be executed independently from EMAS. In the following pages the software is explained with snapshots.

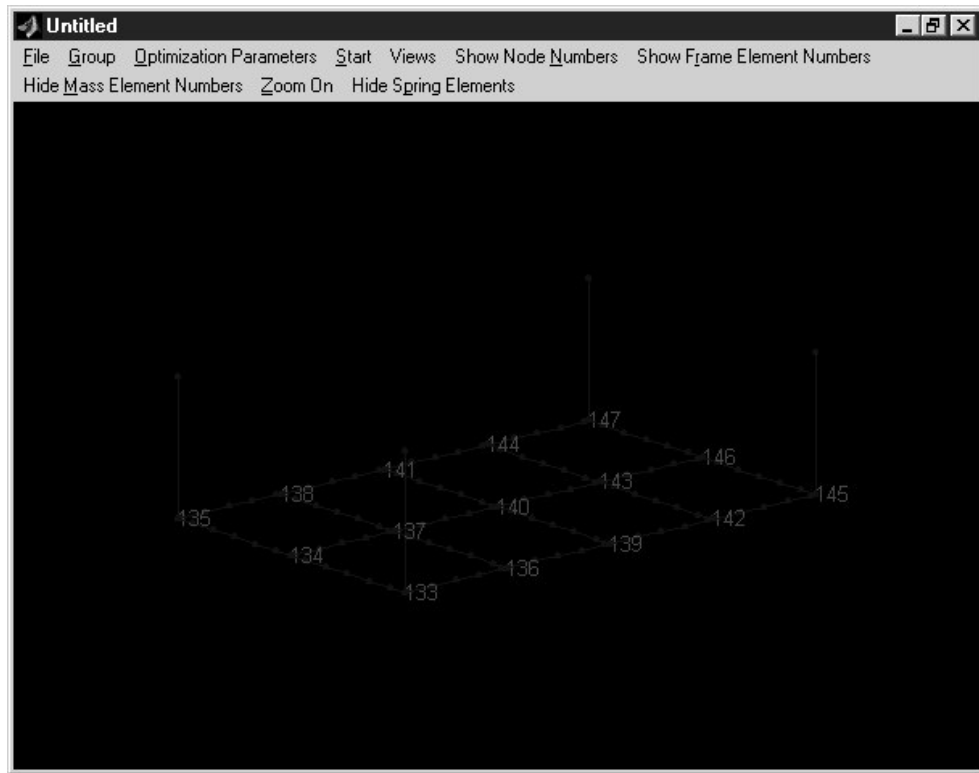


Figure 9-1 Main screen of FEUS

Main screen of the software is shown in Figure 9-1 with a model used for FEU process. When the **Group** menu item is clicked, a new screen (Grouping screen) appears. Grouping screen is shown in Figure 9-2. The groups defined in this screen are used in FEU. The importance of grouping is explained in Section 9.4.2. For the defined groups, group parameters are defined in Optimization parameters screen which is shown in Figure 9-3. According to the selected group type (mass group, frame group, spring group) different screens appear for defining FEU parameters. These screens are shown in Figure 9-4 to Figure 9-6 respectively.

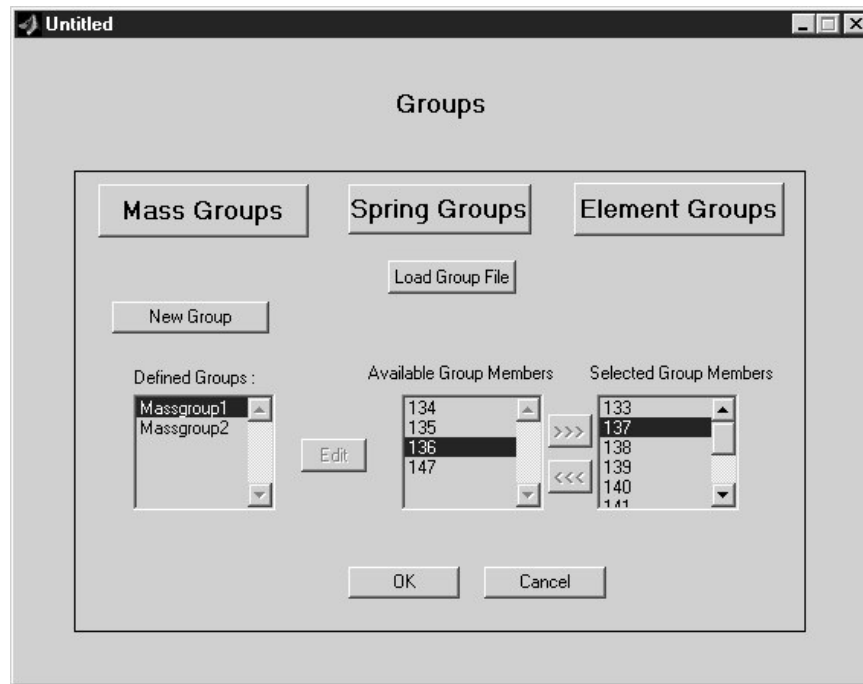


Figure 9-2 Groups Screen

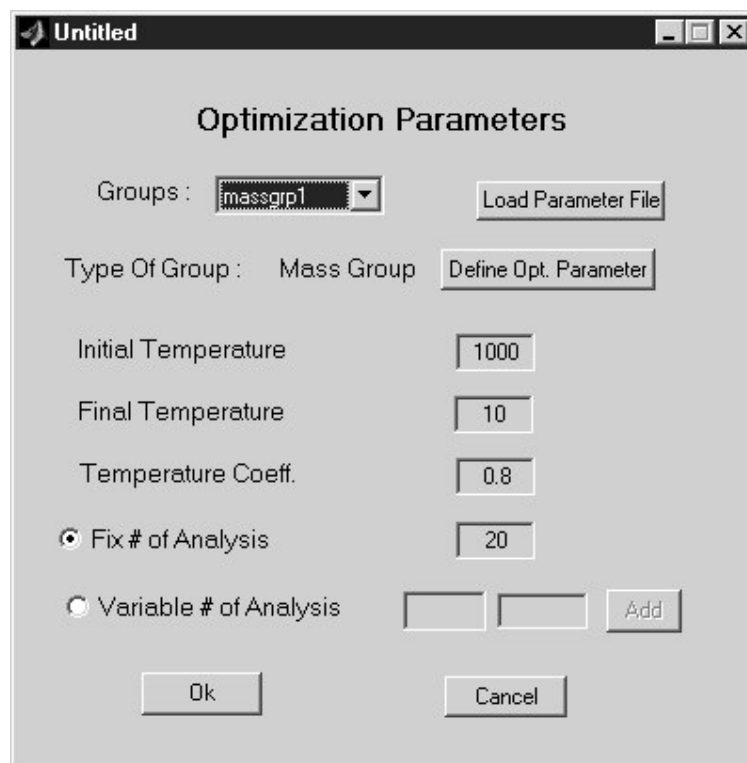
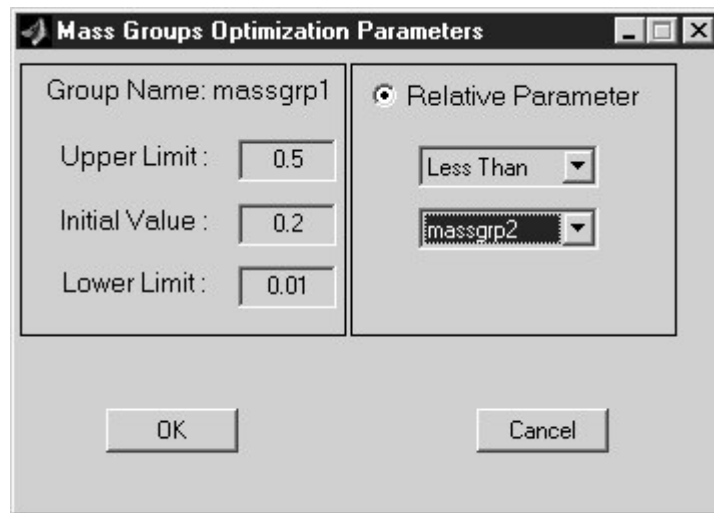


Figure 9-3 Optimization Parameter Screen



Mass Groups Optimization Parameters

Group Name: massgrp1

Upper Limit: 0.5

Initial Value: 0.2

Lower Limit: 0.01

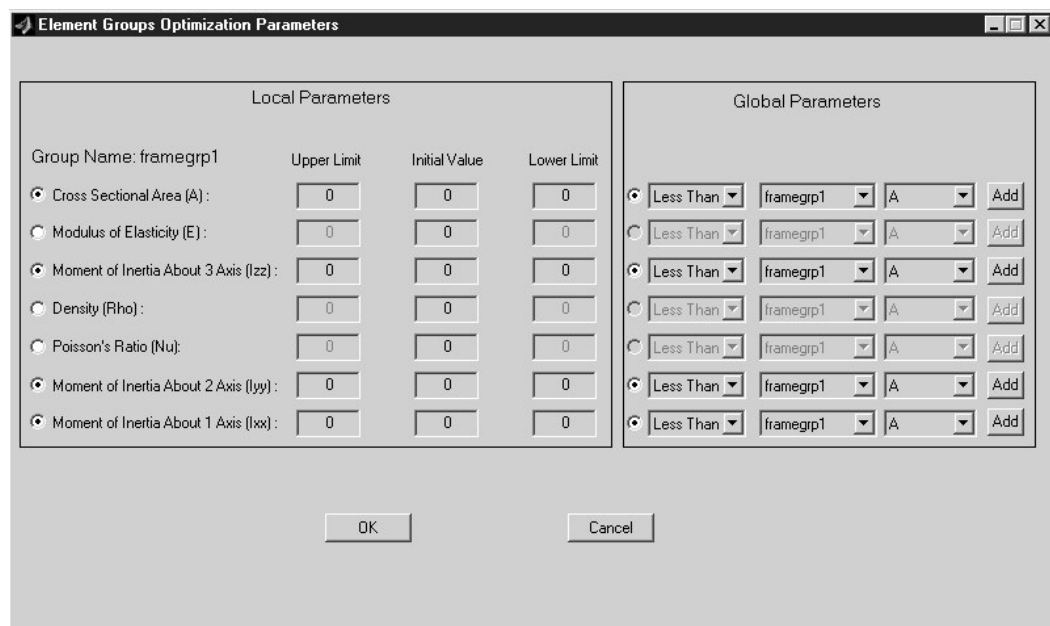
☒ Relative Parameter

Less Than

massgrp2

OK Cancel

Figure 9-4 Mass Group Optimization Parameters



Element Groups Optimization Parameters

Local Parameters				Global Parameters			
Group Name: framegrp1	Upper Limit	Initial Value	Lower Limit				
<input checked="" type="radio"/> Cross Sectional Area (A) :	0	0	0	<input checked="" type="radio"/> Less Than	framegrp1	A	Add
<input type="radio"/> Modulus of Elasticity (E) :	0	0	0	<input type="radio"/> Less Than	framegrp1	A	Add
<input checked="" type="radio"/> Moment of Inertia About 3 Axis (Izz) :	0	0	0	<input checked="" type="radio"/> Less Than	framegrp1	A	Add
<input type="radio"/> Density (Rho) :	0	0	0	<input type="radio"/> Less Than	framegrp1	A	Add
<input type="radio"/> Poisson's Ratio (Nu) :	0	0	0	<input type="radio"/> Less Than	framegrp1	A	Add
<input checked="" type="radio"/> Moment of Inertia About 2 Axis (Iyy) :	0	0	0	<input checked="" type="radio"/> Less Than	framegrp1	A	Add
<input checked="" type="radio"/> Moment of Inertia About 1 Axis (Ixx) :	0	0	0	<input checked="" type="radio"/> Less Than	framegrp1	A	Add

OK Cancel

Figure 9-5 Frame Group Optimization Parameters

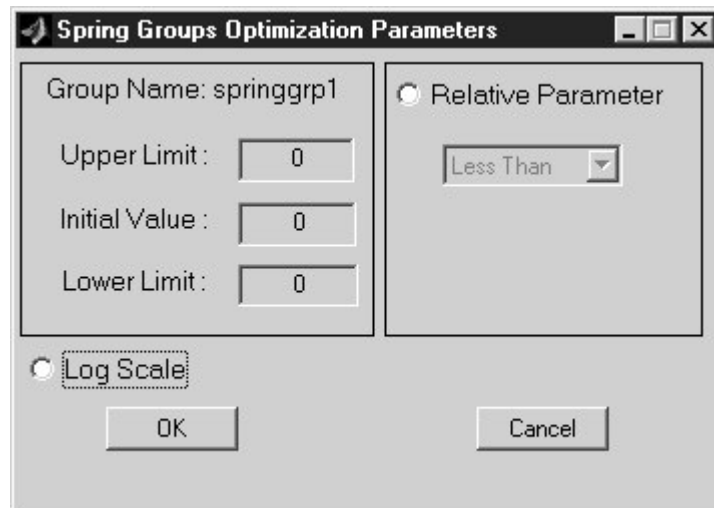


Figure 9-6 Frame Group Optimization Parameters

After defining all the required parameters for FEU clicking **Start** menu item starts the FEU process. The status of the FEU process is shown in Figure 9-7

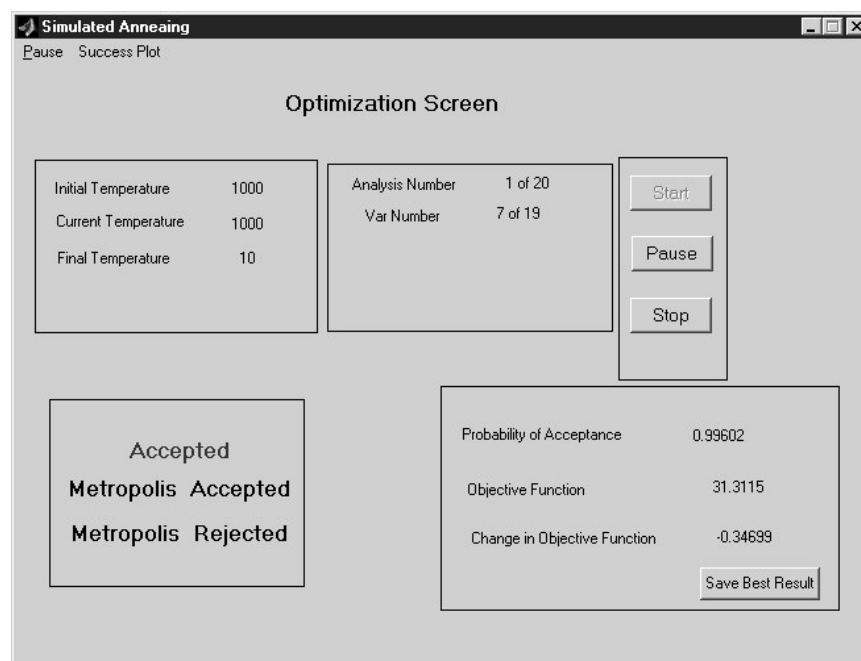


Figure 9-7 FE Updating Process

Whenever a better model is found, it is auto saved into a directory under the software.

CHAPTER 10

APPLICATION OF FE UPDATING SOFTWARE ON SKEWED STEEL GRID FRAME

10.1 Introduction

The skewed steel grid frame was dynamically tested and FRFs were obtained analyzed with EMAS software as discussed in the Chapter 8. Two separate sine-sweep tests were conducted for DC to 260 Hz and DC to 500 Hz. The experimental mode shapes and corresponding natural frequencies were obtained for each test. Those results are then used to calibrate the nominal FE model using model updating techniques. This Chapter concentrates on the Finite Element Updating procedure and discussion of the results obtained from the Finite Element Updating Software (FEUS). The results are listed in tabular format and compared against each other.

10.2 Input File of the Skewed Steel Grid Frame

The input file generation for the developed Experimental Modal Analysis Software (EMAS) program was explained in Chapter 6. An earlier model input file was prepared for the EMAS software for the purpose of experimental modal parameter estimation (i.e., animate mode shapes, define input-output nodal relationships, etc.).

A total of 37 nodes were used in the model for EMAS. For the finite element updating (FEU) purposes, a finer meshed model input file is prepared using a total of 127 nodes. A larger number of nodes were used to generate more members which will be used to fine tune the variations in sectional and other relevant properties. Additional mass elements are defined at the joints for the effect of the actual additional masses at the connection points due to the used plates for bolting and bolt masses. Since the model was tested by hanging the frame in the air using elastic cords, spring elements are defined at six different points on the frame (see Figure 10-3 for the places of the springs). Therefore, FEU model has incorporated larger number of members, additional masses, and springs different than the initial input file used for EMAS. 3D view of the prepared model used for FEU is shown in Figure 10-1. The input file is given in Appendix B.

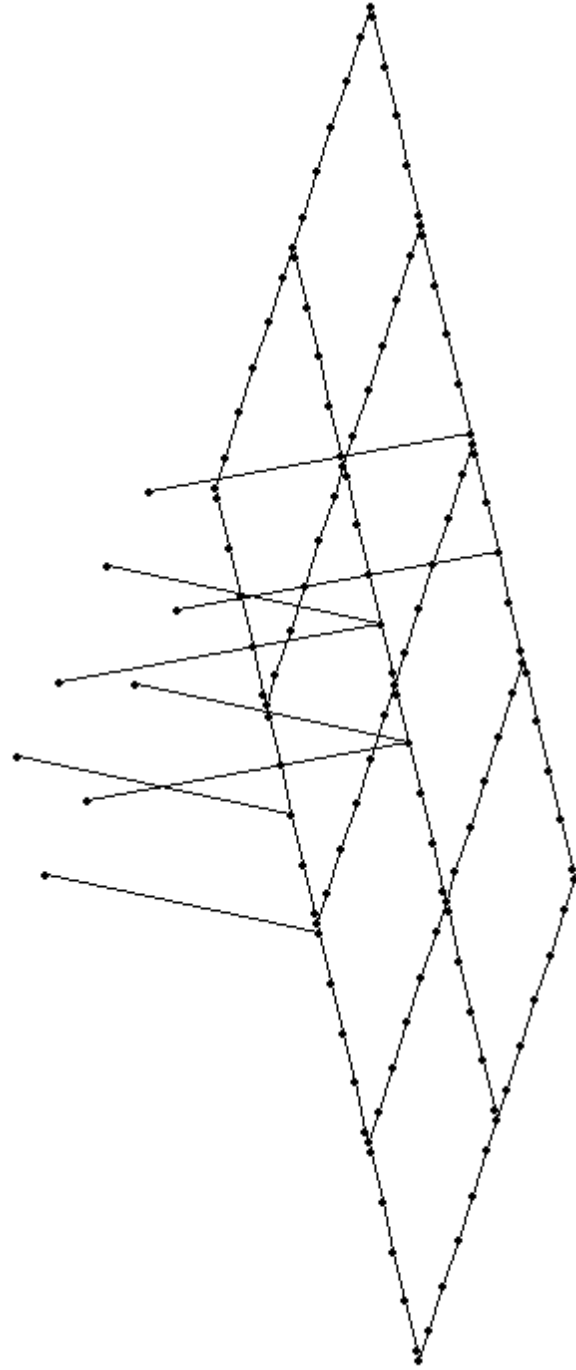


Figure 10-1 3D view of the model used in FEU

10.3 Groups, and Parameters for Each Group

For Finite Element Updating purposes of the skewed steel frame, the following groups and group parameters are defined.

10.3.1 Mass groups and Parameters:

Mass groups are defined according to the plate sizes used for bolting the steel members. Two different types of mass groups are defined based on the used plate sizes. The steel grid is composed of three longitudinal continuous frames. Cover plates used to connect transverse direction members to the longitudinal members are larger for the middle longitudinal frame, and smaller for the side frames. Therefore, the mass parameters used for the middle frame junctions and the side frame junctions are grouped under two variables. For better visualization of mass elements refer to Figure 8-2 and Figure 10-2.

Massgroup1 consists of the elements 133, 135, 136, 138, 139, 141, 42, 44, 45, 147 with the following parameters.

Massgroup1	Initial Value	Upper Limit	Lower Limit
Mass (kg)	0.2098	0.4	0.1

Massgroup2 consist of the elements 134, 137, 140, 143, 146 with the following parameters.

Massgroup2	Initial Value	Upper Limit	Lower Limit
Mass (kg)	0.353	0.5	0.1

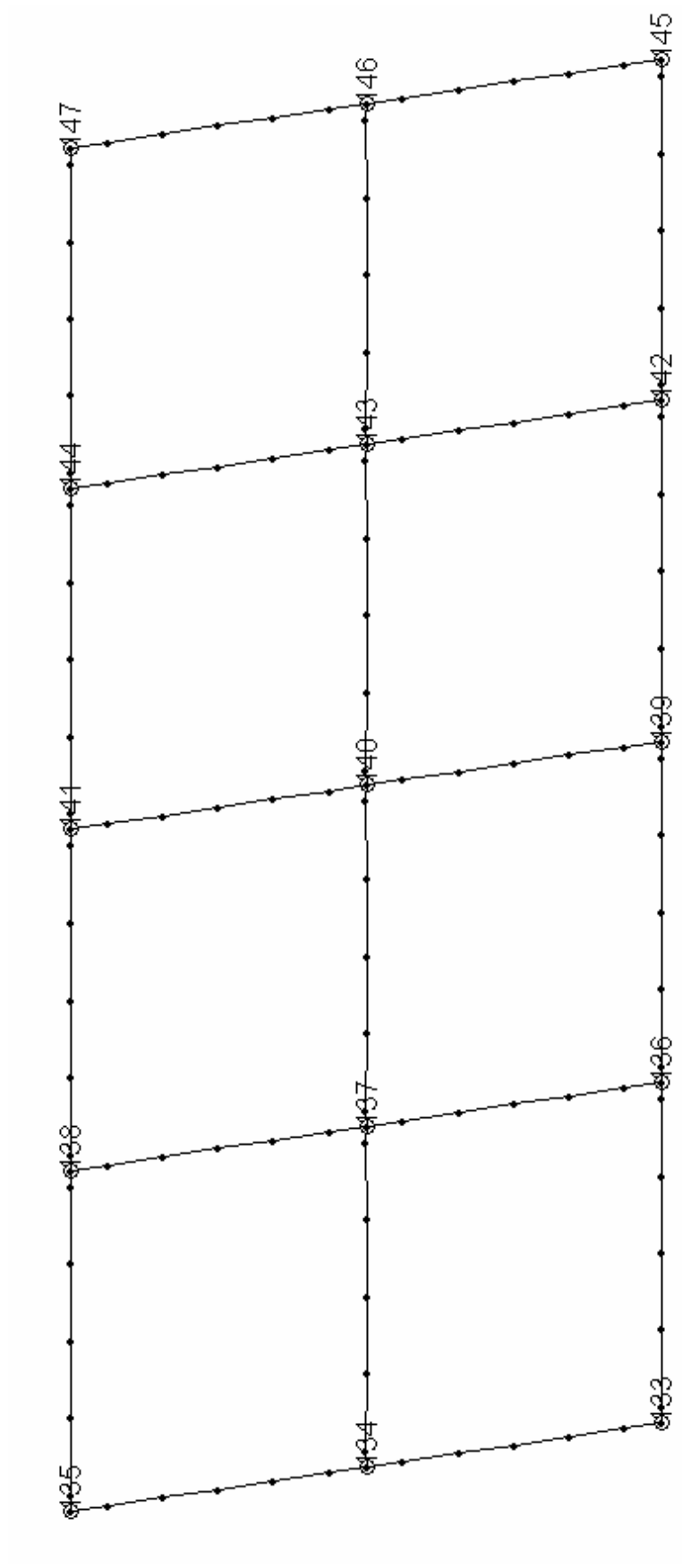


Figure 10-2 Mass Elements

10.3.2 Spring Groups and Parameters

Since all the elastic bands used to test the frame have the same elastic spring coefficient, all the spring elements defined are grouped under one group. The spring element axial stiffness parameter is named as “SpringGroups1” and consists of the elements 148, 149, 150, 151, 152, 153, 154, 155, 156, 157, 158, and 159 with the following properties.

SpringGroups1	Initial Value	Upper Limit	Lower Limit
Spring Coef. (N/m).	1001	100000	1000

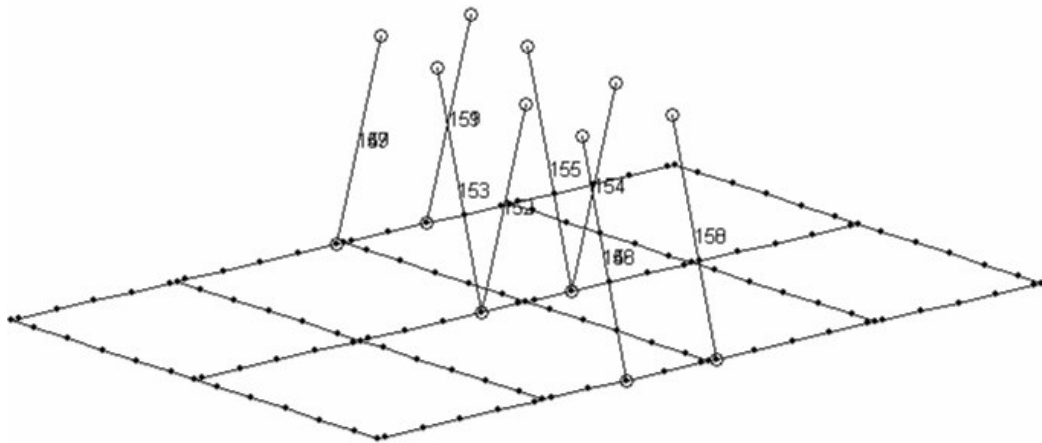


Figure 10-3 Spring Elements

10.3.3 Frame Groups and Parameters

Frame elements used for the FEU model are categorized under 4 groups. These groups and corresponding group parameters are defined below in Table 10-1 through Table 10-4. The frame group member distributions are graphically presented in Figure 10-4 and each group parameter are explained in detail below.

Framegroup1 is defined for the elements at the joints which are connected with plates to the other continuous elements. The existences of cover plates are expected to increase the moment of inertia of the short members under each cover plate. Framegroup1 consist of element numbers 1, 24, 25, 48, 49, 72, 73, 78, 79, 84, 85, 90, 91, 96, 97, 102, 103, 108, 109, 114, 115, 120, 121, 126, 127, and 132 with the parameters listed in Table 10-1. Framegroup1 is shown with circles in Figure 10-4. Parameters related with Framegroup1 are given in Table 10-1.

Table 10-1 Model parameters, limits, and initial values for Frame Group 1

Framegroup1	Initial Value	Upper Limit	Lower Limit
Modulus of Elasticity (N/m ²)	2.1e11	-	-
Cross-sectional area (m ²)	0.000184	0.000276	9.2e-005
Z Moment of inertia (m ⁴)	2.157e-8	3.2355e-008	1.0785e-008
Density (kg/m ³)	7850	-	-
Poisson's Ratio	0.3	-	-
Y moment of inertia (m ⁴)	1.113e-8	1.6695e-8	5.565e-9
X moment of inertia (m ⁴)	2.209e-8	3.3135e-8	1.1045e-8

Upper and lower limits are calculated by increasing and decreasing initial value by %50 and %-50 respectively. (-) indicates that the parameter is constant.

Framegroup2 is defined for the elements at the joints which are connected continuously to the discontinuous elements and shown with oval circles in Figure 10-4. Framegroup2 consist of elements; 6, 7, 12, 13, 18, 19, 30, 31, 36, 37, 42, 43, 54, 55, 60, 61, 66, and 67 with the following parameters. Parameters related with Framegroup2 are given in Table 10-2.

Table 10-2 Model parameters, limits, and initial values for Frame Group 2

Framegroup1	Initial Value	Upper Limit	Lower Limit
Modulus of Elasticity (N/m ²)	2.1e11	-	-
Cross-sectional area (m ²)	0.000184	0.000276	9.2e-005
Z Moment of inertia (m ⁴)	2.157e-8	3.2355e-008	1.0785e-008
Density (kg/m ³)	7850	-	-
Poisson's Ratio	0.3	-	-
Y moment of inertia (m ⁴)	1.113e-8	1.6695e-8	5.565e-9
X moment of inertia (m ⁴)	2.209e-8	3.3135e-8	1.1045e-8

Upper and lower limits are calculated by increasing and decreasing initial value by %50 and %-50 respectively. (-) indicates that the parameter is constant.

Framegroup3 is defined for the main elements which are located between joints without cover plates. Framegroup3 consist of elements; 2, 3, 4, 5, 8, 9, 10, 11, 14, 15, 16, 17, 20, 21, 22, 23, 26, 27, 28, 29, 32, 33, 34, 35, 38, 39, 40, 41, 44, 45, 46, 47, 50, 51, 52, 53, 56, 57, 58, 59, 62, 63, 64, 65, 68, 69, 70, 71, 74, 75, 76, 77, 80, 81, 82, 83, 86, 87, 88, 89, 92, 93, 94, 95, 98, 99, 100, 101, 104, 105, 106, 107, 110, 111, 112, 113, 116, 117, 118, and 119. Framegroup3 is shown with pentagons in Figure 10-4. Parameters related with Framegroup3 are given in Table 10-3.

Table 10-3 Model parameters, limits, and initial values for Frame Group 3

Framegroup1	Initial Value	Upper Limit	Lower Limit
Modulus of Elasticity (N/m ²)	2.1e11	-	-
Cross-sectional area (m ²)	0.000184	0.000276	9.2e-005
Z Moment of inertia (m ⁴)	2.157e-8	3.2355e-008	1.0785e-008
Density (kg/m ³)	7850	-	-
Poisson's Ratio	0.3	-	-
Y moment of inertia (m ⁴)	1.113e-8	1.6695e-8	5.565e-9
X moment of inertia (m ⁴)	2.209e-8	3.3135e-8	1.1045e-8

Upper and lower limits are calculated by increasing and decreasing initial value by %50 and %-50 respectively. (-) indicates that the parameter is constant.

Framegroup4 is defined for the elements which are between joints for only the elements at the right edge of the frame shown with triangles in Figure 10-4. The

section used for the indicated members have slightly thicker walls compared to the rest of the members defined by Framegroup3. Framegroup4 consist of elements; 122, 123, 124, 125, 128, 129, 130, and 131. Framegroup4 is shown with triangles in Figure 10-4. Parameters related with Framegroup1 are given in Table 10-4.

Table 10-4 Model parameters, limits, and initial values for Frame Group 4

Framegroup1	Initial Value	Upper Limit	Lower Limit
Modulus of Elasticity (N/m ²)	2.1e11	-	-
Cross-sectional area (m ²)	0.000184	0.000276	9.2e-005
Z Moment of inertia (m ⁴)	2.157e-8	3.2355e-008	1.0785e-008
Density (kg/m ³)	7850	-	-
Poisson's Ratio	0.3	-	-
Y moment of inertia (m ⁴)	1.113e-8	1.6695e-8	5.565e-9
X moment of inertia (m ⁴)	2.209e-8	3.3135e-8	1.1045e-8

Upper and lower limits are calculated by increasing and decreasing initial value by %50 and %50 respectively. (-) indicates that the parameter is constant.

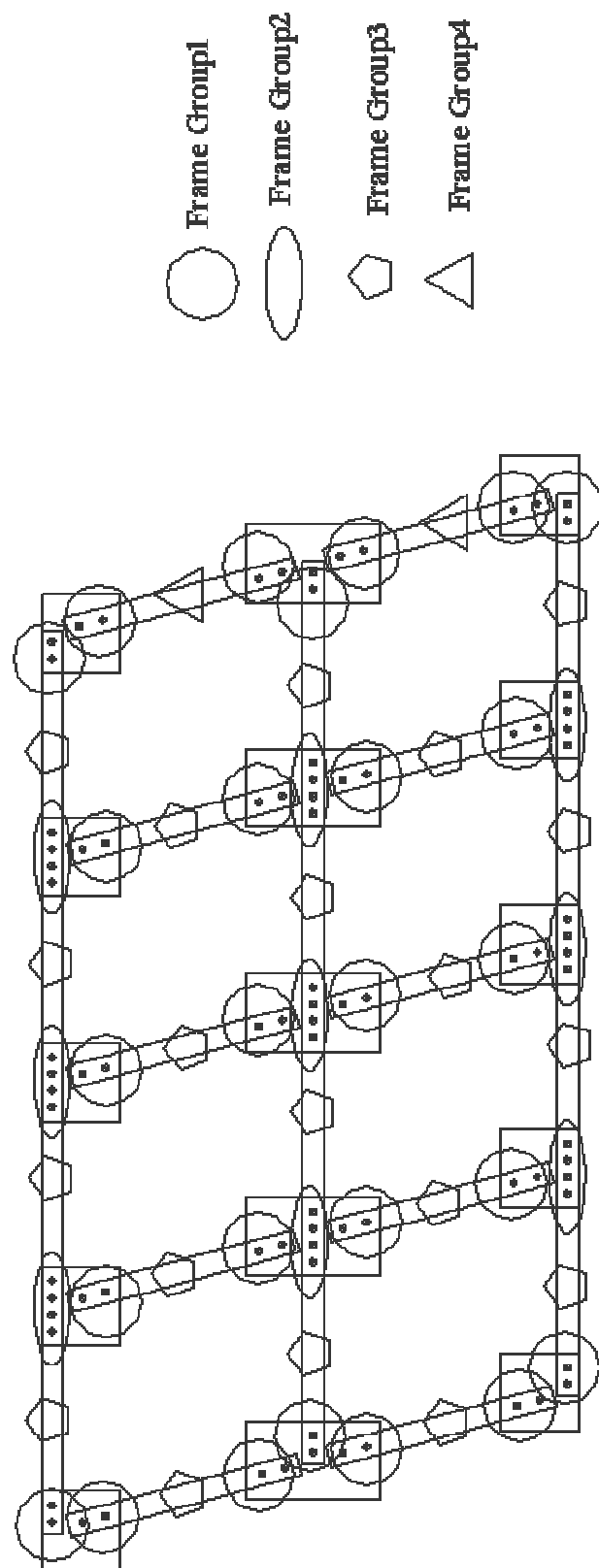


Figure 10-4 Frame Group Member Distributions

10.4 Parameters defined for FEU process

Groups defined for frame properties, lumped mass constants, and spring coefficients are assigned various parameters in order to find an optimal solution that closely matches the experimental results. Parameters are assigned for each FEU group. Additional parameters are used during the Simulated Annealing (SA) processes which are necessary for the optimization process. These SA parameters are provided below:

Initial Temperature = 1000

Final Temperature = 0.0001

Temperature coefficient = 0.95

Number of Outer Loops (linear): Initial: 2, Final: 6

Following new parameters are defined in addition to the above standard SA parameters:

Perturbation limit parameter (linear): Initial: %12, Final %8

Penalty Coefficient (linear): Initial: 1, Final: 1.5

Metropolis Test: Using Boltzman Parameter.

10.4.1 Nominal Models' Comparisons and FEU Results

With the group names and parameters defined in Section 10.3 and FEU parameters defined in Section 10.4, the FEU software is executed with three different experimental models. These models are:

- 1) EMA result set 1 (First experiment 1-260 Hz).
- 2) EMA result set 2 (Second experiment 1-500 Hz).

- 3) Combination of selected meaningful modes from EMA result set 1 and
EMA result set 2.

In the following sub-sections, the comparisons for the three nominal model results and FEU results are explained in detail.

10.4.1.1 EMA Result Set 1

For the comparison of the nominal analytical model against EMA test result set 1, is made using an objective function as described in Section 9.3 by Equation 9-1. Corresponding comparison plots and tables are given in Figure 10-5 and Table 10-5, respectively. The objective function value calculated for the nominal analytical model (in according with Equation 9-1) is 21.85263.

Looking at the Figure 10-5 and

Table 10-5, it is easy to understand that nominal FE model does not correlate well with EMA set 1. Overall impression obtained from examination of Figure 10-5, it is understood that FEU process will not give good results since most of the matched modes have very low MAC values and very low frequency correlation values. At the end of the FEU process, the objective function is lowered to 17.1021. Success plot for FEU of EMA result set 1 is given in Figure 10-6.

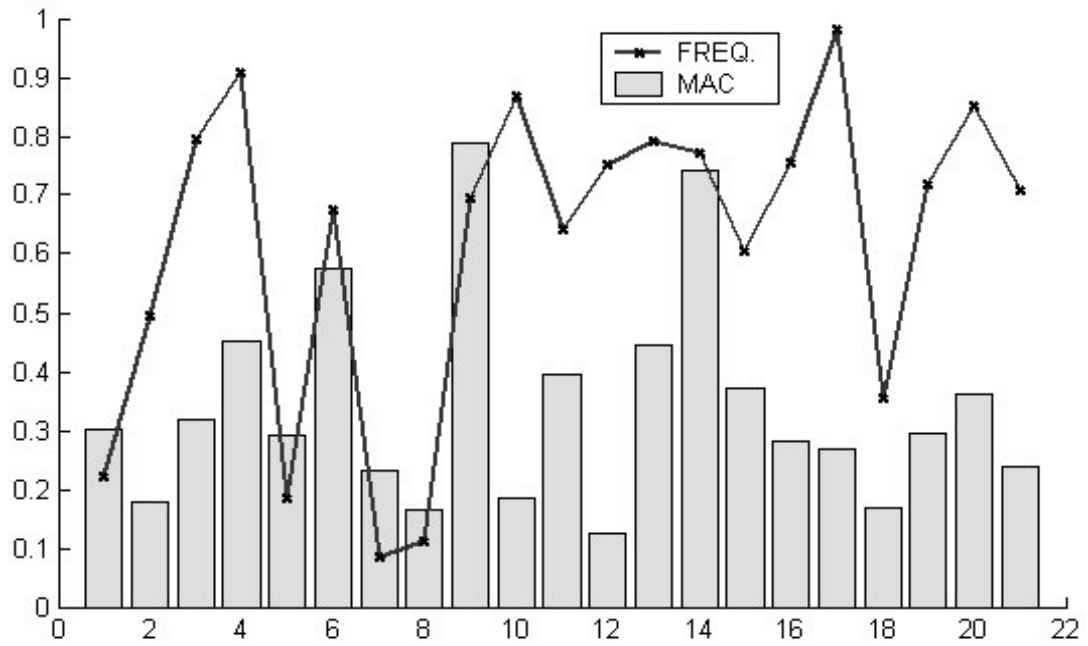


Figure 10-5 Comparison plot for Mode Shapes & Frequencies for the Ema result set 1

Table 10-5 Comparison table for nominal model with Ema result set 1

Matched Modes	Exp. Mode	Theo. Mode	Exp. Freq.	Theo. Freq.	Mac	Freq Corr.
1	1	8	6.1892	27.8308	0.301496	0.222387
2	2	7	13.3584	26.9766	0.178521	0.495186
3	3	5	18.5315	14.7266	0.319736	0.794682
4	4	6	21.2636	23.4166	0.451546	0.908054
5	5	4	35.4435	6.59767	0.29144	0.186146
6	6	7	39.9946	26.9766	0.576298	0.674507
7	7	33	44.2785	511.515	0.230721	0.086563
8	8	38	64.8885	582.474	0.165952	0.111402
9	9	9	77.9366	54.1085	0.78876	0.694263
10	10	13	102.37	88.7602	0.184132	0.867053
11	11	10	110.041	70.5554	0.396111	0.641175
12	12	13	118.139	88.7602	0.125207	0.751322
13	13	15	136.103	107.627	0.44341	0.790776
14	14	15	139.414	107.627	0.743176	0.771995
15	15	14	156.93	94.9382	0.371032	0.604971
16	16	16	171.685	129.645	0.282592	0.755135
17	17	20	179.825	176.312	0.267824	0.980464
18	18	37	206.55	579.624	0.167371	0.356352
19	19	18	222.699	159.726	0.294774	0.717229
20	20	21	232.839	197.928	0.362858	0.850064
21	21	20	249.422	176.312	0.237795	0.706884

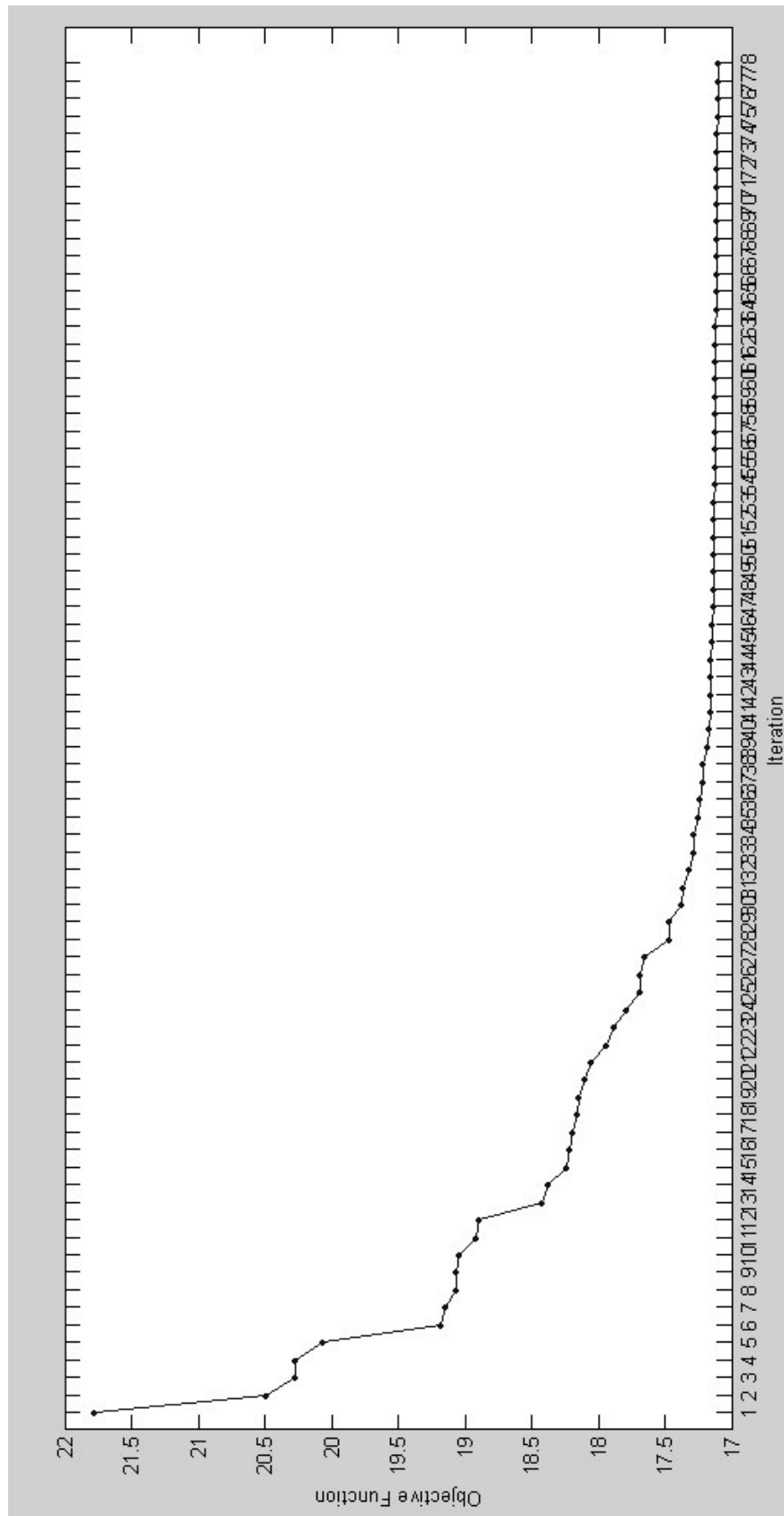


Figure 10-6 Success plot for ema set 1

10.4.1.2 EMA Results Set 2

For the comparison of the nominal analytical model against EMA result set 2, is made using objective function as described in Section 9.3 by Equation 9-1. Corresponding comparison plots and tables are given in Figure 10-7 and Table 10-7 respectively. The objective function value calculated for the nominal analytical model (in according with Equation 9-1) is 26.32330.

For this comparison same as the previous one (EMA results set 1) ,looking at the Figure 10-7 and Table 10-7, it is easy to understand that nominal FE model does not correlate well with EMA set 2. Overall impression obtained from the examination of Figure 10-7, it is understood that FEU process will not give good results since most of the matched modes have very low MAC values and very low frequency correlation values. At the end of the FEU process, the objective function is lowered to 20.6492.

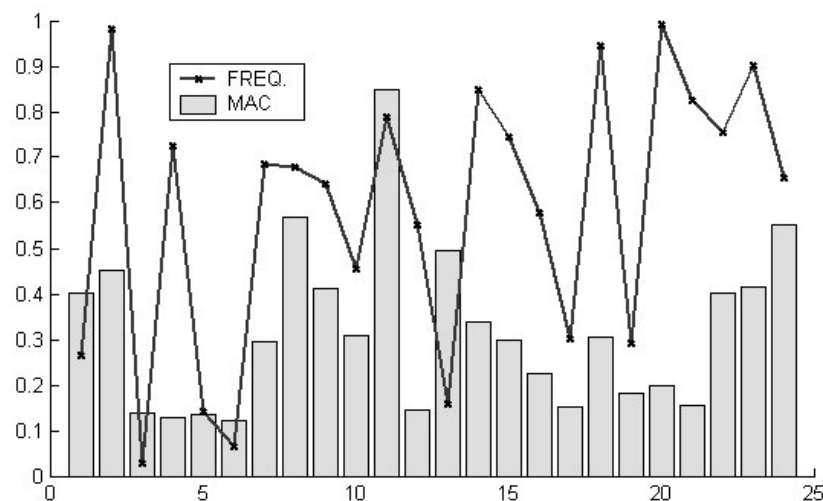


Figure 10-7 Comparison plot for Mode Shapes & Frequencies for the Ema result set 2

Table 10-6 Comparison table for nominal model with Ema result set 2

Matched Modes	Exp. Mode	Theo.Mode	Exp. Freq.	Theo. Freq.	Mac	Freq Corr.
1	1	6	6.23257	23.4166	0.402019	0.26616
2	2	5	14.9984	14.7266	0.45189	0.98188
3	3	47	24.6408	860.988	0.139736	0.028619
4	4	7	37.2949	26.9766	0.128573	0.723333
5	5	4	47.1186	6.59767	0.135169	0.140022
6	6	51	67.2184	1013.96	0.121028	0.066293
7	7	9	79.0423	54.1085	0.296003	0.684551
8	8	10	104.066	70.5554	0.568002	0.677985
9	9	10	109.891	70.5554	0.411422	0.642049
10	10	24	118.218	259.165	0.308474	0.45615
11	11	15	136.269	107.627	0.8473	0.789811
12	12	26	156.695	284.209	0.144272	0.551338
13	13	52	172.872	1083.36	0.493456	0.15957
14	14	17	182.002	154.471	0.338792	0.848736
15	15	17	207.665	154.471	0.298472	0.743848
16	16	16	223.905	129.645	0.223548	0.579018
17	17	10	234.085	70.5554	0.150266	0.301409
18	18	23	250.922	237.369	0.306281	0.945986
19	19	51	296.531	1013.96	0.180444	0.292448
20	20	27	304.296	307.149	0.199674	0.990713
21	21	25	328.367	271.344	0.15379	0.826345
22	22	26	375.774	284.209	0.402714	0.756331
23	23	28	401.75	444.917	0.415023	0.902976
24	24	27	469.608	307.149	0.550719	0.654054

10.4.1.3 EMA Set 3

After comparing the nominal models against the EMA result set 1 and EMA result set 2, it is concluded that a third set of EMA result which consists of the meaningful modes select from EMA result set 1 and EMA result set 2 is necessary. For the third try of the FEU process, meaningful modes from EMA result set 1 and EMA result set 2 are selected and grouped as EMA Set 3 used. From the mode shape animation of the first and second result sets, the modes which have meaningful mode shapes are selected. The selected modes give better correlation in nominal model comparison. These modes are 1,6,8,9,10,11,14, and 20 from EMA result set 1 and 1, 2, 8,11,14,22, and 24 from EMA result set 2. These mode shapes are re-arranged according to their frequencies and used in the FEU process. The objective function value calculated for the nominal model in according with the Equation 9-1 is

12.224. Comparison plot and comparison table are given in Figure 10-8 and Table 10-7 respectively.

The FEU process is executed, and the success plot for FEU is obtained as shown in Figure 10-9.

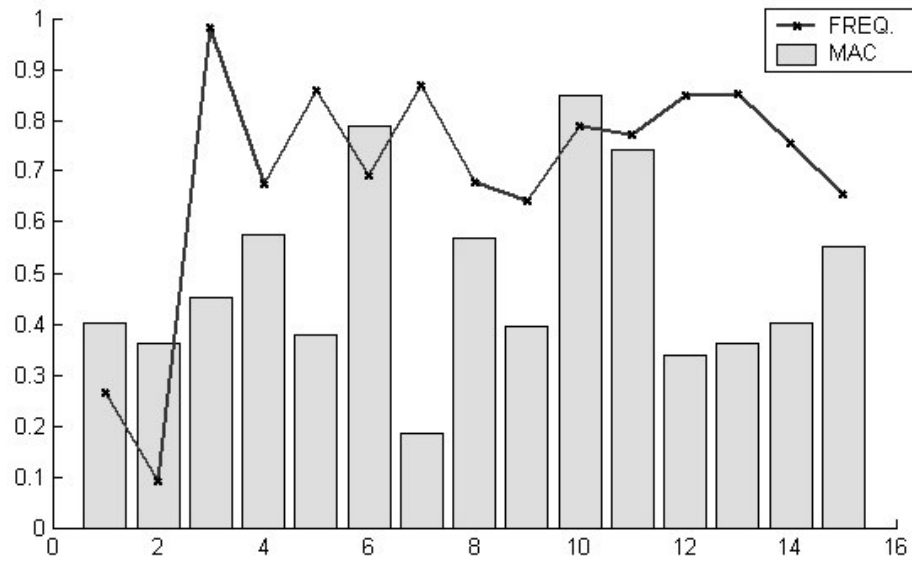


Figure 10-8 Comparison plot for nominal model with Ema result set 3

Table 10-7 Comparison table for nominal model with Ema result sets combination

Matched Modes	Exp. Mode	Theo. Mode	Exp. Freq.	Theo. Freq.	Mac	Freq Corr.
1	1	6	6.23253	23.4166	0.402019	0.266158
2	2	3	8.22362	0.765449	0.361687	0.093079
3	3	5	14.9984	14.7266	0.45189	0.981879
4	4	7	39.9946	26.9766	0.576298	0.674507
5	5	11	64.8894	75.5733	0.37721	0.858629
6	6	9	78.1982	54.1085	0.78876	0.691941
7	7	13	102.37	88.7602	0.184132	0.867052
8	8	10	104.062	70.5554	0.568002	0.678011
9	9	10	110.041	70.5554	0.396111	0.641175
10	10	15	136.269	107.627	0.8473	0.789811
11	11	15	139.414	107.627	0.743176	0.771995
12	12	17	182.002	154.471	0.338792	0.848736
13	13	21	232.839	197.928	0.362858	0.850064
14	14	26	375.774	284.209	0.402714	0.756331
15	15	27	469.609	307.149	0.550719	0.654052

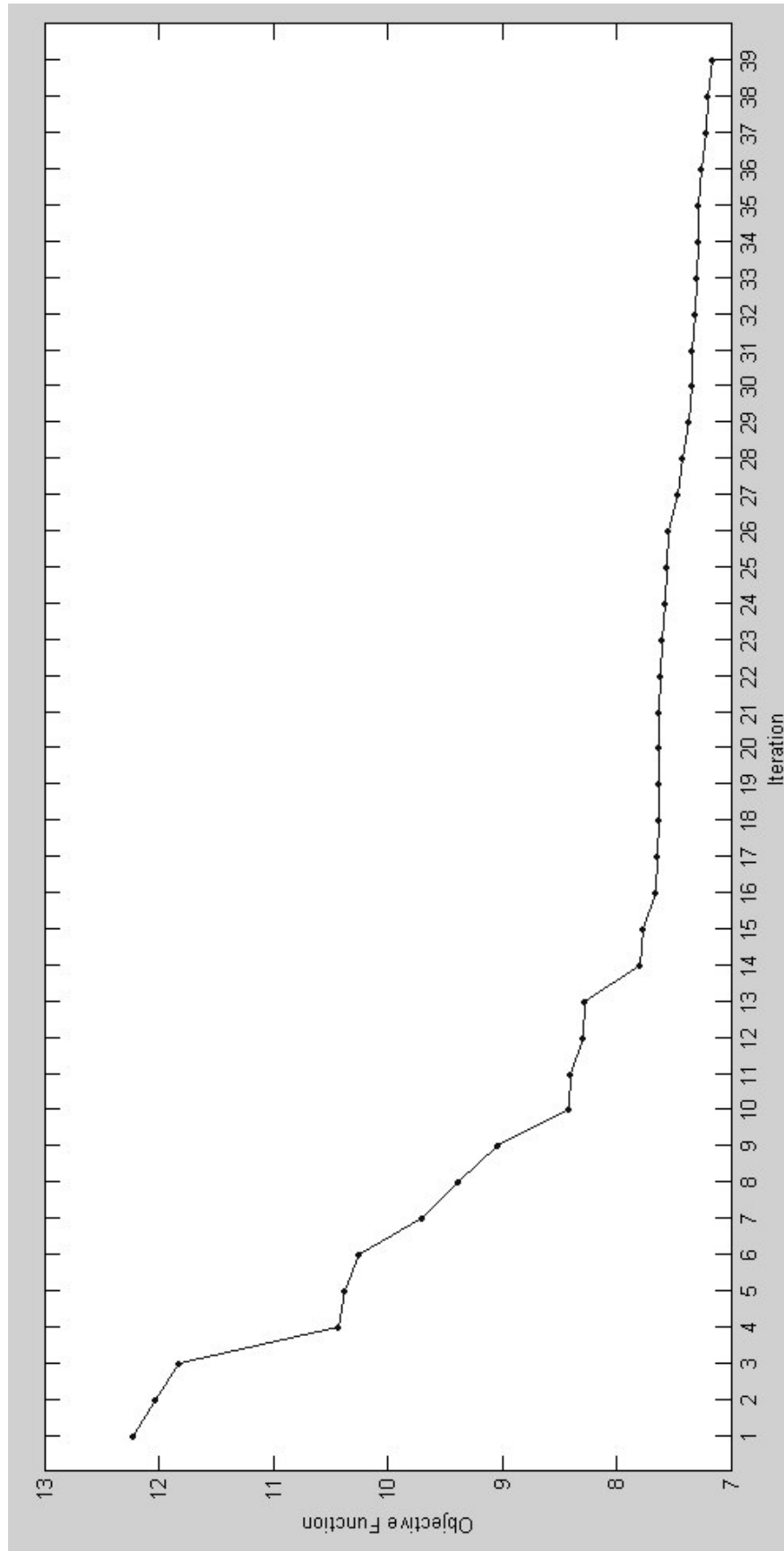


Figure 10-9 Success plot for Ema results sets 3

The objective function is lowered to 7.1564 at the end of FEU process as it can be seen from Figure 10-9. Keeping in mind that 15 modes are used in FEU, min value that the objective function can take is zero (*complete consistency*) and maximum value is 30, which means *complete inconsistency*. The objective function is lowered to 7.1564 (% 76.145 consistency) from 12.224 (%59.25 consistency) showing a positive improvement of % 16.985 in consistency. The improvement consistency percentages and final consistency values for the three EMA sets are listed in Table 10-8 below:

Table 10-8 Improvements consistency percentages.

	Nominal Consistency	Final Consistency	Improvement
EMA Set 1	% 47.97	% 59.281	% 11.311
EMA Set 2	% 45.159	% 50.835	% 5.676
EMA Set 3	% 59.28	% 76.145	% 16.985

Comparison plot and comparison table for FEU results are given in Figure 10-10 and Table 10-9, respectively. The improvement can be easily seen when Figure 10-8 and Figure 10-10 are compared. Almost all MAC values and Frequency values increased.

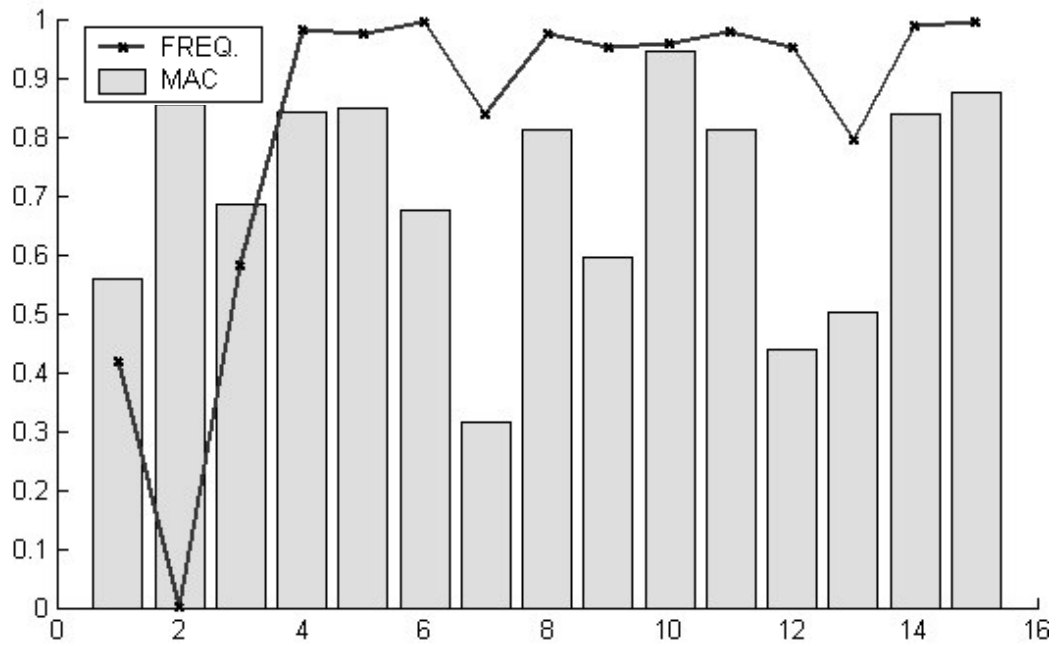


Figure 10-10 Comparison plot for FEU result for Ema result set 3

Table 10-9 Comparison table for FEU result for Ema result set 3

Matched Nodes	Exp. Node	Theo. Node	Exp. Freq.	Theo. Freq.	Mac	Freq Corr.
1	1	6	6.23253	14.887	0.556697	0.418656
2	2	1	8.22362	0.000266	0.855455	3.2e-005
3	3	8	14.9984	25.7204	0.685199	0.583134
4	4	9	39.9946	39.2875	0.840134	0.98232
5	5	12	64.8894	66.549	0.849889	0.975062
6	6	13	78.1982	78.5335	0.676377	0.99573
7	7	18	102.37	122.048	0.315143	0.838771
8	8	15	104.062	101.442	0.812049	0.974824
9	9	16	110.041	115.705	0.594466	0.951044
10	10	20	136.269	142.362	0.943425	0.957201
11	11	20	139.414	142.362	0.810217	0.979291
12	12	23	182.002	191.021	0.438656	0.952786
13	13	29	232.839	292.597	0.502809	0.795765
14	14	36	375.774	379.676	0.837934	0.989722
15	15	45	469.609	466.65	0.876195	0.993699

10.5 Optimized group parameters

Since an increase of %16.985 in consistency was the best result obtained using the third EMA (relative to others), the FEU is accepted to be satisfactory and corresponding group parameters are accepted as optimized group parameters. In the following three tables, optimized mass, spring, and frame group parameters are listed respectively. Optimized mass, spring, and frame parameters are discussed in Chapter11 in Discussion of Results & Conclusion.

Table 10-10 Optimized Mass Parameters

Mass Group Parameters	Property Name	Upper Limit	Lower Limit	Initial Value	Current Value	Change in %
massgroup1	Mass	0.4	0.1	0.2098	0.184065	-12.2664
massgroup2	Mass	0.5	0.1	0.353	0.24032	-31.9207

Table 10-11 Optimized Spring Parameters

Spring Group Parameters	Property Name	Upper Limit	Lower Limit	Initial Value	Current Value	Change in %
springgrpl	Spring Coef.	100000	1000	1001	11689.3	1067.77

Table 10-12 Optimized Frame Parameters

Frame Group Parameters	Property Name	Upper Limit	Lower Limit	Initial Value	Current Value	Change in %
framegroup1	A	0.000276	9.2e-005	0.000184	0.000115954	-36.9815
framegroup1	E			2.1e+011	2.1e+011	Constant
framegroup1	Izz	3.2355e-008	1.0785e-008	2.157e-008	2.10523e-008	-2.40016
framegroup1	Rho			7850	7850	Constant
framegroup1	Nu			0.3	0.3	Constant
framegroup1	Iyy	1.6695e-008	5.565e-009	1.113e-008	1.37149e-008	23.2246
framegroup1	Ixx	3.3135e-008	1.1045e-008	2.209e-008	1.67283e-008	-24.2722
framegroup2	A	0.000276	9.2e-005	0.000184	0.000176383	-4.13977
framegroup2	E			2.1e+011	2.1e+011	Constant
framegroup2	Izz	3.2355e-008	1.0785e-008	2.157e-008	2.18465e-008	1.282
framegroup2	Rho			7850	7850	Constant
framegroup2	Nu			0.3	0.3	Constant
framegroup2	Iyy	1.6695e-008	5.565e-009	1.113e-008	1.05263e-008	-5.42412
framegroup2	Ixx	3.3135e-008	1.1045e-008	2.209e-008	1.89702e-008	-14.1231
framegroup3	A	0.0002208	0.0001472	0.000184	9.85915e-005	-46.4176
framegroup3	E			2.1e+011	2.1e+011	Constant
framegroup3	Izz	2.5884e-008	1.7256e-008	2.157e-008	2.15547e-008	-0.0708372
framegroup3	Rho			7850	7850	Constant
framegroup3	Nu			0.3	0.3	Constant
framegroup3	Iyy	1.3356e-008	8.904e-009	1.113e-008	1.42377e-008	27.9222
framegroup3	Ixx	2.6508e-008	1.7672e-008	2.209e-008	1.22353e-008	-44.6114
framegroup4	A	0.0002208	0.0001472	0.000184	0.000193808	5.33069
framegroup4	E			2.1e+011	2.1e+011	Constant
framegroup4	Izz	2.5884e-008	1.7256e-008	2.157e-008	1.89227e-008	-12.2731
framegroup4	Rho			7850	7850	Constant
framegroup4	Nu			0.3	0.3	Constant
framegroup4	Iyy	1.3356e-008	8.904e-009	1.113e-008	1.5891e-008	42.7762
framegroup4	Ixx	2.6508e-008	1.7672e-008	2.209e-008	1.95153e-008	-11.6555

CHAPTER 11

DISCUSSION OF RESULTS & CONCLUSION

11.1 An Overview of This Study

The major work in this thesis study was on experimental modal testing, modal analysis, and analytical model updating (calibration) based on measured modal parameters. For this purpose a skewed steel grid frame was constructed. The test frame was dynamically tested by using swept sine signals. The signals were generated by the help of a shaker (see Section 3.3.3 for the properties of swept sine signals). The model is tested in free-free boundary conditions after suspended in the air using elastic rubber wires (see Section 8.3 for boundary condition details). HP 35665A 2 channel dynamic signal analyzer is used for processing the data obtained from the transducers. One force transducer and one accelerometer are used to acquire data from the model.

Two separate experiments are conducted on the test frame. Although the testing method is the same for both sets, the force generator location is changed between tests to excite all modes. Furthermore, the latter test focuses on a narrow band which is half the width of the first test to increase the accuracy of measured data by

doubling the number of measurement points (see Section 8.7 for details). The frequency response functions obtained from the experiment are analyzed by the developed experimental modal analysis software (EMAS). Then the results obtained from EMAS are used in Finite Element Updating Software (FEUS). The results are discussed and conclusions are drawn.

11.2 Discussion of Results of Modal Testing

Frequency Response Functions (FRFs) obtained from modal testing are analyzed using EMAS (see Chapter 8). A total of 21 and 24 modes are extracted from the FRFs of the first and second experiments, respectively. By the help of the mode shape animation part of EMAS, these mode shapes are animated (refer to Section 5.3 for the use of mode animation as verification method and refer to Section 6.2.1.3.1 for the mode shape animation part of EMAS). By investigating these mode shapes, it is realized that some of the mode shapes are computational modes and are not likely to be replicated by structural analysis. Since the EMAS software was verified using a cantilever beam's synthetically generated experimental data (refer to Chapter 7 for the verification of EMAS), it is certain that there are no formulation or programming errors in EMAS. The computational modes are excluded from the model updating process. Modal tests that were conducted on the test frame were not possible to replicate due to laboratory and scheduling constraints.

The reason of obtaining unreasonable (computational) mode shapes can be explained with the number of accelerometers used in modal testing. Equipment used for modal data acquisition (or dynamic analyzer) has only 2 input channels, which

are used for one load transducer and one accelerometer. Since there was only one channel for accelerometer, in order to obtain mode shapes, the accelerometer was moved over 37 reference points on the frame. Obtaining all mode shapes correctly using a single accelerometer is not possible, and a larger number of accelerometers are needed in order to obtain healthy results. One of the accelerometers should be stationary (at the driving point) and the other accelerometer(s) should be moved over reference nodes sequentially. The reference accelerometer should be used for determining the sign of the mode shapes and for the magnitude of the modal scaling factor. For the explanation of modal scaling factor refer to Section 2.1 and Section 4.3.1.

Since there was only one channel available for acquiring response of the model in this study, it is assumed that if two accelerometers were used, modal scaling factor obtained in two tests would have been equal and for the reference accelerometer there would be no sign change in the mode shape coefficient

Natural frequency and damping factor can be correctly obtained even if only one accelerometer is used in the modal testing. However, this does not guarantee that the mode shapes are obtained correctly. Although some of the mode shapes may be correctly obtained, some mode shapes may be erroneous.

11.3 Discussion of Results of Finite Element Updating

Modifying FE model in order to bring the FE model prediction into better agreement with the experimental results is referred as **Finite Element Updating (FEU)** (see Chapter 9). Results obtained from EMAS (mode shapes and corresponding natural frequencies) are inputs of FEU.

In Finite Element Updating, mode shapes and natural frequencies obtained from modal testing are compared with the mode shapes and natural frequencies obtained from Finite Element Analysis. The most important criterion in comparing mode shapes is MAC values. MAC values are the main indicator whether the two set of modes are similar or not. The second criterion is the comparison of the **natural frequencies** of the matching modes. Therefore, in order to say that two modes obtained experimentally and analytically are matching, both the MAC values and modal frequencies should match. If either MAC or frequencies do not match, it is not possible to state that the two modes are matching.

In this study, two sets of experimental results are used for FEU purposes. These two sets of results are given in Sections 8.10.1 and 8.10.2, respectively. The Finite Element Updating (FEU) process did not achieve good results because of the weaknesses associated with the measurements (see Table 10-8 for the performance of FEU on different EMA result sets). The third set of EMA results obtained by excluding computational modes from the two sets of EMA results. For this purpose, 17 and 13 computational modes are excluded from the first and second EMA test result sets, respectively. The remaining modes in the first and second set of EMA results were collected in a new set and ordered according to their natural frequencies.

FEUS execution using the third set of EMA results concluded satisfactorily. The nominal model comparison results were acceptable (Table 10.8). The nominal (initial) model comparison to the third experimental set yielded %58.2 consistency

which was almost equal to the final consistency of the first set results. At the end of Finite Element Updating using third set of data, the consistency is obtained as 76.1% (agreement with the third set of EMA results), which is a 17.9% consistency improvement.

11.3.1 Optimized Mass Parameters

Mass groups were defined according to the plate sizes used for bolting the steel members. Two different types of mass groups were defined based on the used plate sizes (refer to Figure 8-2 and Section 10.3.1 for plates sizes and mass parameters, respectively).

For the first mass group (small plates) the optimized weight is found to be 0.184 (kg) which is 12.27% less than the initial value. Also for the second mass group (larger plates) optimized weight is found to be 0.24032 (kg) which is 31.92% less than the initial value. It is concluded from the above results that the initial values of the plates used were over estimated. The optimized value for mass group 2 is higher than the optimized value of mass group1, as expected.

11.3.2 Optimized Spring Parameters

The model was tested in free-free boundary conditions after suspended in the air using elastic ropes. The dynamic response of the test model becomes close to a free-free support condition since the stiffness of the elastic ropes are much smaller than the frame stiffness. Elastic rods and steel frame are shown in Figure 8-5 and Figure 8-6. Increasing or decreasing elastic rod stiffness (within the given range) does not affect bending or torsional modes of the model, but only affects the rigid body

modes' natural frequencies. Bending and torsional modes are insensitive to elastic rod stiffness value within the selected range. The initial value of spring elements axial stiffness was defined as 1001 N/m and the optimized parameter is found to be 11698.3 N/m. The large difference between the nominal and calibrated spring stiffness is due to the fact that nominal spring stiffness was just a guess (no preliminary experiment was conducted to determine the stiffness of elastic ropes), since it had no significant effect on natural modes of the test frame other than rigid body mode frequencies.

11.3.3 Optimized Frame Parameters

Frame elements used for the FEU were categorized under 4 groups. Frame group member distributions were graphically presented in Figure 10-4. The upper limits, lower limits, and initial values of the frame group parameters are initially defined same for all frame groups (refer to Table 10-1 through Table 10-4.). For the optimization process, the upper and lower limits of all parameters are defined by increasing and decreasing their initial values by 50%. Since the perturbation limit parameter was initially defined as %12, it would have been unfair to define different ranges for the optimization parameters. (More information on the perturbation limit parameter can be reached at Section to 9.4.3).

Framegroup1 was defined for the short members (with cover plates) at the joints, which are not continuous, and attached to the longitudinal (continuous) frame members by cover plates. The moment of inertia of this group (I_{zz}) about the major bending axis was 2.4% over estimated relative to the nominal model. The calibrated

value came out to be slightly lower than the nominal section since the transverse members are not continuous. The moment of inertia (I_{yy}) about the minor bending axis was 23.22 percent less estimated relative to the nominal value. The minor bending direction was largely affected by the cover plates (Figure 10-4). Finally torsional moment of inertia (I_{xx}) was 24.27 percent over estimated.

Framegroup2 was defined for the short members at the joints in longitudinal direction, which are formed by the continuous members and bolted cover plates. The calibrated moment of inertia for framegroup2 about the major bending axis (I_{zz}) was 1.28 percent more than the initial (nominal) value. The calibrated moment of inertia about major bending axis (I_{yy}) was found to be 5.42% less than the nominal value. Finally, calibrated torsional moment of inertia (I_{xx}) was 14.12% lower than the initial value.

Framegroup3 was defined for the main elements in longitudinal and transverse direction which are located between joints and without cover plates. The calibrated moment of inertia about the major bending axis (I_{zz}) turned about to be 0.07% smaller than the nominal value with almost no change at all. The calibrated moment of inertia about the minor bending axis (I_{yy}) was 27.92% larger than the nominal value. The calibrated torsional moment of inertia (I_{xx}) was 44.6% smaller than the nominal value.

The above results show that the changes in major bending moment of inertia (I_{zz}) values remained within reasonable and expected ranges. The framegroup1 sections

(with cover plates in transverse direction) had smaller I value due to discontinuity, whereas the framegroup2 (with cover plates in longitudinal direction) had a small inertia increase probably because of the holes in compression and tension flanges, and poor shear transfer (voids) in the bolted connections at low loading levels. The unusual variations in the minor and torsional inertia values are due to the insensitivity of parameters in vertical bending modes. The study had included only the vertical modes, and minor moment of inertia values were not exited by taking transverse vibration mode shapes. The effects of torsional and lateral bending moment of inertias had little effect on vertical mode shapes, therefore were not properly calibrated using measured dynamic data.

Framegroup4 is defined for the members which are located at the right edge of the frame shown with triangles in Figure 10-4. The section used for the indicated members have slightly different dimensions compared to the rest of the members defined by Framegroup3. The calibrated moment of inertia for framegroup4 about the major bending axis (I_{zz}) is found to be 12.27% smaller than the nominal value. The calibrated moment of inertia about the minor bending axis (I_{yy}) was 42.78% larger than the nominal value. The calibrated torsional moment of inertia (I_{xx}) was 11.66% smaller than the nominal value.

The framegroup4 sections were slightly larger than the rest of the members. Therefore, major bending axis inertias were expected to be larger than the nominal values. On the other hand, minor bending axis moment of inertia found to be larger than the nominal values. The unclear variations in the group 4 member properties

(calibration results being smaller than the expected values) are attributed to a) the reduced number of members not being able to affect the overall behavior, and b) coupled effect of group1 and group4 elements that coexist. Nevertheless, the calibration results of group 4 were worse than what was expected. Certain percentage of low performance obtained for group4 members might also be attributed to the quality of dynamic measurements. If the tests are repeated using better equipment and larger number of accelerometers, the success rate of calibration might have been improved.

As it can be noticed, changes in cross sectional area for all frame groups given above were not mentioned. Within the given ranges, changes in cross-sectional area do not change the objective function. Change in cross-sectional area is an insensitive variable in FEU since all of the measured dynamic data are affected predominantly by bending properties of sections.

11.4 A Few Comment about FEU

Process of experimental modal analysis and calibration can be considered as a chain. Finite Element Updating is the last link of that chain, whereas modal testing is the first, and modal parameter estimation is in the middle. Therefore a problem at any ring level of the chain will affect the final ring. In order to obtain accurate results from Finite Element Updating, Modal parameter estimation should be accurate. In order to obtain accurate modal parameter estimation, Frequency Response Functions should be accurate. Finally in order to obtain accurate Frequency Response Functions, modal testing should be accurate. Success in a link

of the chain is highly related with the successes in previous links. In order to say that the result of FEU process is completely successful, there should be at least % 90-95 correlation between experimental results and finite element results (analytical results). But in our case there was only % 76.145 consistency between experimental results and finite element results (analytical results). If there were more than 90-95 percent correlation and the optimized values were similar to the ones above, then it would be correct to say that there is something wrong either in Finite Element Analysis or in Finite Element Updating.

Under these circumstances, it is only possible to say that FEU process was successful as much as modal parameters were. And finally modal parameters were accurate as much as modal testing was. Therefore the success in this study was limited (and dominantly affected by) modal testing part of this study. If at least a 4 channel data acquisition system (or a 4 channel dynamic analyzer) had been available, the modal parameters would have been more accurate and therefore FEU would have had a higher success rate. Nonetheless, majority of the calibration results obtained (especially for major bending moment of inertias and concentrated mass values) were meaningful. The modal testing, modal analysis, and model updating phases might be deemed as successful considering the difficulties with the measurement phase.

It is concluded that minor axis bending properties could be better estimated if lateral and longitudinal direction modal parameters were also obtained (in addition to the vertical modal parameters). The number of accelerometers used for the testing

should be increased for higher success rate in measurements. Smaller frequency windows should be tested at a time to have shorter frequency intervals between each reading. Measurement of 1 to 260 Hz and 1 to 500 Hz range was too coarse and individual data points were too sparse.

11.5 Future Studies

In PhD studies, it is planned to use EMAS and FEUS with data obtained from large scale actual and existing structures (such as bridges and buildings). Small size bridges will be dynamically tested but a better data acquisition system will be used. With a better data acquisition system (4, 8, 16 channels) it will be proven that EMAS and FEUS are working properly.

The next topic for future studies is “Modal Parameter Estimation using Ambient Response data”. Ambient data is generated by environmental excitation (such as traffic, wind, earthquakes, etc.) and the input force to the system is unknown. For bridges, the input forces are generally the traffic loads. For the buildings, the input forces are generally heavy street traffic, human/machinery activity in the building, wind, and with a small probability an earth quake.

Custom design testing tools, wireless sensors, and commercially available modal analysis programs will also be investigated as a part of future studies.

REFERENCES

Allemang, R. J. (1998). Vibrations: VIBRATIONS: EXPERIMENTAL MODAL ANALYSIS Structural Dynamics Research Laboratory. Department of Mechanical, Industrial and Nuclear Engineering. University of Cincinnati.

Avaitable, P., (1998). Could you explain modal analysis for me. Society of Experimental Techniques. February 1998

Avaitable, P., (1998). Could you explain the difference between time domain , frequency domain and modal space. Society of Experimental Techniques. April 1998

Avaitable, P., (1998). Is there any difference between a modal test with shaker excitation and impact excitation. Society of Experimental Techniques. June 1998

Avaitable, P., (1998). Which shake excitation is best? Is there any difference? Society of Experimental Techniques. December 1998

Avaitable, P., (1999). Curve fitting is so confusing me! What do all the techniques mean?. Society of Experimental Techniques. February 1999

Avaitable, P., (1999). I still Don't Understand Curve fitting... How do you get Mode Shapes from FRF? Society of Experimental Techniques. April 1999

Avaitable, P., (1999). I am still overwhelmed by all this stuff. Give me the big picture. Society of Experimental Techniques. December 1999

Avaitable, P., (1999). Are you sure you get mode shapes from one row or column of H? Society of Experimental Techniques. August 1999

Avaitable, P., (1999). I heard someone say "Pete doesn't do windows" What is the scoop. Society of Experimental Techniques. October 1999

Avaitable, P., (2000). How many point are enough when running a modal test? Society of Experimental Techniques. June 2000

Avaitable, P., (2000). Someone told me Structural dynamic modification will never work. Society of Experimental Techniques. February 2000

Avaitable, P., (2000). Why is mass loading and data consistency so important? Society of Experimental Techniques. October 2000

Avaitable, P., (2001). I heard about SVD all the time. Could you explain it simply to me?. Society of Experimental Techniques. January 2001

Awaitable, P., (2002). Is there any real advantage to MIMO testing?, Why not just use SISO and then move the shaker. Society of Experimental Techniques. September 2002

Ashory M. R., (1999). High Quality modal testing methods. (Phd study). University of London.

Bathe, K. J., (1982). Finite Element Procedures in Engineering Analysis, Prentice Hall.

Brown, D., (1997). Advanced Modal Parameter Estimation Concepts. UC/SDRL Prepared for the System Dynamics Course

Catbas F.N, Lenett, M., Brown, D.L., Doebling, S.W., Farrar, C.R., Turer, A., (1998). Modal Analysis of Multi-Reference impact test data for steel stringer bridges. Presented at 15th International Modal Analysis Conference

Chandrupatla,T.R., Belegundu, A.D., (1997). Introduction to Finite Elements in Engineering, Prentice Hall

Chen, G., Ewins, D. J., (2000). A Perspective on Model Updating Performance. Presented at 20th IMAC Conference

Chen, G., Ewins, D. J., (2001). Verification of FE Models for Model Updating. Presented at 21st International Modal Analysis Conference.

Chopra, A. K., (1995). Dynamics of Structures. Prentice Hall.

Cook, R.D., (1989). Concepts and Application of Finite Element Analysis, John Wiley & Sons.

Dascotte, E.,(2001). Applications of Finite Element Model Updating Using Experimental Modal Data. Dynamic Design Solutions, <http://www.femtools.com>.

Ewins, D.,(1995).Modal Testing: Theory and Practice. John Wiley and Sons, Inc

Elliott, A. S., Richardson M. H., (1998). Virtual Experimental Modal Analysis. Presented at 16th International Modal Analysis Conference.

Haapaniemi, H., Saarenheimo, A., Smeekes, P.,Talja H, (2002). Numerical simulation of piping vibrations using updated FE model. Presented at 20th International Modal Analysis Conference.

Hasançebi, (2001). Optimum structural design using analogies to natural processes.(Phd Study). Middle East Technical University.

Kwon, Y. W., (1982). The Finite Element Method Using MATLAB, CRC Press.

Kashani, R., State–Space Formulation of Linear Systems, DEICON (Design, Imaging, & Control, Inc) www.deicon.com.

Marchand, P.,(1999).Graphics and GUIs with Matlab. CRC Press.

Meirovitch, L., (1996). Elements of Vibration Analysis. McGraw-Hill International Editions.

Michael, L., Richardson, M., (1992). Determining the Accuracy of Modal Parameter Estimation Methods, Presented at 10th International Modal Analysis Conference.

Potter, R., Richardson M., (1982). Mass, Stiffness and Damping Matrices from Measured Modal Parameters. Presented at 1st IMAC Conference.

Ventura,C.E., Brincker, R., Dascotte, E., Andersen, P. (2001). Finite Element Model Updating of the Heritage Court Building Structure. Presented at 21st International Modal Analysis Conference

Richardson, M. H., (1978). Fundamentals of the Discrete Fourier Transform. Sound & Vibration Magazine,1978.

Richardson, M. H., (1986). Global Frequency and Damping Estimates from Frequency Response Measurements. Presented at 4th International Modal Analysis Conference.

Richardson, M. H., (2000). Modal Mass, Stiffness and Damping. Presented at 20th International Modal Analysis Conference

Schwarz, B. J., Richardson M. H., (1997). Structural Modifications Using Higher Order Elements . Presented at 15th International Modal Analysis Conference.

Schwarz, B., Richardson,M., (2001) Modal Parameter Estimation From Ambient Response Data. Presented at 21st International Modal Analysis Conference.

Schwarz, B., Richardson, M., (2001),Post- Processing Ambient and Forced Response Bridge Data to Obtain Modal Parameters. Presented at 21st International Modal Analysis Conference .

Shih, C. Y., Tsuei, Y. G., Allemang, R. J., Brown D. L, (1989). Complex Mode Indication Function and its Applications to Spatial Domain Parameter Estimation. Presented at 7th International Modal Analysis Conference.

Shye, K., Richardson, M., (1987). Mass, Stiffness, and Damping Matrix Estimates from Structural Measurements. International Modal Analysis Conference.

Shye, K., Richardson, M.(1985). Mass, Stiffness, and Damping Matrix Estimates from Structural Measurements. Presented at 5th International Modal Analysis Conference.

Wallack, P., Skoog, P., Richardson, M., (1989). Comparison of Analytical and Experimental Rib Stiffener Modifications to a Structure. Presented at 7th International Modal Analysis Conference.

Weisstein, E., Singular Value Decomposition. <http://mathworld.wolfram.com>

APPENDIX A

Report generated by EMAS for 3 d.o.f. system

Date: 06-Jan-2004

Time: 16:31

This is a report generated by experimental modal analysis software(EMAS)

Title: 3 d.o.f. cantilever beam model

N O D E S

NODE ID	X CORD	Y CORD	Z CORD
1	0	0	0
2	1	0	0
3	2	0	0
4	3	0	0

E L E M E N T S

ELEMENT TYPE	START NODE	END NODE
2	1	2
2	2	3
2	3	4

C O N S T R A I N T S

NODE ID	X-TRANS	Y-TRANS	Z-TRANS	X-ROT	Y-ROT
1	1	1	1	1	1

M A S T E R D O F S

NODE ID	X-TRANS	Y-TRANS	Z-TRANS	X-ROT	Y-ROT
2	0	0	1	0	0
3	0	0	1	0	0

	4	0	0	1	0	0
0						

M O D A L P A R A M E T E R S

MODE	FREQUENCY (Hz)	DAMPING (%)
1	7.598	0.119
2	21.397	0.336
3	32.802	0.515

M O D E S H A P E S

MODE 1

NODE	DOF	FACTOR
2	3	-0.2801
3	3	-0.5642
4	3	-0.7767

MODE 2

NODE	DOF	FACTOR
2	3	-0.6200
3	3	-0.5962
4	3	0.5100

MODE 3

NODE	DOF	FACTOR
2	3	-0.8251
3	3	0.5489
4	3	-0.1340

M A C C O R R E L A T I O N

M O D E 1

	MODE 1
MODE 1	1.0000
MODE 2	0.0130

MODE 3	0.0006
--------	--------

M O D E 2

MODE 2

MODE 1	0.0130
--------	--------

MODE 2	1.0000
--------	--------

MODE 3	0.0135
--------	--------

M O D E 3

MODE 3

MODE 1	0.0006
--------	--------

MODE 2	0.0135
--------	--------

MODE 3	1.0000
--------	--------

APPENDIX B

Input file of skewed frame used in FEUS.

```
title skewed frame Problem
! Main nodes which are used in FEUS
! these are nodes that are selected as master
node 1,      0,      0.0,      0.0
node 5,     -0.194114283826891,  0.724444369716801,  0.0
node 33,      3,      0.0,      0.0
node 37,      2.80588571617311,  0.724444369716801  , 0
nodegen 1    33  3    9    8
nodegen 5    37  3   13    8
nodegen 1     5  3    2    1
nodegen 33   37  3   34    1
nodegen 9    13  3   10    1
nodegen 17   21  3   18    1
nodegen 25   29  3   26    1
nodegen 1     9  1    6    1
nodegen 25   33  1   30    1
nodegen 6    30  2   14    8
nodegen 3     11  1    7    1
nodegen 27   35  1   31    1
nodegen 7    31  2   15    8
nodegen 5    13  1    8    1
nodegen 29   37  1   32    1
nodegen 8    32  2   16    8
! Nodes used to define connection regions
node 38,      0.037,      0.0,      0.0
node 39,      0.715,      0.0,      0.0
node 40,      0.785,      0.0,      0.0
node 41,      1.465,      0.0,      0.0
node 42,      1.535,      0.0,      0.0
node 43,      2.215,      0.0,      0.0
node 44,      2.285,      0.0,      0.0
node 45,      2.963,      0.0,      0.0
node 46,     -0.01216449512  0.04539851384,  0.0
node 50,      2.987835505  0.04539851384,  0.0
nodegen 46  50  3  47    1
node 51      -0.08489264679,  0.316823671,  0.0
node 55      2.91510735320637,  0.316823671,  0.0
nodegen 51  55  3  52    1
node 64      -0.109221637033264,  0.407620698693987,  0.0
node 68      2.89077836296674,  0.407620698693987,  0.0
nodegen 64  68  3  65    1
node 69      -0.181949788707072,  0.679045855881215,  0.0
node 73      2.81805021129293,  0.679045855881215,  0.0
```



```

nodegen 69 73 3 70 1
node 56 -0.0600571419134455, 0.362222184858401, 0.0
node 57 0.617942858086555, 0.362222184858401, 0.0
node 58 0.687942858086555, 0.362222184858401, 0.0
node 59 1.36794285808655, 0.362222184858401, 0.0
node 60 1.43794285808655, 0.362222184858401, 0.0
node 61 2.11794285808655, 0.362222184858401, 0.0
node 62 2.18794285808656, 0.362222184858401, 0.0
node 63 2.86594285808656, 0.362222184858401, 0.0
node 74 -0.157114283826891, 0.724444369716801, 0.0
node 75 0.520885716173109, 0.724444369716801, 0.0
node 76 0.590885716173109, 0.724444369716801, 0.0
node 77 1.27088571617311, 0.724444369716801, 0.0
node 78 1.34088571617311, 0.724444369716801, 0.0
node 79 2.02088571617311, 0.724444369716801, 0.0
node 80 2.09088571617311, 0.724444369716801, 0.0
node 81 2.76888571617311, 0.724444369716801, 0.0
! Nodes that are used to get fine mesh
! One additional node is added between two nodes
! which are wide enough
nodegen 6 38 1 82 1
nodegen 6 39 1 83 1
nodegen 14 40 1 84 1
nodegen 14 41 1 85 1
nodegen 22 42 1 86 1
nodegen 22 43 1 87 1
nodegen 30 44 1 88 1
nodegen 30 45 1 89 1
nodegen 2 46 1 90 1
nodegen 2 51 1 91 1
nodegen 4 64 1 92 1
nodegen 4 69 1 93 1
nodegen 34 50 1 94 1
nodegen 34 55 1 95 1
nodegen 36 68 1 96 1
nodegen 36 73 1 97 1
nodegen 8 74 1 98 1
nodegen 8 75 1 99 1
nodegen 16 76 1 100 1
nodegen 16 77 1 101 1
nodegen 24 78 1 102 1
nodegen 24 79 1 103 1
nodegen 32 80 1 104 1
nodegen 32 81 1 105 1
nodegen 90 94 3 106 1
nodegen 91 95 3 109 1
nodegen 92 96 3 112 1
nodegen 93 97 3 115 1
nodegen 82 98 1 118 1
nodegen 83 99 1 119 1
nodegen 84 100 1 120 1
nodegen 85 101 1 121 1
nodegen 86 102 1 122 1
nodegen 87 103 1 123 1
nodegen 88 104 1 124 1
nodegen 89 105 1 125 1
node 126 1.125 0.1 0.5
node 127 1.27088571617311, 0.624444369716801, 0.5
node 128 1.535, 0.1, 0.5

```

```

node 129    1.68088571617311,    0.624444369716801    , 0.5
node 130    1.19794285808655,0.26222184858401,0.5
node 131    1.19794285808655,        0.46222184858401,    0.5
node 132    1.60794285808655, 0.262222184858401,    0.5
node 133    1.60794285808655, 0.462222184858401,    0.5
!node 134    0 -0.5 0
!node 135    -0.194114283826891,    1.224444369716801,    0
!node 136    3,    -0.5,    0
!node 137    2.80588571617311,    1.24444369716801    , 0
elemtype beam3d    1.84e-4,    2.e11,    2.157e-8,    7850, 0.3 , 1.113e-
8,    2.209e-8
elem 1 1 38
elem 2 38 82
elem 3 82 6
elem 4 6 83
elem 5 83 39
elem 6 39 9
elem 7 9 40
elem 8 40 84
elem 9 84 14
elem 10 14 85
elem 11 85 41
elem 12 41 17
elem 13 17 42
elem 14 42 86
elem 15 86 22
elem 16 22 87
elem 17 87 43
elem 18 43 25
elem 19 25 44
elem 20 44 88
elem 21 88 30
elem 22 30 89
elem 23 89 45
elem 24 45 33
elem 25 3 56
elem 26 56 118
elem 27 118 7
elem 28 7 119
elem 29 119 57
elem 30 57 11
elem 31 11 58
elem 32 58 120
elem 33 120 15
elem 34 15 121
elem 35 121 59
elem 36 59 19
elem 37 19 60
elem 38 60 122
elem 39 122 23
elem 40 23 123
elem 41 123 61
elem 42 61 27
elem 43 27 62
elem 44 62 124
elem 45 124 31
elem 46 31 125
elem 47 125 63
elem 48 63 35

```

elem 49 5 74
elem 50 74 98
elem 51 98 8
elem 52 8 99
elem 53 99 75
elem 54 75 13
elem 55 13 76
elem 56 76 100
elem 57 100 16
elem 58 16 101
elem 59 101 77
elem 60 77 21
elem 61 21 78
elem 62 78 102
elem 63 102 24
elem 64 24 103
elem 65 103 79
elem 66 79 29
elem 67 29 80
elem 68 80 104
elem 69 104 32
elem 70 32 105
elem 71 105 81
elem 72 81 37
elem 73 1 46
elem 74 46 90
elem 75 90 2
elem 76 2 91
elem 77 91 51
elem 78 51 3
elem 79 3 64
elem 80 64 92
elem 81 92 4
elem 82 4 93
elem 83 93 69
elem 84 69 5
elem 85 9 47
elem 86 47 106
elem 87 106 10
elem 88 10 109
elem 89 109 52
elem 90 52 11
elem 91 11 65
elem 92 65 112
elem 93 112 12
elem 94 12 115
elem 95 115 70
elem 96 70 13
elem 97 17 48
elem 98 48 107
elem 99 107 18
elem 100 18 110
elem 101 110 53
elem 102 53 19
elem 103 19 66
elem 104 66 113
elem 105 113 20
elem 106 20 116
elem 107 116 71

```

elem 108 71 21
elem 109 25 49
elem 110 49 108
elem 111 108 26
elem 112 26 111
elem 113 111 54
elem 114 54 27
elem 115 27 67
elem 116 67 114
elem 117 114 28
elem 118 28 117
elem 119 117 72
elem 120 72 29
elem 121 33 50
elem 122 50 94
elem 123 94 34
elem 124 34 95
elem 125 95 55
elem 126 55 35
elem 127 35 68
elem 128 68 96
elem 129 96 36
elem 130 36 97
elem 131 97 73
elem 132 73 37
elemtype mass3d 0
elem      133, 1
elemgen 133 4 136 3 8
elemgen 133 2 134 1 2
elemgen 136 2 137 1 2
elemgen 139 2 140 1 2
elemgen 142 2 143 1 2
elemgen 145 2 146 1 2
elemtype spring3d 102
elem 148 14 126
elem 149 77 127
elem 150 42 128
elem 151 24 129
elem 152 121 130
elem 153 121 131
elem 154 122 132
elem 155 122 133
elem 156 14 126
elem 157 77 127
elem 158 42 128
elem 159 24 129
! Fix Spring Supports
constnode 126
constnode 127
constnode 128
constnode 129
constnode 130
constnode 131
constnode 132
constnode 133
allmasterdof 3

```

APPENDIX C

Mode shapes extracted from the first experiment.

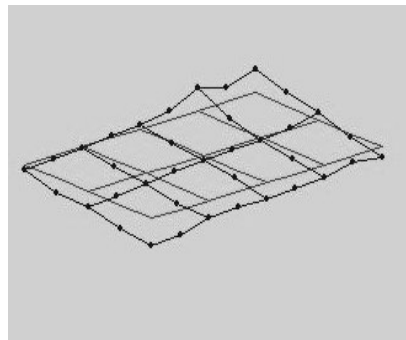


Figure C-1 6.23 Hz

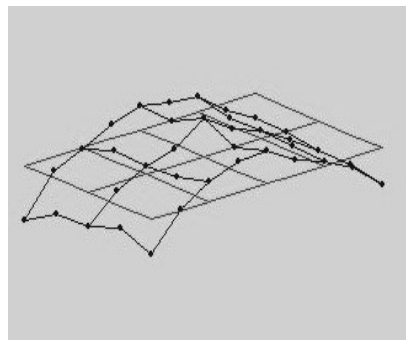


Figure C-2 14.72 Hz

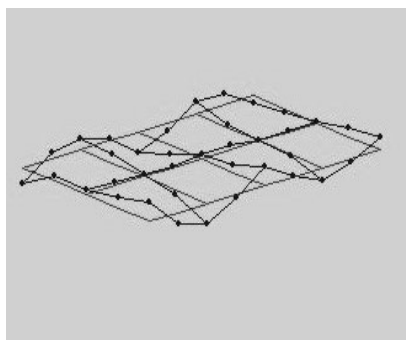


Figure C-3 104.06 Hz

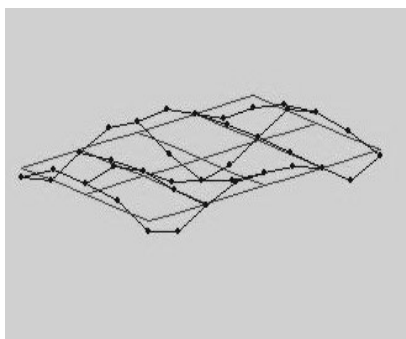


Figure C-4 136.27 Hz

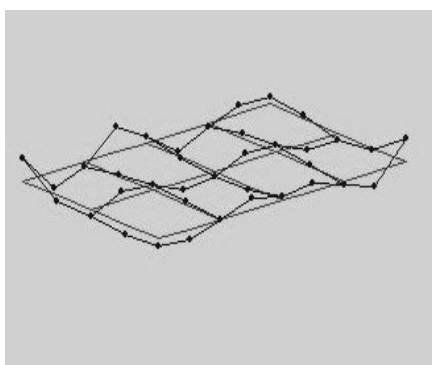


Figure C-5 182.0014 Hz

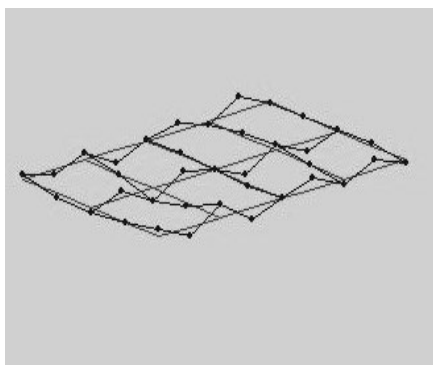


Figure C-6 182.0014 Hz

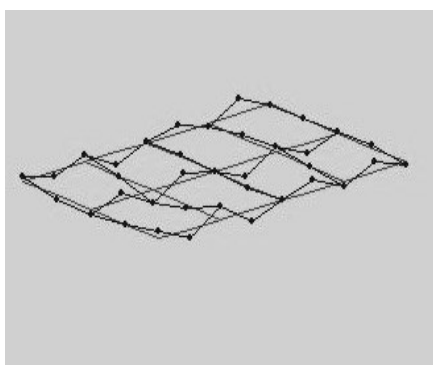


Figure C-7 375.77 Hz

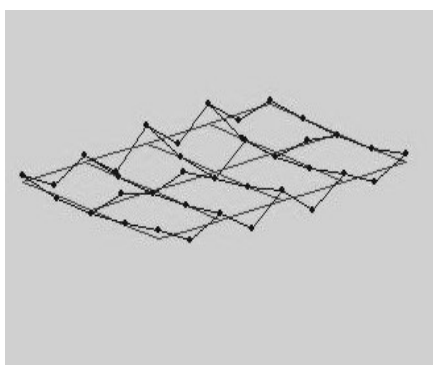


Figure C-8 469.60 Hz

APPENDIX D

Mode shapes extracted from the second experiment.

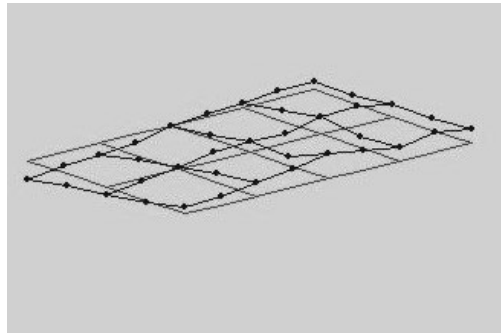


Figure D-1 8.22 Hz

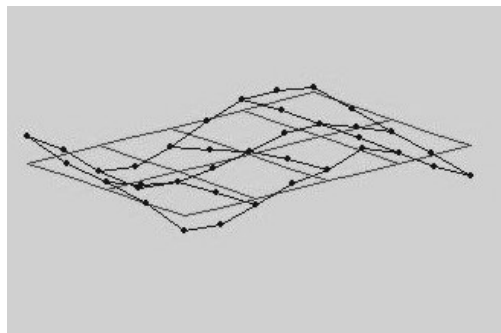


Figure D-2 39.995 Hz

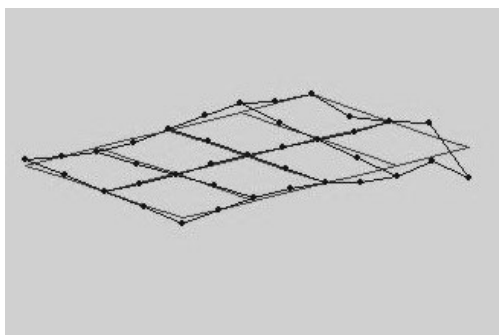


Figure D-3 64.889 Hz

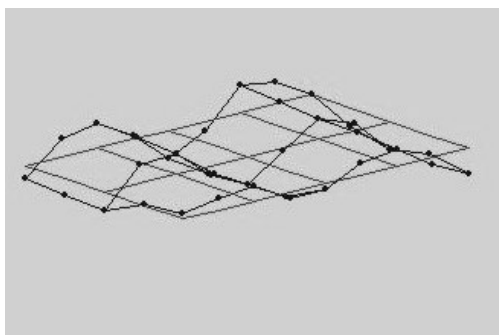


Figure D-4 78.19 Hz

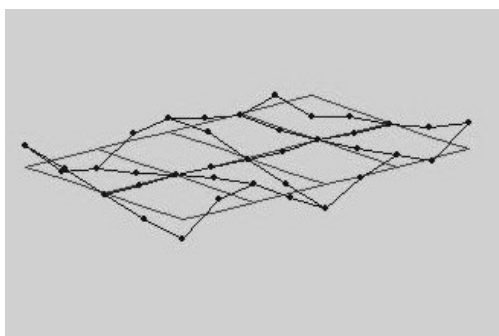


Figure D-5 102.37 Hz

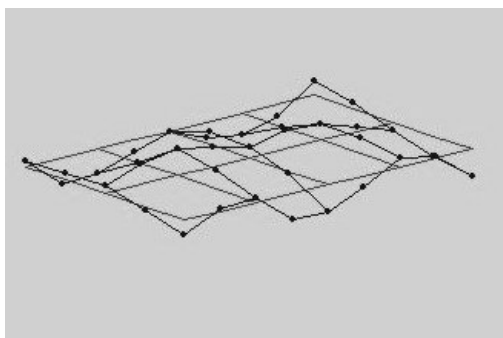


Figure D-6 110.04 Hz

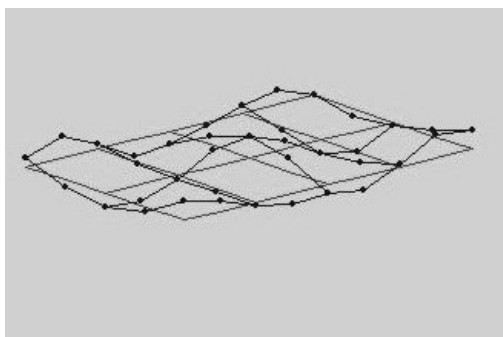


Figure D-7 139.41 Hz

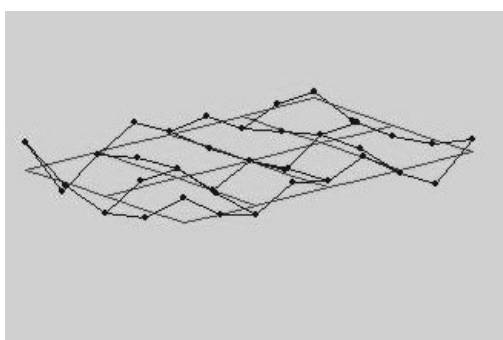


Figure D-8 232.84 Hz